N°d'ordre NNT : 2020LYSEI012

THESE de DOCTORAT DE L'UNIVERSITE DE LYON
opérée au sein de
INSA-LYON

Ecole Doctorale N° EDA160
Électronique, Électrotechnique, Automatique

Spécialité/ discipline de doctorat :
Traitement du Signal et de l'Image

Soutenue publiquement le **14/02/2020**, par:
Fei GE

Titre de la thèse

The lattice Boltzmann method dedicated to medical image processing

---

Devant le jury composé de :

RUAN, Su	Professeure des Universités	Université de Rouen	Rapporteuse
THIRAN, Jean-Philippe	Professeur ordinaire	EPFL	Rapporteur
NAVARRO, Laurent	Chargé de Recherche - HDR	ENSMSE	Examinateur
CHEN, Yu	Professeur associé	YanchengTeachers University	Examinateur
FOURNEL, Thierry	Professeur des Universités	Université Jean Monnet	Examinateur
COURBEBAISSE, Guy	IR HC - HDR	INSA Lyon	Directeur de thèse

Département FEDORA – INSA Lyon - Ecoles Doctorales – Quinquennal 2016-2020

SIGLE	ECOLE DOCTORALE	NOM ET COORDONNEES DU RESPONSABLE
CHIMIE	**CHIMIE DE LYON** **http://www.edchimie-lyon.fr** Sec. : Renée EL MELHEM Bât. Blaise PASCAL, 3e étage **secretariat@edchimie-lyon.fr** INSA : R. GOURDON	**M. Stéphane DANIELE** Institut de recherches sur la catalyse et l'environnement de Lyon IRCELYON-UMR 5256 Équipe CDFA 2 Avenue Albert EINSTEIN 69 626 Villeurbanne CEDEX **directeur@edchimie-lyon.fr**
E.E.A.	**ÉLECTRONIQUE, ÉLECTROTECHNIQUE, AUTOMATIQUE** **http://edeea.ec-lyon.fr** Sec. : M.C. HAVGOUDOUKIAN **ecole-doctorale.eea@ec-lyon.fr**	**M. Gérard SCORLETTI** École Centrale de Lyon 36 Avenue Guy DE COLLONGUE 69 134 Écully Tél : 04.72.18.60.97 Fax 04.78.43.37.17 **gerard.scorletti@ec-lyon.fr**
E2M2	**ÉVOLUTION, ÉCOSYSTÈME, MICROBIOLOGIE, MODÉLISATION** **http://e2m2.universite-lyon.fr** Sec. : Sylvie ROBERJOT Bât. Atrium, UCB Lyon 1 Tél : 04.72.44.83.62 INSA : H. CHARLES **secretariat.e2m2@univ-lyon1.fr**	**M. Philippe NORMAND** UMR 5557 Lab. d'Ecologie Microbienne Université Claude Bernard Lyon 1 Bâtiment Mendel 43, boulevard du 11 Novembre 1918 69 622 Villeurbanne CEDEX **philippe.normand@univ-lyon1.fr**
EDISS	**INTERDISCIPLINAIRE SCIENCES-SANTÉ** **http://www.ediss-lyon.fr** Sec. : Sylvie ROBERJOT Bât. Atrium, UCB Lyon 1 Tél : 04.72.44.83.62 INSA : M. LAGARDE **secretariat.ediss@univ-lyon1.fr**	**Mme Sylvie RICARD-BLUM** Institut de Chimie et Biochimie Moléculaires et Supramoléculaires (ICBMS) - UMR 5246 CNRS - Université Lyon 1 Bâtiment Curien - 3ème étage Nord 43 Boulevard du 11 novembre 1918 69622 Villeurbanne Cedex Tel : +33(0)4 72 44 82 32 **sylvie.ricard-blum@univ-lyon1.fr**
INFOMATHS	**INFORMATIQUE ET MATHÉMATIQUES** **http://edinfomaths.universite-lyon.fr** Sec. : Renée EL MELHEM Bât. Blaise PASCAL, 3e étage Tél : 04.72.43.80.46 **infomaths@univ-lyon1.fr**	**M. Hamamache KHEDDOUCI** Bât. Nautibus 43, Boulevard du 11 novembre 1918 69 622 Villeurbanne Cedex France Tel : 04.72.44.83.69 **hamamache.kheddouci@univ-lyon1.fr**
Matériaux	**MATÉRIAUX DE LYON** **http://ed34.universite-lyon.fr** Sec. : Stéphanie CAUVIN Tél : 04.72.43.71.70 Bât. Direction **ed.materiaux@insa-lyon.fr**	**M. Jean-Yves BUFFIÈRE** INSA de Lyon MATEIS - Bât. Saint-Exupéry 7 Avenue Jean CAPELLE 69 621 Villeurbanne CEDEX Tél : 04.72.43.71.70 Fax : 04.72.43.85.28 **jean-yves.buffiere@insa-lyon.fr**
MEGA	**MÉCANIQUE, ÉNERGÉTIQUE, GÉNIE CIVIL, ACOUSTIQUE** **http://edmega.universite-lyon.fr** Sec. : Stéphanie CAUVIN Tél : 04.72.43.71.70 Bât. Direction **mega@insa-lyon.fr**	**M. Jocelyn BONJOUR** INSA de Lyon Laboratoire CETHIL Bâtiment Sadi-Carnot 9, rue de la Physique 69 621 Villeurbanne CEDEX **jocelyn.bonjour@insa-lyon.fr**
ScSo	**ScSo*** **http://ed483.univ-lyon2.fr** Sec. : Véronique GUICHARD INSA : J.Y. TOUSSAINT Tél : 04.78.69.72.76 **veronique.cervantes@univ-lyon2.fr**	**M. Christian MONTES** Université Lyon 2 86 Rue Pasteur 69 365 Lyon CEDEX 07 **christian.montes@univ-lyon2.fr**

*ScSo : Histoire, Géographie, Aménagement, Urbanisme, Archéologie, Science politique, Sociologie, Anthropologie

Abstract

Lattice Boltzmann Method (LBM) is a numerical tool working with a methodology based on microscopic particle models and mesoscopic kinetic equations. As a numerical tool LBM has proved its capability to simulate complex fluid flow behaviours and more recently to process medical images. In the framework of image analysis, LBM is implemented to perform denoising operation, image boundary detection and image segmentation. In addition, the lattice Boltzmann method possesses the feature of strong amenability to parallel computing, especially on low-cost powerful graphics hardware (GPU).

The main purpose of this thesis is to develop a general segmentation algorithm described by four main parts. The first part proposes an original segmentation methodology created by combining a direct volume rendering technique (2D histogram based clustering method) and a Lattice Boltzmann 3D method. The applied strategy allows to segment medical images sequences by grey-level values and gradient of grey-level values. In this part, the results are compared with the k-means clustering method, and the manually segmentation results show that the algorithm can improve both on segmentation accuracy and denoising performances. But applying this method on more complex data sets results in poor accuracy. Hence, in the second part introduces multiple thresholds based on LBM and clustering algorithm. The LBM of the first part is basically realized by solving the diffusion reaction equation. This equation takes into account a threshold that is usually calculated by the Otsu method, thereby solving the diffusion reaction equation. An innovative multi-threshold collision function is elaborated, and a new formulation for the lattice Boltzmann method is established for the clustering of 3D images. Moreover, the thresholds are fixed by the k-means clustering method. Under this new concept, 2D images from the Berkeley segmentation database and 3D volume data-set including cerebral aneurysm sequences are segmented through the new approach. The performances are evaluated with the Dice similarity coefficient, Relative volume difference, and Hausdorff distance. Then, in order to

extend the universality of the algorithm, more potential geometry and statistic properties are introduced in the LBM-based segmentation method. In addition, an innovative multivariate clustering-based collision function is introduced, which causes a new formulation of the lattice Boltzmann method for the clustering of 3D volume data-set. The centroids in the collision function are still being fixed by the k-means method. The performances are also validated by segmenting three-dimensional (3D) tomography angiography images, and also evaluated with the Dice similarity coefficient and Hausdorff distance. The last part investigates the LBM-based segmentation method on parallel computing. In order to deal with large scale image, we take advantage of parallel LBM by using Graphic Processors Units (GPU) architectures to improve the performance of LBM. It has been proved efficiency can be improved by segmenting aneurysms and parent vessel walls, whole-brain data sets and stent-assisted aneurysms. The parallel segmentation method has been operated on NVIDIA graphic cards and demonstrates that the proposed method achieves at least 131 speedups under the same precision.

Keywords: segmentation algorithm, cerebral aneurysm segmentation, lattice Boltzmann method, clustering algorithm, stent-assisted aneurysm, 2D histogram GPU acceleration.

Résumé

La méthode de Boltzmann sur rseau (LBM) est un outil numérique avec une méthodologie basée sur des modèles microscopiques de particules et des équations cinétiques mésoscopiques. Elle repose sur des mécanismes de propagation et de collision au cours du temps de distributions de particules se propageant sur un réseau régulier. Si les lois de conservation sont imposées en chaque noeud du réseau, alors la solution générée correspondra à la modélisation de phénomènes physiques à l'échelle macroscopique. Dans ce contexte la méthode de Boltzmann est tout à fait adaptée pour résoudre un problème de mécanique des fluides qui équivaut à résoudre indirectement l'équation de Navier-Stokes. Récemment des travaux en traitement d'images ont été réalisés en adaptant la méthode de Boltzmann sur réseau pour des opérations de segmentation, de débruitage,... LBM a également l'avantage d'être très adapté au calcul parallèle, notamment sur du matériel graphique puissant et peu coûteux (GPU).

Le but principal de cette thèse est de développer un algorithme général de segmentation. Cette thèse se compose de quatre parties principales. La première partie propose une méthodologie de segmentation originale créée en couplant une technique de rendu volumique direct (méthode de clustering à base d'histogrammes 2D) et une méthode de Boltzmann sur réseau 3D. La stratégie réside dans la possibilité de segmenter des séquences d'images médicales par niveaux de gris et gradient de niveaux de gris. Dans cette partie, les résultats sont comparés avec la méthode de classification par k-moyennes et les résultats de segmentation manuelle montrent que l'algorithme a amélioré à la fois la rapidité du traitement et la limitation du bruit de calcul numérique. Mais nous avons constaté que la méthode peut s'appliquer à des ensembles de données plus complexes, mais que la précision des résultats n'est pas suffisante. La deuxième partie propose donc un processus de multi-euillages basé sur la LBM et un algorithme de partionnement. LBM de la première partie est essentiellement mis en œuvre pour la segmentation en résolvant une équation de réaction-diffusion prenant en compte un seuil communément cal-

culé par la méthode de Otsu. Une fonction innovante de collision multi-seuils est élaborée, conduisant à une nouvelle formulation de la méthode de Boltzmann sur réseau pour le partitionnement d'images 3D, les seuils étant fixés par la méthode de partitionnement par k-moyenness. Dans le cadre de ce nouveau concept, des images 2D de la base de données de segmentation de Berkeley et des données en volume 3D comprenant des séquences d'anévrismes cérébraux traités par endoprothèse sont segmentées par la nouvelle approche. Les performances sont évaluées via le coefficient de similarité de Dice, la différence de volume relative et la distance de Hausdorff. Ensuite, afin d'étendre l'universalité de l'algorithme basée sur les propriétés potentielles de la géométrie et de données statistiques sont introduits dans la méthode de segmentation basée sur la LBM, et une fonction de collision innovante basée sur un partitionnement multivarié est élaborée conduisant à une nouvelle formulation de la méthode de Boltzmann pour le traitement de données volumiques 3D. Les performances sont également validées par la segmentation d'images tomographiques tridimensionnelles (3D) d'angiographie. La dernière partie examine la méthode de segmentation basée sur une version parallélisée de LBM. Pourour traiter les images à grande échelle, nous tirons parti de la LBM parallèle en utilisant des architectures de processeurs graphiques (GPU) afin d'améliorer la performance de la LBM. Nous avons prouvé l'efficacité du LBM parallèle en segmentant la paroi d'un anévrisme traité pas stent et des vaisseaux sanguins parents. La méthode de segmentation parallèle a été testée sur une carte graphique nVIDIA et démontre que la méthode proposée reduit les temps de calcul d'un facteur supérieur à 100.

Mots-clés: algorithme de segmentation, segmentation de l'anévrisme cérébral, méthode de Boltzmann sur réseau, algorithme de clustering, anévrisme traité par stent , histogramme 2D, accélération GPU.

Contents

List of Figures

List of Tables

Acknowledgments

In the beginning, I would like to appreciate my supervisor Guy COURBEBAISSE for guiding me well throughout the research work, including the title selection and the result finding. His immense knowledge, motivation and patience always motivate me to complete research work. Without his help, I could not finish this research work. He is my mentor and a better advisor for my doctorate study beyond the imagination.

Apart from my Supervisor, I would like to appreciate Yu CHEN, Laurent NAVARRO, and Romain NOEL for giving encouragement and sharing insightful suggestions. They all play crucial roles in polishing my research writing skills.

I am also pleased to thank Patrick CLARYSSE and Mathilde GI- AGALONE, who made it easier for me to visit research institutes and laboratory and gave an opportunity to become a member of their teams. It is impossible to conduct this research without their precious support. They all really mean a lot to me.

I also would like to remember my fellow labmates for the fun-time we spent together, precious experience when we cooperate with each other to complete tasks before deadlines and discussion problems. And I feel fairly happy to work along with these dear friends from CREATIS: Mathilde Giacalone, Pierre-Antoine Ganaye, Sarah Leclerc, Anchen Chai, Noelie Debs, Yunyun Sun, Bingqing Xie, Pei Niu, Yuemeng Feng, and Hoai-Thu Nguyen. Thanks for your inspirations and help for my research, the Monday and Friday cake and the "soire", especially for all the moments that we shared together.

Finally, I would like to thank my wife Bowen ZHNAG and my family for their continuous support and priceless encourage throughout my thesis.

Synthèse

La segmentation d'images comme méthode de post-traitement est une étape importante dans de nombreux domaines de recherche tels que l'imagerie médicale, la vision par ordinateur, la biologie... L'objectif de ce post-traitement est de prélever une (ou des) région(s) d'intérêt (RDI) dans une image (2D - composée de pixels) ou dans des données volumétriques (3D - composée de voxels). Cette opération est toujours un défi parce que la variété des images à segmenter et des dispositifs d'imagerie, ne cesse d'évoluer. En définitive la motivation principale de cette thèse est l'élaboration d'une méthode de segmentation d'image 3D généralisée efficace. Un modèle original de segmentation multi-seuils basé sur l'algorithme des k-moyennes couplé au calcul d'un histogramme 2D et sur la méthode de Boltzmann sur réseau dans une version 'réaction-diffusion' adaptée à la segmentation d'image, est ici proposé comme candidat à la problématique posée. Pour présenter les développements théoriques et les résultats des calculs numériques obtenus pendant la durée de la thèse, le manuscrit est organisée comme suit.

Après le chapitre 1 qui donne l'état de l'art sur les travaux scientifiques portant à la fois sur le rendu volumique direct [Drebin et al., 1988] et la méthode de Boltzmann sur réseau [McNamara and Zanetti, 1988], le chapitre 2 présente les automates cellulaires de type gaz sur réseau (Lattice Gas Cellular Automata - LGCA) précurseurs de la méthode de Boltzmann sur réseau, tels que le modèle Hardy-Pomeau-Pazzis (HPP) [Raabe, 2004] et le modèle Frisch-Hasslacher-Pomeau (FHP) [Frisch et al., 1986], ce dernier permettant de résoudre les équations de Navier-Stokes utilisées dans le domaine de la simulation numérique en mécanique des fluides. Émerge de ces travaux, la méthode de Boltzmann sur réseau qui est formulée en terme de distributions de particules alors que les gaz sur réseau ne considèrent que la propagation et la collision de particules sur réseaux réguliers. L'effet attendu est notamment la réduction du bruit de calcul numérique. Différentes versions de la méthode de Boltzmann sur réseau ont été développées en une dimension (1D), en deux dimensions (2D) et en trois dimensions (3D) suivant

des distributions de vitesses variées, dont le nombre varie en fonction des propriétés d'anisotropie escomptées notamment dans le domaine du traitement d'images. La méthode de de Boltzmann sur réseau 4D n'est pas abordé dans ce manuscrit [Wang et al., 2016].

Le chapitre 3 introduit ensuite la méthode de Boltzmann sur réseau dédiée au traitement d'image [Jade], dans laquelle la fonction de collision est formulée suivant une équation de diffusion pour effectuer des opérations de lissage et de filtrage. Dans ce contexte, l'équation de diffusion est résolue via la méthode de Boltzmann sur réseau réalisant le lissage et le filtrage d'images 2D et 3D. Dans un deuxième temps, une fonction de diffusion anisotrope est implémentée dans la formulation de la fonction de collision de la méthode de Boltzmann sur réseau pour la segmentation d'images 2D et 3D.

Le chapitre 4 présente la couplage de la méthode de Boltzmann sur réseau et de la technique du rendu de volume direct (méthode de partitionnement ou clustering, basée sur un histogramme 2D). La stratégie employée consiste à classer des séquences d'images en considérant à la fois la valeur de niveau de gris des voxels et à la fois le module des gradients de gris calculé sur chaque voxel en fonction des niveaux de gris des voxels voisins, ce qui pourrait être utilisée comme deuxième propriété pour la segmentation.

Le chapitre 5 présente le développement de la méthode décrite au chapitre 4 et donne un aperçu du cadre proposé pour la segmentation multi-seuils 3D via la méthode de Boltzmann sur réseau. La méthode à seuils-multiples proposée peut effectuer une classification plus sophistiquée des données volumétriques et ainsi produire des objets volumétriques mieux partitionnés. Cela permet à l'algorithme de localiser de manière flexible des groupes de sous-volumes ayant des caractéristiques communes; par exemple dans le cas de l'application médicale traitant d'anévrismes cérébraux (un des domaines d'applications abordés dans la thèse), les groupes de sous-volumes vont correspondre à des catégories de tissus vivants rencontrés dans la cavité crânienne. La méthode de Boltzmann de segmentation multi-seuils est ensuite testée pour vérifier son efficacité sur des données volumétriques ayant une composition complexe et ceci pour des grands volumes de données. Pour valider l'exactitude de cette nouvelle approche associant plusieurs outils numériques en rendu volumique et en calcul scientifique, plusieurs sources de données émanant de bibliothèques d'images de référence et de différentes applications médicales telles que celle des anévrismes cérébraux traités par stent (prothèse endovasculaire) sont analysées. Également les résultats obtenus par la méthode de Boltzmann sur réseau

multi-seuils sont comparés avec les méthodes classiques de segmentation. Les performances de cette méthode originale sont évaluées suivant des critères d'évaluation basés sur le calcul du coefficient de similarité de Dice (DSC) [Sørensen, 1948], d'une différence de volume relatif (RVD) [Altman and Bland, 1983] et de la distance de Hausdorff [Rockafellar and Wets, 2009]. Ensuite, la méthode de Boltzmann sur réseau est proposée dans une formulation multivariée de la fonction de collision, conduisant à une nouvelle formulation de partitionnement de volumes de données 3D. Cette formulation permet de prendre en compte des paramètres caractéristiques inusités tels que courbure, opérateur Laplacien... qui sont implémentés dans la fonction de collision proposée.

Le chapitre 6 étudie la mise en œuvre de l'algorithme proposé au chapitre 5 sur carte graphique (GPU) et d'un algorithme de calcul parallèle de la méthode de Boltzmann multi-seuils. Le programme de déploiement sur carte GPU est implémenté principalement en langages python et CUDA (NVidia-10.0), qui permettent d'améliorer sensiblement les performances de calcul.

Le chapitre 7 conclut la thèse et propose des pistes de futurs travaux prometteurs.

Introduction

Dans le domaine de la segmentation d'images, les équations aux dérivées partielles jouent un rôle important dans l'opération de segmentation d'images. La première utilisation d'une fonction de diffusion permettant de réduire le bruit dans une image est celle de Koenderink [Koenderink, 1984]. Partant de ce concept, la méthode de Boltzmann sur réseau (Lattice Boltzmann method - LBM) est ici utilisée en tant que méthode numérique pour résoudre des équations aux dérivées partielles (EDP) à l'échelle mésoscopique, et qui présente l'avantage d'être adaptée naturellement à la parallélisation en comparaison d'autres méthodes de résolutions des EDP. Par ailleurs, les codes de segmentation sont de plus en plus ancrés au système informatique sur lequel ils sont implémentés. La méthode de Boltzmann sur réseau (Lattice Boltzmann method - LBM) illustre bien cette évolution et a prouvé sa capacité à simuler des comportements d'écoulement de fluides complexes et plus récemment à traiter des images médicales avec des temps de calcul optimisés. Également, les implémentions de codes parallèles sont directes en raison des opérations locales effectuées sur chaque noeud du réseau régulier sur lequel des distributions de particules se propagent et entrent en collision et ceci en fonction du

temps. En effet sur un domaine partitionné en plusieurs sous-domaines, chaque partition peut-être implémentée sur cartes graphiques ou processeurs graphiques (Graphical Processing Unit en anglais - GPU), pour du calcul parallèle et seules les distributions de particules en bordures de ces partitions sont à propager, ce qui se traduit par une optimisation des temps de calcul. En conséquence, un code de segmentation optimisé a été mis en œuvre sur la base de l'algorithme des k-moyennes dont les conditions initiales sont données via un histogramme 2D et la méthode de Boltzmann sur réseau dans une version où la fonction de collision est construite pour résoudre une EDP de réaction-diffusion adaptée pour prendre en compte les seuils déterminés via la méthodes des k-moyennes . Cette méthode originale est ici appliquée pour réaliser la segmentation de séquences d'images médicales traitant d'anévrismes cérébraux.

Dans des travaux récents de Yan[Wang et al., 2016], la méthode de Boltzmann sur réseau a été utilisée pour segmenter la lumière et le thrombus d'anévrismes partiellement thrombosés, débouchant sur des résultats sensiblement meilleurs que ceux obtenus par les méthodes classiques (Chen-Vase, Otsu...). Il faut noter qu'il s'agit d'une méthode dans laquelle la méthode de Otsu calcule un seuil influant sur un terme de diffusion de la fonction de collision. Dans le continuité des travaux de Yan Wang et Yu Chen, l'originalité de cette thèse réside dans la création d'une méthode de segmentation à seuils multiples dont l'implémentation sur carte graphique conduit à des temps de calcul réduits d'un facteur supérieur à cent.

La segmentation d'images (2D) ou de données volumétriques (3D) en imagerie médicale nous a conduit à élaborer une méthode de segmentation d'images 3D couplant une technique de rendu volumique direct [Max, 1995] et la méthode de Boltzmann sur réseau (LBM). La segmentation de séquences d'images médicales basée sur le rendu de données volumétriques par la méthode de rendu volumique qui projette des données 3D sur un plan 2D, devient une technique incontournable. Le cœur de cette technique est basé sur la conception d'une fonction de transfert, qui consiste à projeter des données volumétriques dans les espaces des couleurs et d'opacité. L'élément clé du rendu volumique est l'utilisation de l'analyse de l'espace de l'image considéré et de l'analyse de l'espace des données, facilitant ainsi le rendu, qui peut par exemple conduire à dissocier différents tissus dans des séquences d'imagerie médicale. Sur la base de ce mécanisme, la fonction de transfert peut être divisée sous la forme de deux expressions, l'une centrée sur l'image et l'autre centrée sur les données:

- Dans les algorithmes centrés sur l'image, l'interface utilisateur permet d'interagir de manière directe sur le résultat du rendu afin de modifier les propriétés optiques, mais les interactions prennent du temps et sont difficiles à régler avec précision.

- Dans les algorithmes centrés sur les données, des fonctions de données sont introduites. Cela améliore la capacité de reconnaissance des caractéristiques de la fonction de transfert en étendant ou en manipulant l'espace des caractéristiques telles que la visibilité et la divergence de l'information,

Cependant, les travaux antérieurs sont difficiles à optimiser et généralement ils ne peuvent s'appliquer qu'à des images liées à une application spécifique. Le choix d'une équation aux dérivées partielles (EDP) joue un rôle important dans la segmentation d'images. La méthode de Boltzmann sur réseau en tant qu'approche numérique pour résoudre l'EDP à l'échelle mésoscopique, est une méthode d'ordre inférieur qui présente l'avantage intrinsèque de la parallélisation par rapport aux autres solutions résolvant une EDP. La relation entre les codes de segmentation et le matériel des systèmes informatiques est de plus en plus intégrée. La méthode de Boltzmann sur réseau illustre bien cette évolution ; La méthode de Boltzmann sur réseau a prouvé sa capacité à simuler des comportements d'écoulement de fluides complexes et plus récemment à traiter des images médicales avec un temps de calcul optimisé. En fait, l'implémentation du code parallèle est directe car la méthode de Boltzmann sur réseau est une méthode travaillant à l'échelle mésoscopique (entre échelle microscopique et macroscopique) qui utilise la valeur de niveau de gris en chaque noeud du réseau 3D lors de la phase de propagation.

Dans le domaine de la segmentation de séquences d'images médicales, le rendu de données volumétriques par la méthode de rendu volumique, qui projette des données 3D sur des plans 2D, devient une technique incontournable. Le cœur de cette technique est basé sur la conception d'une fonction de transfert (FT) et la projection les données volumétriques suivant des espaces de couleurs et d'opacité. L'élément clé du rendu volumique est l'utilisation simultanée de l'espace d'image et de l'espace des données pour faciliter le rendu, permettant par exemple de caractériser les différents tissus représentés dans les images médicales. Sur la base de ce mécanisme, la conception de la fonction de transfert peut prendre deux expressions, l'une centrée sur l'image et l'autre centrée sur les données. Les méthodes centrées sur les données extraient diverses caractéristiques des données de volume et attribuent des propriétés optiques en fonction de celles-ci. Les méthodes centrées sur l'image sont généralement plus intuitives et se basent directement sur le rendu de l'image la plus attrayante dans l'espace des rendus.

Méthode de Boltzmann sur réseau dédiée au traitement d'images

Méthode de Boltzmann sur réseau et lissage d'images

En 2008, Yu Chen a proposé d'utiliser la LBM pour le lissage d'image [Chen et al., 2008], et il prouve que l'équation d'évolution de la LBM est un processus assimilable à un processus de diffusion directe par expansion Chapman-Enskog, qui atténue les effets de marches d'escalier. Le modèle anisotrope de diffusion basé sur LBM est présenté dans l'Eq.1:

$$\begin{aligned} f_i(\vec{r}+\Delta r, t+\Delta t) &= g_i(\vec{r})\{f_i(\vec{r})\frac{1}{\tau}[f_i^{eq}(\vec{r},t) - f_i(\vec{r},t)] \\ &+ (1-g_i(\vec{r}))\{f_i(\vec{r}+\Delta r,t) + \frac{1}{\tau}[f_i^{eq}(\vec{r}+\Delta r,t) - f_i(\vec{r}+\Delta r,t)]\} \end{aligned} \tag{1}$$

où f_i est une fonction de distribution de particules et correspond ici au niveau de gris en chaque nœud lié à un pixel de l'image traitée. $f_i(\vec{r}+\Delta r, t+\Delta t)$ est la fonction de distribution des particules au nœud $\vec{r}+\Delta r$, et au temps $t+\Delta t$, Δr et Δt désignent respectivement l'espacement du réseau et le pas de temps. f_i^{eq} est la fonction de distribution d'équilibre. L'introduction d'une membrane semi-perméable qui agit comme un filtre selectif g_i, permet à certaines particules de se propager à travers la membrane, ce qui en fait une diffusion anisotrope [Chen et al., 2008]. g_i est ici une probabilité de passer à travers la membrane, c'est-à-dire que l'état du nœud à la prochaine fois est égal à la somme des les particules ont rebondi à partir du membrane et les particules voisines voyageant à travers le membrane. Un modèle D2Q9 à deux dimensions et neuf directions de propagations auxquelles sont associées neuf vitesses, est choisi comme l'indique l'équation d'évolution dans la Fig.1.

Des séquences d'images obtenues en angiographie par tomodensitométrie (Angioscanner - AngioCT ou Computed Tomography Angiography - CTA) sont utilisées pour l'analyse d'anévrismes. Les résultats obtenus par la méthode de Boltzmann sur réseau (LBM) sont comparés avec les résultats obtenus avec la méthode de diffusion anisotrope classique aussi appelée méthode de diffusion Perona–Malik (Méthode P-M). Le résultat donné Fig.2 montre que la méthode proposée peut filtrer des images et en même temps accentuer les transitions de niveaux de gris. Cependant, la fonction de diffusion anisotrope P-M ou modèle P-M, met en évi-

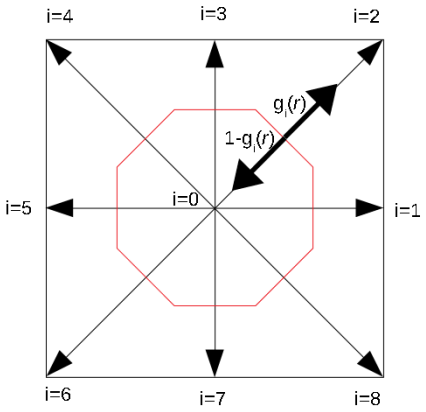

Figure 1: LBM D2Q9 lattice.

dence un effet d'escalier alors qu'il a disparu avec la méthode de Boltzmann proposée, comme l'illustre la figure 2[3][4].

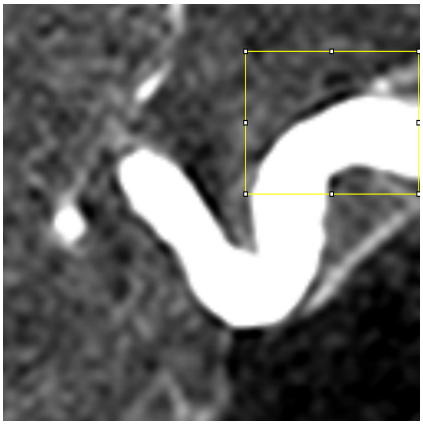

(1) Résultat méthode P-M

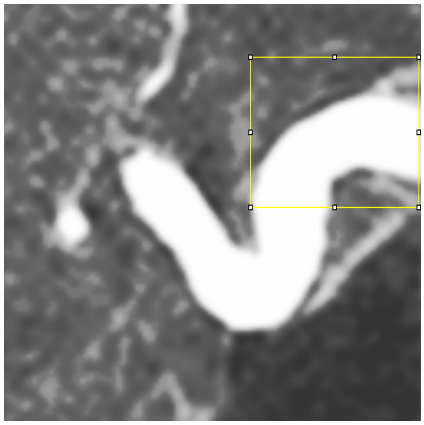

(2) Résultat lissage via LBM

(3) Grossissement de la figure (1)

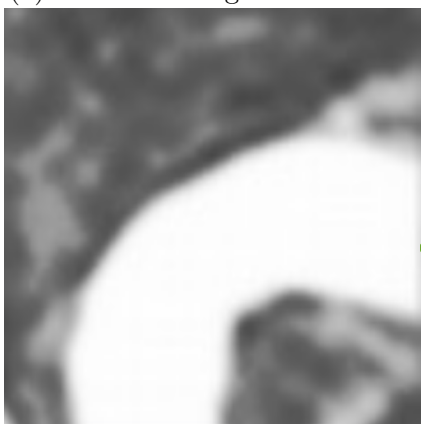

(4) Grossissement de la figure (2)

Figure 2: Effet d'escalier estompé via la méthode de Boltzmann sur réseau.

Fonction de diffusion anisotrope LBM pour la segmentation d'image

Yu Chen [Chen et al., 2014] a proposé une segmentation de l'image basée sur la fonction de diffusion anisotrope via la LBM. Il utilise le même modèle D2Q9 que celui illustré à la Fig.1. Afin d'améliorer l'image, une source de diffusion $a\Delta t[T-\rho(\rho(\vec{r})]$ est ajoutée au modèle, et l'équation d'évolution LBM s'écrit alors:

$$\begin{aligned} f_i(\vec{r}+\Delta r, t+\Delta t) &= g_i(\vec{r})\{f_i(\vec{r},t)+\frac{1}{\tau}[f_i^{eq}(\vec{r},t)-f_i(\vec{r},t)]\} \\ &+ (1-g_i(\vec{r}))\{f_i(\vec{r}+\Delta r,t)+\frac{1}{\tau}[f_i^{eq}(\vec{r}+\Delta r,t)-f_i(\vec{r}+\Delta r,t)]\} \\ &+ a\Delta t[T-\rho(\vec{r})] \end{aligned} \tag{2}$$

où f_i est une fonction de distribution de particules et correspond ici au niveau de gris en chaque nœud lié à un pixel de l'image traitée. $f_i(\vec{r}+\Delta r, t+\Delta t)$ est la fonction de distribution des particules au nœud $\vec{r}+\Delta r$, et au temps $t+\Delta t$, Δr et Δt désignent respectivement l'espacement du réseau et le pas de temps. f_i^{eq} est la fonction de distribution d'équilibre.

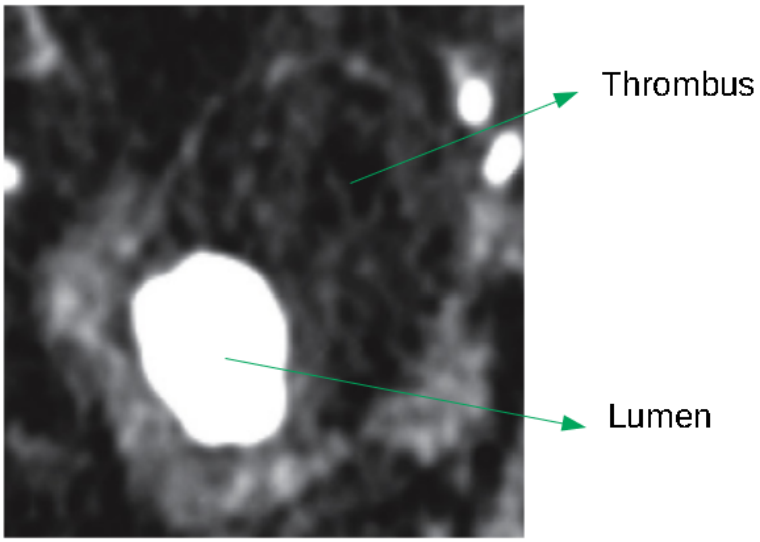

Figure 3: Lumière et Thrombus de l'anévrisme cérébral.

Dans cette équation Δt correspond à un pas de temps, Δr à un pas spatial permettant de parcourir la distance Δr pendant Δt, et T à un seuil de segmentation, a est une constante. Cette équation a été proposée par Yan Wang qui permet de segmenter la lumière de l'anévrisme issue de l'image originale (Fig.3) en utilisant la méthode de Otsu [Wang et al., 2016].

Puis en 2014, Yu Chen a proposé la méthode LBGM (LBM Geodesic active contour method) dans laquelle la fonction d'évolution GAC du LBM est résolue [Chen et al., 2014] pour segmenter le thrombus d'anévrismes cérébraux en 3D.

Contributions

En raison de la complexité des images CTA (Computed Tomography Angiography) et du temps nécessaire à la segmentation des images médicales résultant des méthodes actuelles, cette thèse propose une solution originale basée sur la méthode de Boltzmann en réseau dédiée au traitement d' images. Pour pallier ce défaut, une version originale de la méthode de Boltzmann sur réseau est proposée dans la continuité des recherches de Chen [Chen, 2009].

Une stratégie originale de segmentation multi-seuils via la méthode de Boltzmann est proposée et appliquée à des données 2D et 3D. L'élaboration d'une fonction de collision originale couplée à un algorithme des k-moyennes réalisant une division en "K" partitions ("clusters") des niveaux de gris de l'image considérée, permet une segmentation efficace à seuils multiples. La précision et l'efficacité de la solution proposée ont été validées sur des images de références et sur des séquences d'imagerie médicale traitant d'anévrismes cérébraux.

Dans ce dernier cas d'applications, l'imagerie médicale apporte une contribution essentielle à la détection et à l'analyse de l'anévrisme cérébral de patients. Dans ce contexte, l'angiographie par tomodensitométrie (CTA) joue un rôle crucial dans le diagnostic et le suivi des patients chez qui un anévrisme cérébral a été détecté. Les anévrismes étudiés ont été enregistrés sur 464 coupes avec un CTA scan 3D (Fig. 4) et sont issus de la base de données du projet Thrombus (FP7-269966). Un anévrisme cérébral est un trouble vasculaire assimilable à une petite hernie due à un affaiblissement de la paroi d'un vaisseau sanguin et se produit notamment à la bifurcation de vaisseaux sanguins. Un anévrisme peut se rompre, entraînant parfois une hémorragie sous-arachnoidienne ayant pour conséquence des taux de mortalité élevés. De nombreux projets portent sur le traitement des anévrismes cérébraux et leur évolution après un traitement endovasculaire (traitement par stent). Aussi un besoin spécifique d'analyse de formation d'un thrombus conduisant à la guérison s'est fait sentir. Dans ce cadre, les techniques de traitement d'images apportent des moyens essentiels pour le diagnostic, le traitement et le suivi des patients.

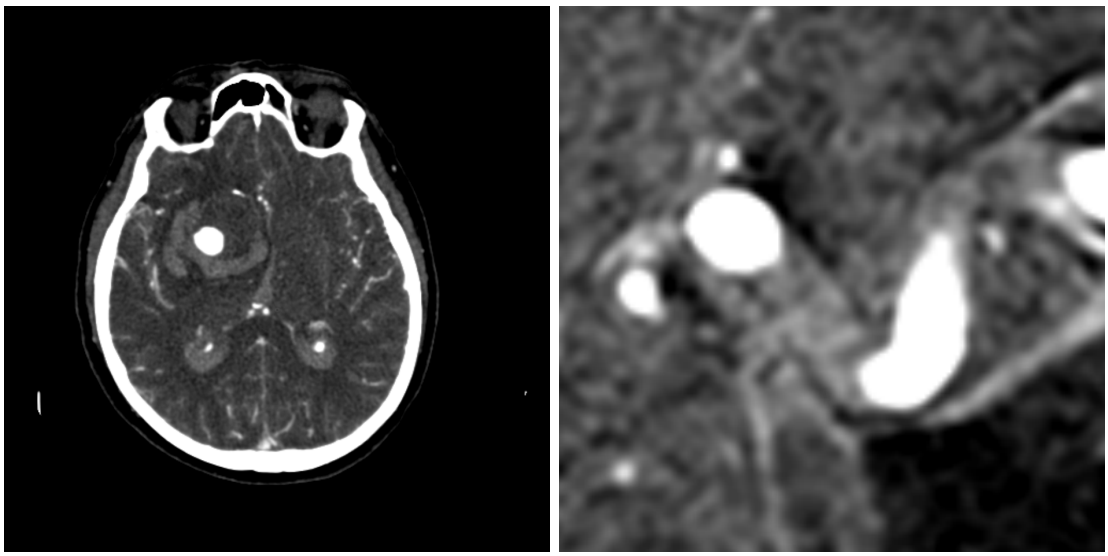

Figure 4: CTA de l'anévrisme cérébral: (1) CTA du cerveau, (2) CTA d'anévrisme.

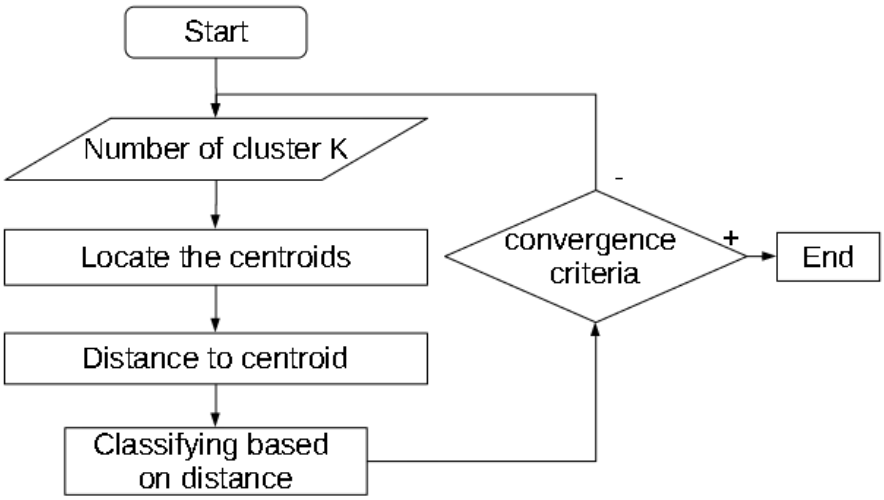

Figure 5: Pipeline d'algorithmes k-moyennes.

Dans un premier temps, nous allons construire une méthode avec une seuil de segmentation et nous étendrons ensuite le modèle à la segmentation à plusieurs seuils permettant un partitionnement de données 2D et 3D. Cette méthode est basée sur le couplage des K-moyennes avec l'histogramme 2D et la méthode de Boltzmann sur réseau. La méthode de partitionnement des k-moyennes permet de calculer les seuils pour la classification de données volumiques. Le pipeline de partitionnement basé sur les k moyennes de base est illustré à la Fig.5 et dans

lequel l'Eq.3 correspond à la minimisation de la distance intra-clusters.

$$\arg\min_{C} \sum_{j=1}^{k} \sum_{\rho \in C_j} |\rho - m_j|^2 , T_j = m_j \tag{3}$$

où ρ est la valeur en niveaux de gris de l'ensemble de données de volume ; m_j est la valeur moyenne de la classe T_j. (ρ et m_j sont deux variables multidimensionnelles). T_j sont les seuils de partitionnement.

La Fig.6 présente le pipeline itératif construit qui couple la méthode de Boltzmann sur réseau et la méthode de partitionnement à k-moyennes via un histogramme 2D IGM (2D Intensity-Gradient Magnitude histogram) permettant la segmentation d'images médicales avec un gain de temps de calcul sensible.

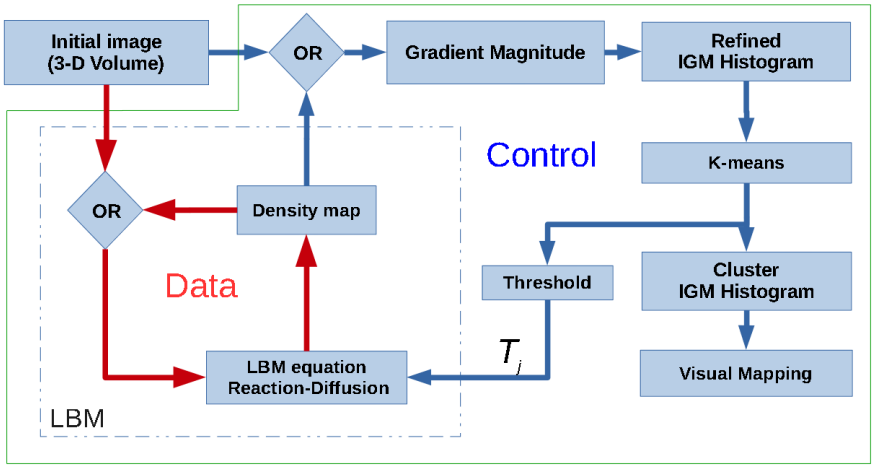

Figure 6: Méthode de couplage de la méthode de Boltzmann sur réseau et de la méthode de partitionnement par k-moyennes.

Initialement, avec l'ensemble des données sur le volume, la valeur du niveau de gris de chaque pixel est recueillie, et le gradient est calculé pour chaque voxel ou pixel avec la fonction de gradient dans l'Eq.4:

$$\bigtriangledown f(x_0, x_1, ..., x_n) = (\frac{\partial f}{\partial x_0}, ..., \frac{\partial f}{\partial x_j}, ..., \frac{\partial f}{\partial x_n}) \tag{4}$$

dans l'algorithme proposé, la norme du vecteur gradient est calculé via Eq.5:

$$|\bigtriangledown f| = \sqrt{(\frac{\partial f}{\partial x_0})^2 + ... + (\frac{\partial f}{\partial x_j})^2 + (\frac{\partial f}{\partial x_n})^2}. \tag{5}$$

La construction de l'histogramme 2D IGM est réalisée à partir de deux ensem-

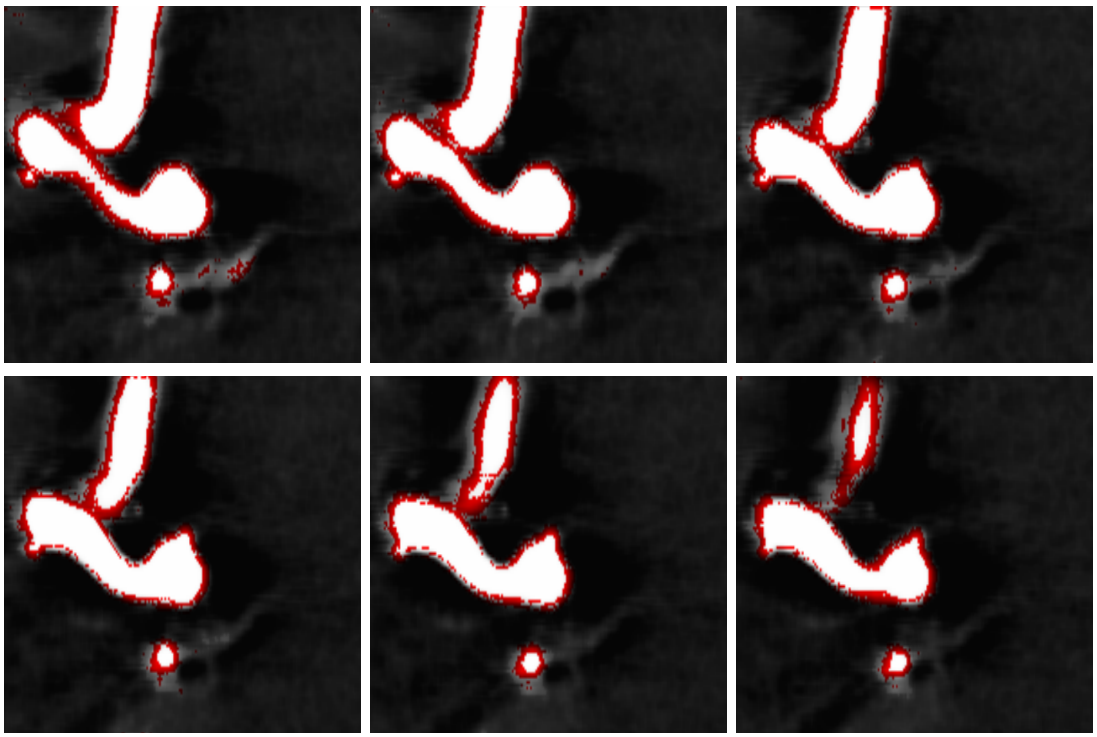

Figure 7: Résultat de segmentation CTA de l'anévrisme cérébral du premier patient, qui prend six coupes d'anévrisme cérébral comme exemples de segmentation 2D. La partie rouge correspond aux frontières vasculaires, la partie blanche est l'intérieur du vaisseau. Les parties noires et grises sont les autres tissus.

bles de données synthétiques, que sont le gradient et la valeur de niveau de gris. Ensuite, avec la carte de densité produite à chaque itération LBM, l'algorithme de partitionnement à k-moyennes regroupe les classes du volume, puis calcule les seuils optimaux dans le but de différencier différents tissus vivants rencontrés dans le domaine médical. Ces seuils sont adressés au bloc LBM de la Fig. 6 qui est implémenté pour résoudre une équation de réaction-diffusion. L'histogramme IGM 2D est calculé à chaque itération pour obtenir le seuil optimal. Le résultat de la segmentation CTA 2D est représenté Fig.7 et Fig.8 [GE et al., 2017]. Les contours rouges se superposent à l'image originale, et correspondent à la limite du vaisseau. L'algorithme de segmentation proposé dans cette section est appliqué à deux séquences d'images médicales CTA respectivement de 131 et 128 coupes et dont la taille des images correspond aux régions d'intérêt pertinentes pour l'analyse des données.

Nous avons appliqué l'algorithme à toute la séquence de l'anévrisme cérébral. Le résultat montre que la méthode proposée est comparable à la méthode de partitionnement par K-moyennes. Les Fig.9 et Fig.10 affichent les résultats du

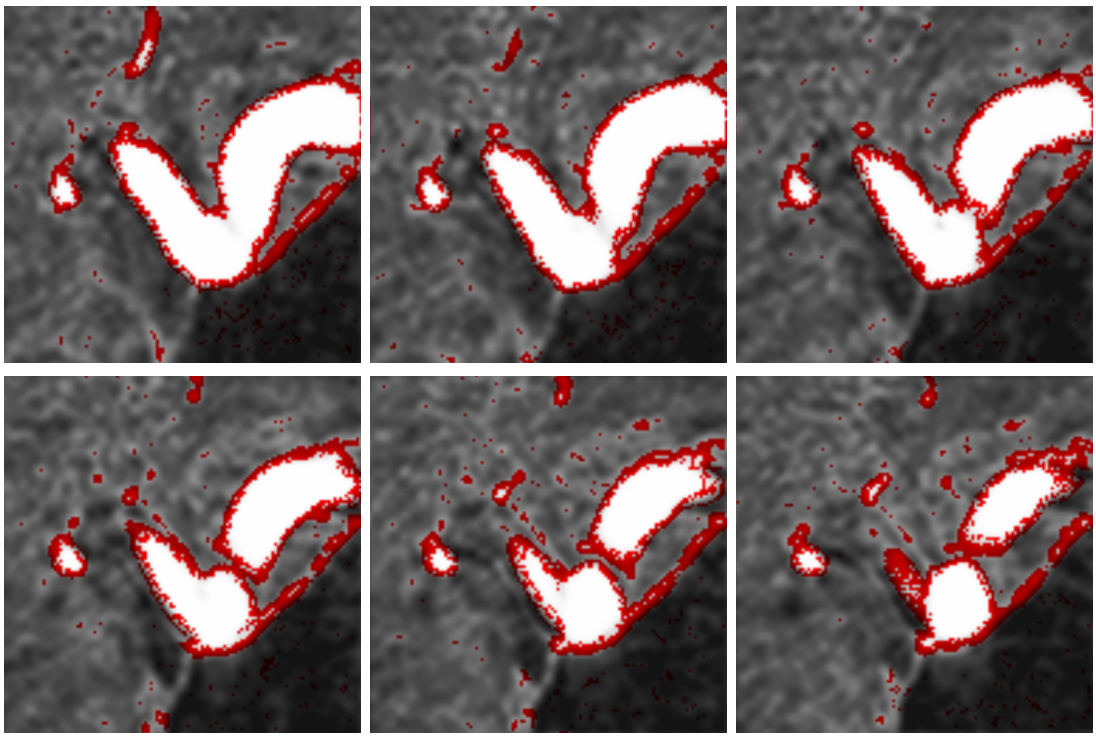

Figure 8: Résultat de la segmentation CTA de l'anévrisme cérébral du deuxième patient, qui prend six coupes d'anévrisme cérébral comme exemples de segmentation 2D. La partie rouge correspond aux frontières vasculaires, la partie blanche est l'intérieur du vaisseau. Les parties noires et grises sont les autres tissus.

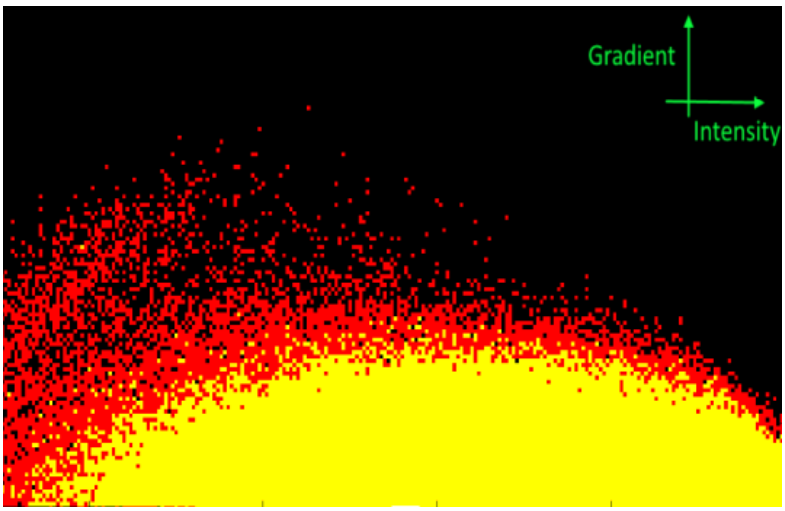

Figure 9: 2D IGM histogramme initial (sans LBM).

calcul de l'histogramme IGM de l'algorithme de partitionnement (sans LBM). On peut voir que l'algorithme K-moyennes partitionne l'IGM en 2 parties, la partie rouge est la limite du vaisseau, la partie jaune est le sang dans les anévrismes cérébraux et les vaisseaux sanguins parents. Fig.11 affiche l'histogramme IGM de la méthode proposée avec LBM. En comparant avec les résultats de la Fig.12, on peut voir que l'ensemble de données est moins sensible au bruit que sans LBM. Les résultats de rendu du volume sont plus discriminants et plus clairs que ceux de la Fig.12. En utilisant le LBM, l'objectif sous-jacent est de mieux révéler les arcs de l'histogramme 2D IGM afin de détecter les différentes natures de tissus vivants dans les images médicales. En utilisant un seuil T issu de K-moyennes, la résolution de l'équation de réaction-diffusion via LBM permet de révéler plusieurs arcs. Dans cet exemple, les arcs jaunes correspondent au sang et les arcs rouges correspondent aux vaisseaux parents.

Conception de la méthode de Boltzmann sur réseau multi-seuils

La méthode construite est basée sur le modèle précédent à un seuil dans laquelle la fonction de collision de la méthode de Boltzmann sur réseau a été réécrite en fonction d'un terme d'extra force dans lequel plusieurs seuils sont déterminés via l'histogramme 2D et la méthodes des K-moyennes. Il en résulte l'équation

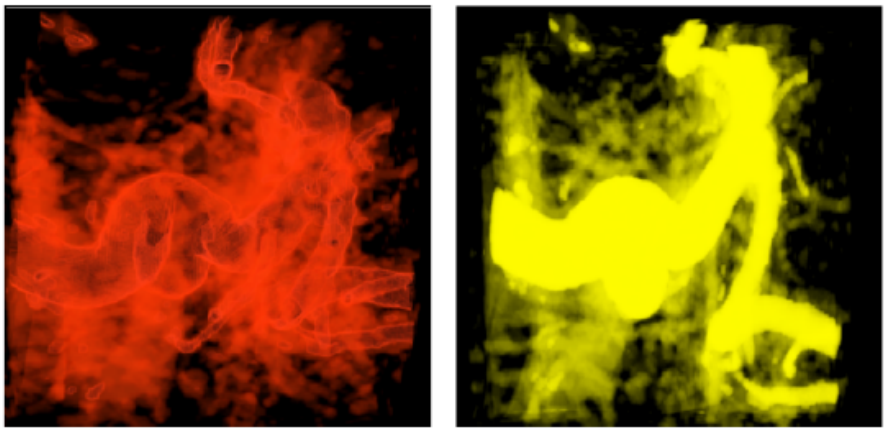

Figure 10: Segmentation résultats: la gauche: vaisseau parent (rouge), la droite: phase sanguine (jaune).

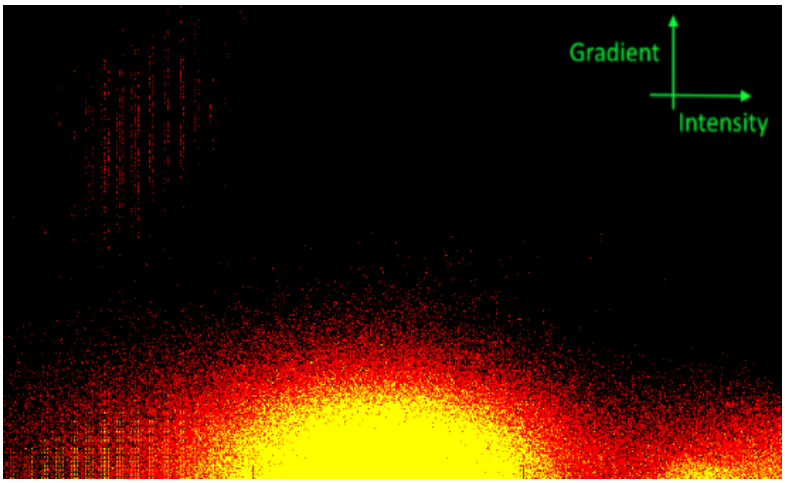

Figure 11: 2D IGM histogramme par la méthode proposée.

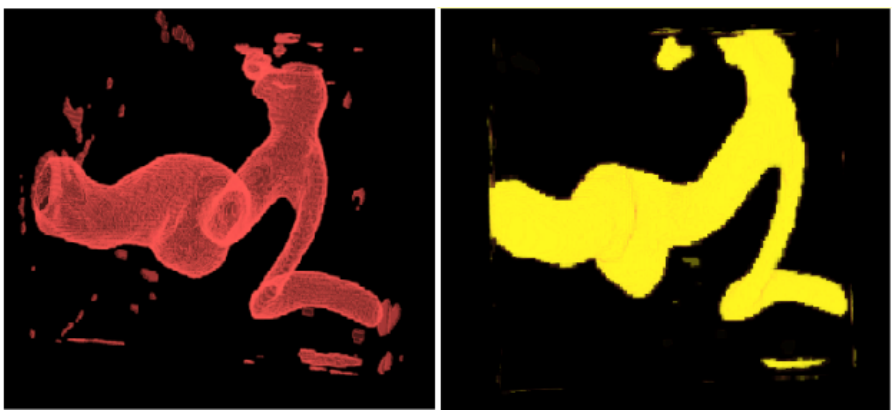

Figure 12: Segmentation par la méthode proposée: la gauche: vaisseau parent (rouge), la droite: phase sanguine (jaune).

d'évolution LBM suivante:

$$f_i(\vec{r}+\Delta r, t+\Delta t) = f_i(\vec{r}+\Delta r, t) + \frac{1}{\tau}[f_i^{eq}(\vec{r}+\Delta r, t) - f_i(\vec{r}+\Delta r, t)] + R(\rho, T_j) \tag{6}$$

où f_i est une fonction de distribution de particules. $f_i(\vec{r}+\Delta r, t+\Delta t)$ est la fonction de distribution des particules au nœud $\vec{r}+\Delta r$, et au temps $t+\Delta t$, Δr et Δt désignent respectivement l'espacement du réseau et le pas de temps. f_i^{eq} est la fonction de distribution d'équilibre. ρ représente la densité et correspond ici au niveau de gris en chaque nœud lié à un pixel de l'image traitée. τ est le temps de relaxation. Dans le chapitre précédent, la méthode de segmentation implémentée avec un seuil n'est pas idéale pour le traitement de séquences d'images complexes. En conséquence la fonction de collision du LBM est proposée dans une version spécifique, où $R(\rho, T_j)$ représente un terme d'extra force supplémentaire (cf. Eq.6) dans le modèle LBM. Dans ce nouvel algorithme, un nouveau terme de collision à plusieurs seuils est proposé suivant l'Eq.7 , T_j étant le critère principal pour réguler ρ.

$$R(\rho, T_j) = \alpha(T_m - \rho), \exists m : |T_m - \rho| = min|T_j - \rho| \tag{7}$$

où T_m est le seuil le plus proche du niveau de gris pour chaque pixel. $\alpha = \frac{2}{1+\frac{1}{1+\nabla\rho}}$ est une fonction non décroissante pour assurer que la procédure de propagation améliore le contraste à la frontière, représentée sur la Fig.13.

Pour obtenir une segmentation automatique sous différentes formes, nous obtenons T_j par l'algorithme de partitionnement par k-moyennes, qui est représentatif des méthodes de partitionnement de fonctions objectives basées sur des prototypes. Le partitionnement par la méthode K-moyennes est ici utilisé. L'algorithme de partitionnement est décrit suivant l'équation 9 [MacQueen, 1967]:

$$\arg\min_{T} \sum_{j=1}^{k} \sum_{\rho \in T_j} |\rho - m_j|^2 , T_j = m_j \tag{8}$$

où p est un voxel de l'ensemble de données de volume ; m_i est la valeur moyenne de la classe T_j. (p et m_i sont deux variables multidimensionnelles). T_j sont les seuils qui sont utilisés comme paramètres de segmentation LBM.

Puis la méthode proposée est comparée avec la méthode de segmentation Chan-Vese dans les Fig.14 à Fig.16. Les premières images sont des images originales, les

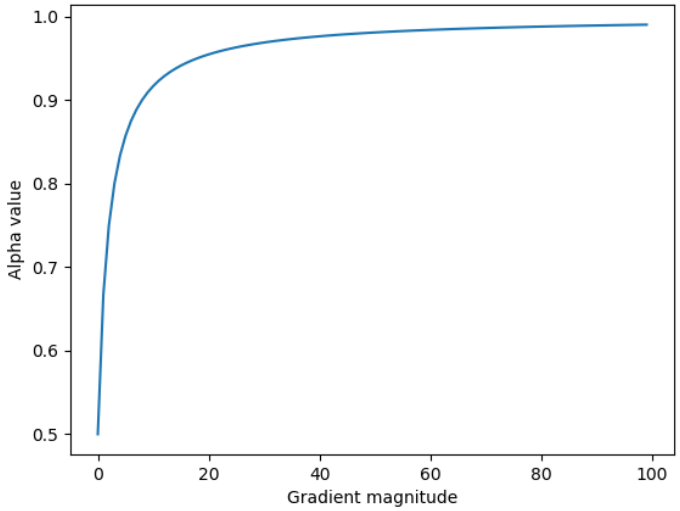

Figure 13: La fonction non-décroissante du paramètre α.

deuxièmes images sont les résultats de segmentation par la méthode de segmentation Chan-Vese, les troisièmes images sont les résultats de la méthode proposée. Les dernières images sont étiquetées à la main.

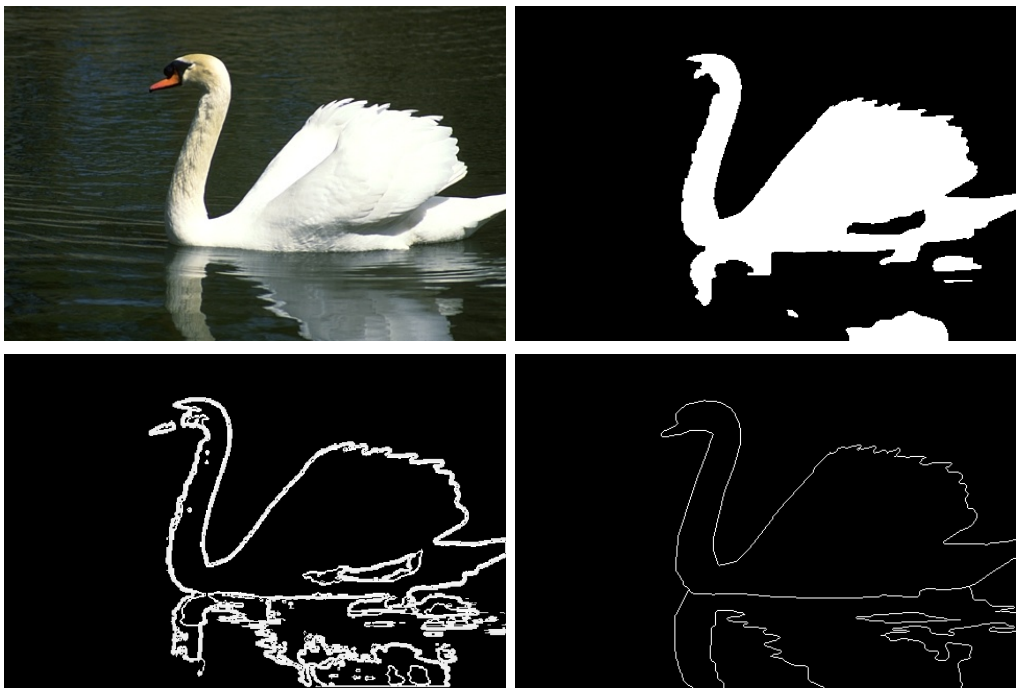

Figure 14: Résultat de segmentation: (1) Image 2D (2) Méthode Chan-Vese (3) Méthode proposée (4) Référence.

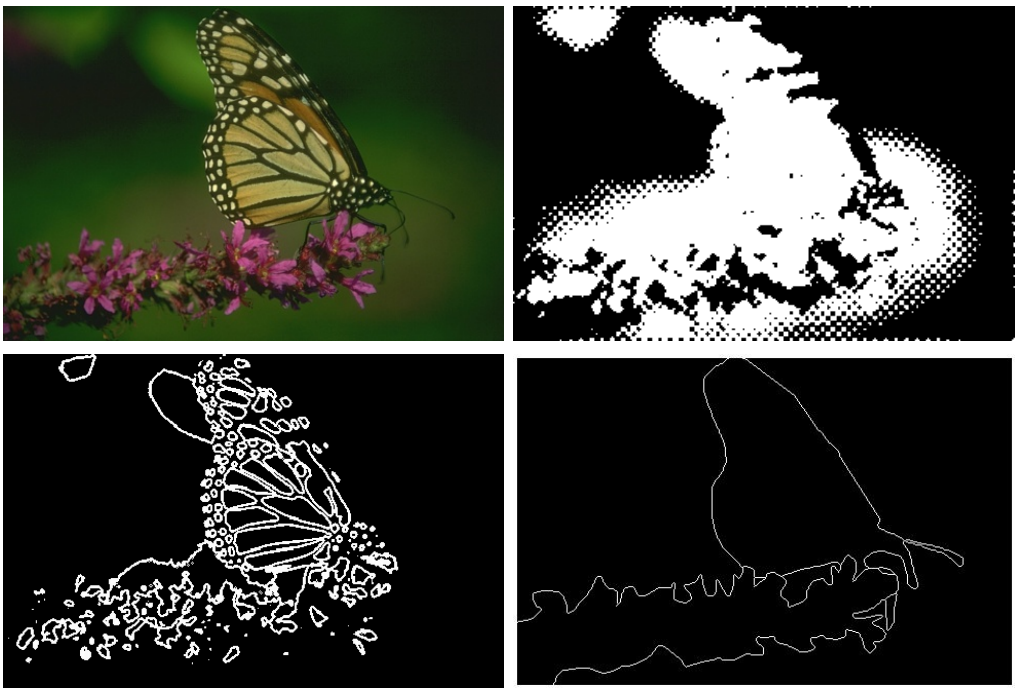

Figure 15: Résultat de segmentation: (1) Image 2D (2) Méthode Chan-Vese (3) Méthode proposée (4) Référence.

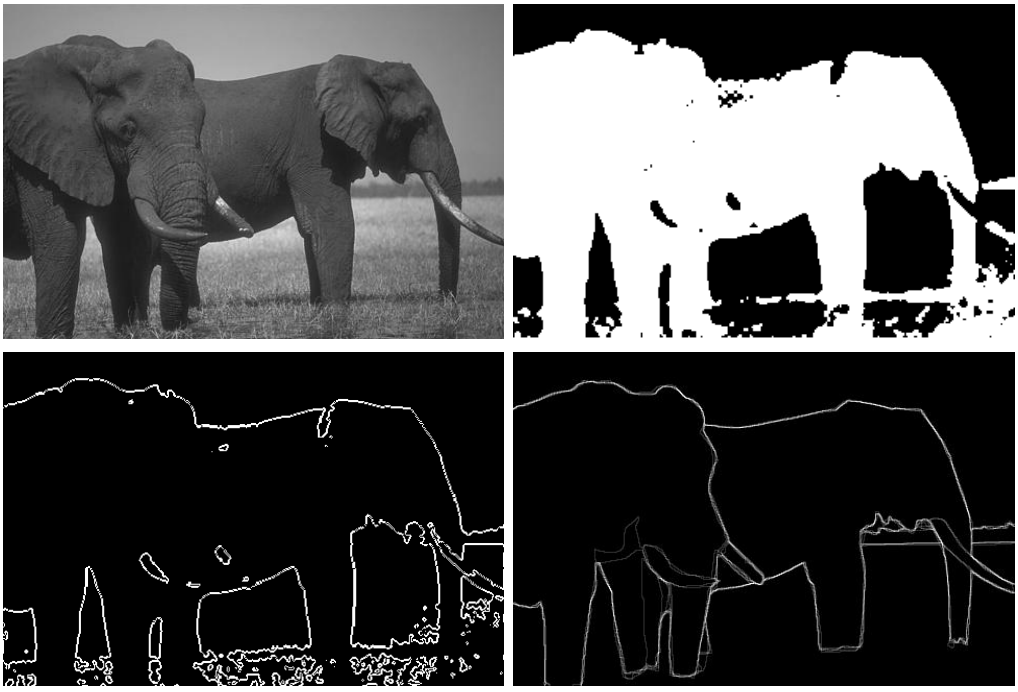

Figure 16: Résultat de segmentation : (1) Image 2D (2) Méthode Chan-Vese (3) Méthode proposée (4) Référence.

Ensuite, la méthode proposée est appliquée sur l'ensemble des données du volume 3D:

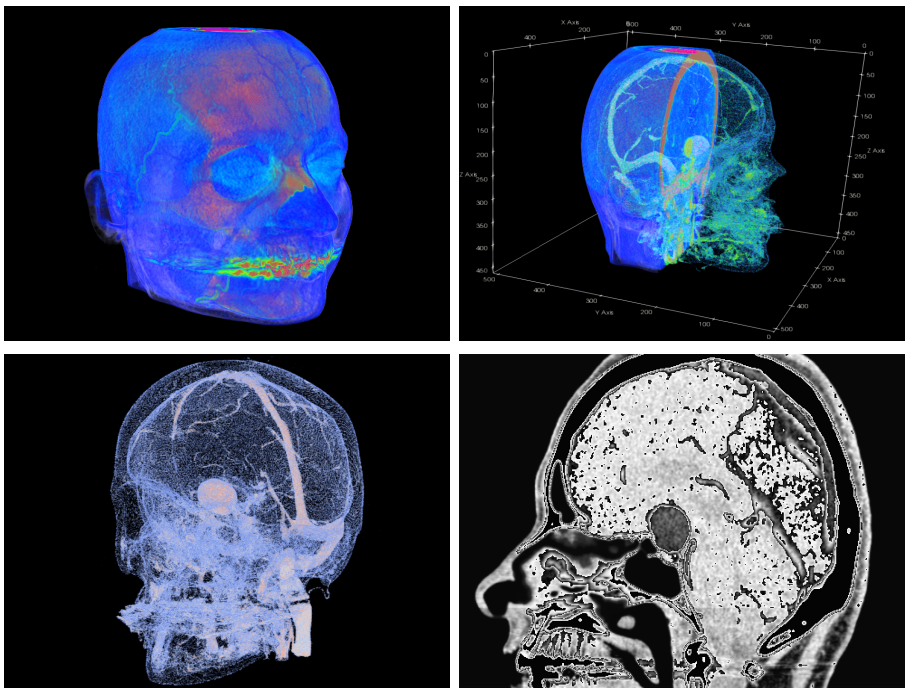

Figure 17: Résultat de la segmentation - crâne segmenté en utilisant $iter = 2, ths = 7$. (1) Données du volume d'origine en vue 3D, (2) données "demi-volume" en vue 3D, (3) résultat de la segmentation en vue 3D, (4) résultat de la segmentation en vue 2D.

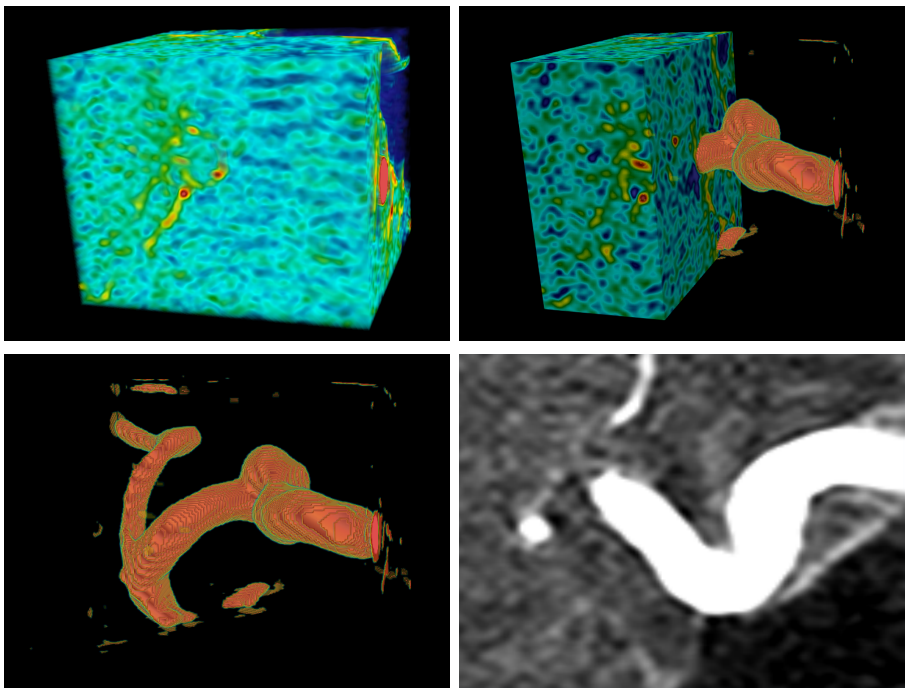

Figure 18: Résultat de la segmentation - anévrisme segmenté en utilisant $iter = 3, ths = 4$.(1) Données du volume d'origine en vue 3D, (2) données "demi-volume" en vue 3D, (3) résultat de la segmentation en vue 3D, (4) résultat de la segmentation en vue 2D.

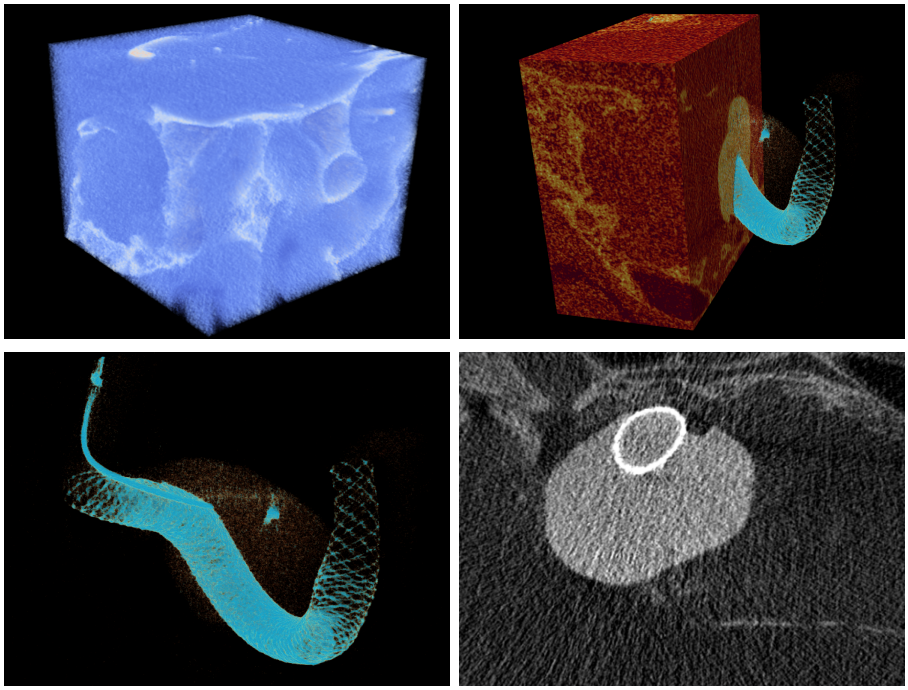

Figure 19: Résultat de la segmentation - anévrisme traité par stent, segmenté en utilisant $iter = 3, ths = 5$. (1) Données du volume d'origine en vue 3D, (2) données "demi-volume" en vue 3D, (3) résultat de la segmentation en vue 3D, (4) résultat de la segmentation en vue 2D.

Méthode de Boltzmann sur réseau multi-variées

L'objet de ce chapitre est d'adapter l'approche élaborée durant la thèse, basée sur la méthode de Boltzmann sur réseau multi-seuils (LBMTM) et de l'appliquer aux traitement de volumes de composition complexe (cas des séquences traitant d'anévrismes cérébraux). Dans l'algorithme LBMTM, la valeur du gradient calculée dans l'histogramme 2D a fortement amélioré le résultat de la segmentation. Nous introduisons donc ici d'autres propriétés potentielles implémentées dans le terme d'extra force de l'Eq.7. Les résultats démontrent qu'en construisant la fonction de collision multi-variée du LBM basée sur le partitionnement ('Clustering'), la capacité de segmenter les données de volume à plusieurs composantes est sensiblement améliorée.

Dans le terme d'extra force, on considère ici la valeur des niveaux de gris et leur courbure, et l'histogramme 2D est maintenant construit à partir de ces deux paramètres. Ensuite, en utilisant l'histogramme 2D pour calculer les centres de gravité pour l'itération suivante, on détermine les seuils jusqu'à ce que la condition de convergence soit atteinte.

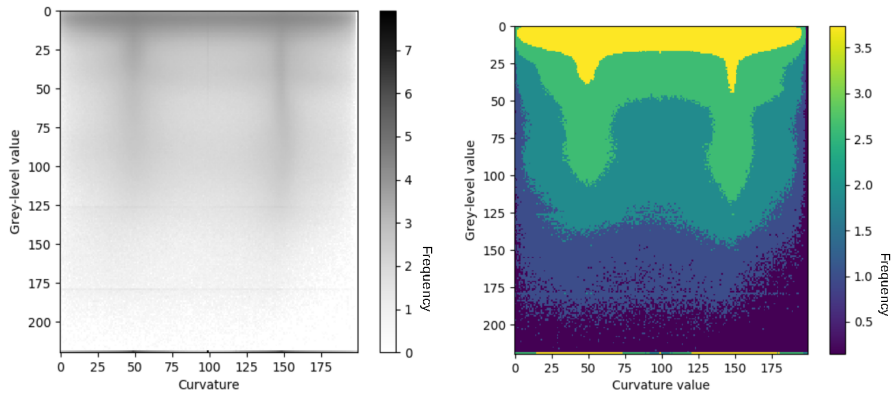

(1) Histogramme 2D 'courbure-niveau de gris' (2) Partitionnement de l'histogramme 2D 'courbure-niveau de gris'

Figure 20: Histogramme 2D multi-varié du crâne.

Nous avons appliqué la méthode proposée à l'ensemble des données sur le volume du crâne, les histogrammes 2D montrant les partitions de différentes couleurs sont illustrés à la Fig.20. L'ensemble du crâne est segmenté en 4 parties et chaque couleur de l'histogramme 2D correspond à des tissus différents tels que vaisseaux sanguins et anévrismes, des tissus mous et l'os du crâne comme montré sur la Fig.21.

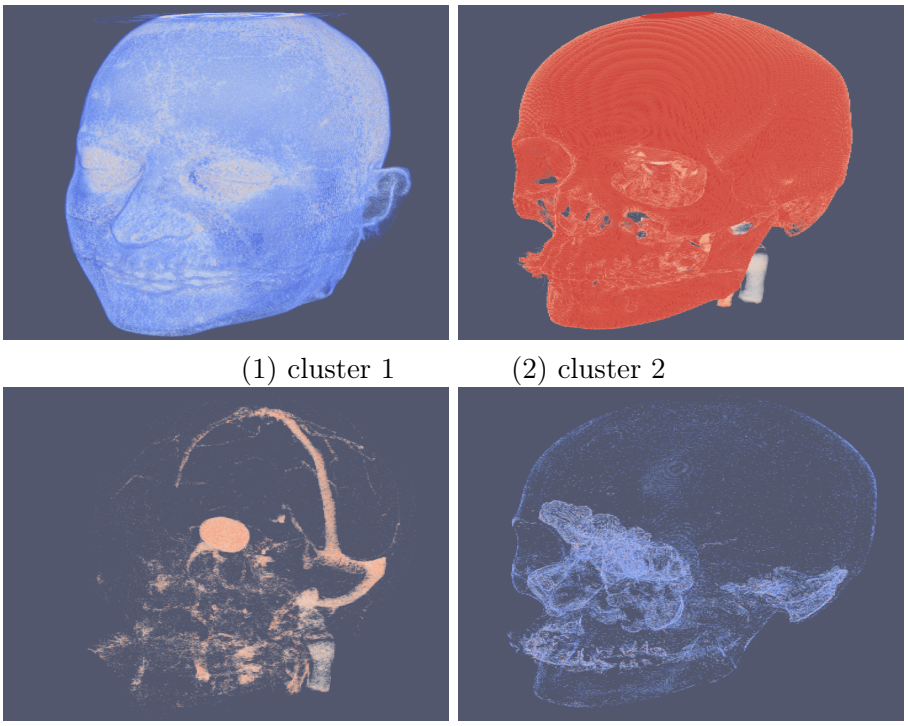

(1) cluster 1 (2) cluster 2

(3) cluster 3 (4) cluster 4

Figure 21: Résultat de la segmentation pour chaque cluster en vue 3D.

Parallélisation de la Méthode de Boltzmann sur réseau multi-seuils

La méthode de Boltzmann sur réseau (Lattice Boltzmann method - LBM) est intrinsèquement adaptée au cacul parallèle et son implementation sur carte GPU est naturelle. La tâche principale exécutée ici sur GPU, consiste à calculer l'évolution de la carte des densités f_i. La carte des densités de distributions est initialisée via la fonction de distribution d'équilibre, et les multi-seuils T_i sont calculés par l'histogramme IGM. Sur le GPU, chaque voxel du volume (lié aux nœuds du réseau) est mappé sur un thread du GPU pour calculer la distribution d'équilibre sur un réseau 3D avec 19 vitesses (D3Q19). Sur chaque thread, $f_i(\vec{r} + \Delta\vec{r}, t + \Delta t)$ est calculé et ensuite les 19 vitesses sont additionnées pour mettre à jour la carte de densité à l'itération suivante. Le calcul se terminera par des critères de convergence ou par un temps d'itération maximum; l'arborescence du code noyau est montrée dans la Fig.22.

```
__global__ void Kernel_3DLBMD3Q19(float *result, float *fin, float *feq)
{
 Obtain the 19 LBM velocities by *fin

 Parameter initialization

 for iterations{

         for 19 velocities{

          Compute the equilibrium distribution function to *feq

          Compute the centroids of gradient *d

          Calculate the distrubution(density map) of next time step
          by proposed collision function(*fin and *feq)

          Add all 19 velocities together to current *result

         if(meet the convergence condition)
         break;
        }
 }
}
```

Figure 22: Pseudo code du noyau sur le GPU.

Dans un premier temps, nous avons implémenté la méthode proposée sur une carte graphique NVIDIA de l'ordinateur portable, la Quadro M1000M avec 4 giga-octets de mémoire GPU et une programmation par python et CUDA-10.0. Par contre la taille mémoire n'est pas suffisante pour traiter des données de grandes

tailles, et nous avons donc implémenté la méthode LBM sur la carte graphique NVIDIA Tesla-P100 avec 16 Go de mémoire (cluster "saki" de CREATIS). Les résultats montrent que pour la segmentation de l'anévrisme de $128 \times 128 \times 128$ voxels par la méthode proposée sous 15 itérations, le coût est 0,25 seconde sur GPU en comparaison des 28,84 secondes réalisées sur CPU. Afin d'évaluer la performance de la méthode proposée, nous avons fait une comparaison qui consiste à exécuter le code proposé sur un thread du CPU i7-6820HQ CPU à 2.70 GHz. Tab.7.1 compare les performances entre CPU et GPU, les résultats montrent que la méthode proposée sur GPU donne un résultat pertinent en termes d'efficacité (réduction des temps de calcul d'un facteur supérieur à 100) et de précision de calcul.

Conclusion et perspectives

La méthode de Boltzmann sur réseau (LBM) est un outil numérique utilisé pour résoudre les équations aux dérivées partielles à l'échelle mésoscopique, permettant ainsi de simuler des phénomènes à l'échelle macroscopique. La thèse porte sur l'étude de la méthode de Boltzmann sur réseau pour la segmentation d'images. Les principales contributions sont les suivantes.

Une méthodologie de segmentation originale créée en couplant une méthode de partitionnement à base d'histogrammes 2D et la méthode de Boltzmann sur réseau 3D est proposée; la stratégie réside dans la réalisation d'une classification de séquences d'images médicales en prenant en compte non seulement la valeur des niveaux de gris des voxels, mais aussi des gradients de niveaux de gris existants entre voxels voisins, et qui dans notre application médicale sont liés à la loi de comportement des tissus vivants à caractériser. Dans le cadre de ce nouveau concept, une séquence d'anévrisme cérébral est traitée dans le but de segmenter la paroi de l'anévrisme et les vaisseaux sanguins parents.

Il résulte de ce travail de thèse la conception originale d'une méthode de Boltzmann sur réseau multi-seuils, dans laquelle la résolution d'une équation de réaction-diffusion à l'échelle mésoscopique est réalisée via l'élaboration d'une fonction de collision multi-seuils. Ceci conduit à l'optimisation d'une méthode de rendu de volume cohérente en rapport avec la complexité des images médicales cérébrales pour l'étude d'anévrismes cérébraux traités entre autres par stent (prothèse endovasculaire). En introduisant l'algorithme de partitionnement et l'histogramme 2D IGM, un nouveau concept est proposé et réside dans l'utilisation de plusieurs

seuils mis à jour au fil des itérations successives du code LBM, conduisant au concept de classification dynamique des séquences d'images médicales.

Annexe: Logiciel et interface utilisateur développés pour implémenter les algorithmes de segmentation

Un logiciel a été développé pour implémenter des méthodes de segmentation d'images basées sur la méthode Boltzmann sur réseau en langage Python et une interface utilisateur est construite pour fixer les paramètres en utilisant la bibliothèque graphique Qt. L'interface graphique du logiciel est scindée en trois parties à savoir, une vue d'ensemble des données de volume 3D, des vues par tranche 2D et un panneau de contrôle des paramètres. Les algorithmes implémentés dans ce logiciel correspondent aux deux méthodes originales que sont la méthode multi-seuils de Boltzmann sur réseau (LBMTM) et la méthode multivariée de Boltzmann sur réseau (LBMVM-courbure). Le logiciel intègre par ailleurs plusieurs algorithmes de segmentation classiques telles que méthode de diffusion, la méthode de partitionnement en k-moyennes , la méthode de partitionnement basée sur un histogramme 2D, la méthode de Otsu, la méthode des lignes de niveau, et la méthode de Chen-Vase. Des fonctionnalités de comparaison des résultats ont également été développées en intégrant des méthodes d'évaluation basées sur le calcul d'un coefficient de similarité de Dice, d'une différence de volume relatif et d'une distance de Hausdorff. Des fonctions de base de visualisation 2D et 3D sont également développées, par exemple pour charger et visualiser une image 2D (fichier * .jpg, * .png) ou des ensembles de données de volume (fichier *.mhd et *.raw). Des fonctions ont été aussi implémentées pour enregistrer les résultats de segmentation dans un fichier spécifique permettant ensuite de visualiser directement les résultats de segmentation 2D ou 3D en vue 2D ou 3D.

Introduction

Image segmentation as a post processing method is becoming an important tool in many research fields such as medical imaging, computer vision, biology, etc. This topic is to separate the region of interest (ROI) from the 2D image or 3D volumetric data-set. It is still challenging because of the increasing image varieties and the imaging devices for segmentation. The motivation is to elaborate an efficient general 3D image segmentation method. We propose a novel segmentation framework that is based on clustering algorithm [Maciejewski et al., 2013] and Lattice Boltzmann Method (LBM) within a diffusion-reaction version [He and Luo, 1997] for image segmentation. The main two research fields of previous image segmentation algorithms are either difficult to fine-tune to apply to limited tasks, or difficult to have ideal computational efficiency [Sonka et al., 2007]. The partial differential equation (PDE) plays an important role in the image segmentation. As a numerical method for solving PDE, the lattice Boltzmann method (LBM) is a low-order method. Compared to other solutions of PDE, it also has the advantage of being inherently adapted to the parallelization of the implemented algorithm. In addition, the relationship between segmentation codes and the computer hardware is becoming much more closed and integrated, and the LBM can illustrate this evolution. The lattice Boltzmann method has the capability to simulate complex fluid flow behaviors [Succi, 2001] and treat medical images [Chen et al., 2008] [Wang et al., 2016] [Ge and Courbebaisse, 2019] with the optimized time of computation more recently. In fact, the implementation of parallel computation code is simple for LBM, because it only locally operates the gray-level value on each node of the 3D lattice at each step for the particle propagation, without data exchange between neighbor voxels. Hence, the calculation code can be easily mapped and optimized on the thread of GPUs.

In a recent work [Wang et al., 2016], the LBM was used to segment the thrombus part of aneurysm data-sets. The experiments and results on computed tomography angiography (CTA) images demonstrated better segmentation accuracy

compared with the Chan–Vese method, Sen's model, and Luca's model. In this LBM-based segmentation method, the Otsu method [Otsu, 1979] was used to find one threshold as the diffusion penalty value in the collision function of the considered version of the lattice Boltzmann method. Although their method improved the accuracy of aneurysm segmentation, this lack of robustness of the LBM make it only used on limited applications. In this thesis, a universal LBM-based segmentation framework is proposed, which has been implemented with the 2D histogram based clustering method [Cai et al., 2013] combined with parallel lattice Boltzmann method for performing 2D images and 3D volume data-sets segmentation algorithm. In particular, the LBM within a diffusion-reaction version of the collision function [He and Luo, 1997] is dedicated to the proposed framework.

0.1 Thesis Organization

The thesis is organized as follows. After the presentation of the state of the art in chapter 1, chapter 2 presents a short history of the lattice Boltzmann method, including lattice-gas cellular automata, HPP model, FHP model, Boltzmann equation, and Lattice Boltzmann models. Then, the models with different distributions of velocities are introduced in 1D, 2D or 3D versions.

Chapter 3 introduces the image processing form based on lattice Boltzmann method, in which diffusion equations form collision terms is to achieve image smoothing. The diffusion equation is solved by the mean of the lattice Boltzmann method. In the same spirit, an anisotropic diffusion function is implemented to segment images.

Chapter 4 combines the lattice Boltzmann method and direct volume rendering technique (2D histogram based clustering method). The strategy classifies images sequences by considering both the grey-level value of voxels and the gradient magnitude calculated on each voxel, which could be used as second property for segmentation.

Chapter 5 extends the method introduced in chapter 4, and gives an overview of the proposed framework for the 3D multi-thresholds segmentation method. Multiple threshold methods are considered to perform a more sophisticated classification of volumetric data and thus deliver better separated volumetric objects or structures. This gives the algorithm the flexibility to subdivide related clusters, such as the structure corresponding to a particular tissue or volume dataset. Then, the lattice Boltzmann multi-thresholds clustering method for the segmentation of

2D images and 3D volume data-sets with complex compositions is implemented and operated with adapted parameters. To identify the accuracy of this new approach and versatility of the methodology, three evaluation methods involving the Dice similarity coefficient (DSC), Relative volume difference (RVD) and Hausdorff distance are selected to compare the results obtained with conventional methods. Then, under the proposed framework, other potential properties (geometry information) are integrated into the segmentation method in order to improve the adaptability of the algorithm. According to this new concept and to evaluate performance, the cranial volume data-set and brain aneurysm sequence are segmented. The experimental validation is performed by the Dice similarity coefficient and Hausdorff distance.

Chapter 6 studies the implementation of the framework proposed in Chapter 5 on Graphic processing units (GPU) by taking advantage of local propagation of LBM. The results show that the parallel computational scheme is suitable for both GPU computing as well as the large data-sets segmentation.

Chapter 7 concludes the thesis and proposes some promising future perspectives.

Chapter 1

State-of-the-art

Abstract

In this chapter, we introduce the general segmentation methods, meanwhile we describe a state of art review of volume rendering transfer function design. The segmentation techniques can be divided into classes in many ways, depending on the classification scheme. The most common used segmentation techniques is classified into three board categories in this chapter including thresholding algorithm, edge-based algorithm and region-growing algorithm. The transfer function design mainly has two categories, image-centric transfer function design and data-centric transfer function design.

Résumé

Dans ce chapitre, nous reprenons les méthodes générales de segmentation. Egalement, nous présentons un état d'art du rendu de volumes et du concept de fonction de transfert. Les techniques de segmentation peuvent être divisées en classes de plusieurs façons, selon le schéma de classification. Les techniques de segmentation les plus utilisées sont classées en trois catégories: l'algorithme de seuillage basic, l'algorithme de détection de contours et l'algorithme de croissance de région. La fonction de transfert est également utilisée dans deux versions, fonction de transfert centrée sur l'image et fonction de transfert centrée sur les données.

1.1 Introduction

Understanding the image as well as extracting image information to conduct certain tasks is a crucial application area of digital image technology. Image segmentation is expected as the first step to understand the image. In the medical field, images are acquired via various modalities such as magnetic resonance imaging (MRI), computed tomography (CT), ultrasound, etc. It can be applied as an effective tool to check the inside of the human body and allows doctors to make a more accurate diagnosis. Extracting useful information from images has become an essential task in both fields. Image segmentation can be used as an important post processing method various fields such as medical imaging, computer vision, bioinformatics, etc. The main topic of this thesis is to separate the region of interest (ROI) from the 2D image or 3D volumetric data, which is still challenging because of the increase in image types and the segmentation of imaging equipment.

The motivation of this thesis is the elaboration of a high efficiency and general 3D image segmentation method. Also, in the domain of 3D medical images segmentation, projecting 3D data to a 2D screen by rendering volume data using volume rendering [Drebin et al., 1988] method is commonly becoming an irreplaceable technique. Transfer function (TF) design as one of the technique cores can locate the ROI in images, and project the volumetric data into colors and opacity space. In both domains, whether it is a segmentation algorithm or TF design, it is a process of dividing an image into multiple components. Therefore, each component is meaningful, corresponding to different objects or natural parts of objects.

In this chapter, we firstly give an overview of the general segmentation algorithm including thresholding algorithm, edge-based algorithm and region-growing algorithm. Then, a state-of-the-art of volume rendering TF, image-centric TF design and data-centric transfer function are given, respectively.

1.2 General segmentation algorithm

Segmentation refers to the process of partitioning an image into regions with similar properties such as intensity and texture. Its goal is to find regions that represent objects or meaningful parts of objects. Meanwhile, segmentation plays an important role in medical image processing. It can help physicians and neurosurgeons, including: (1) Investigation and diagnosis. (2) Study of anatomical structure, e.g.,

cortical or sub-cortical structures, blood vessels, tumors etc. (3) Identification of regions of interest or detect abnormalities. (4) Measure growth or decrease in size of tumor. (5) Treatment planning prior to radiation therapy. (6) Computer-guided surgery. It is still challenging because of the increase in image types and the segmentation of imaging equipment. The motivation is the elaboration of a high efficiency and general 3D image segmentation method. Segmentation methods are classified into two broad categories: (1) region segmentation techniques that identify the regions satisfying a given-homogeneity criterion, and (2) edge-based segmentation techniques that search edges between regions with different characteristics [Gonzalez and Woods, 2006] [Mitiche and Aggarwal, 1985] [Sonka et al., 2007].

Thresholding is a common method of regions segmentation. In this technique, thresholds are selected, and an image is divided into groups of pixels with values below the threshold as well as groups of pixels with values greater than or equal to the threshold. There are several thresholding methods, such as global methods based on gray-level s, global methods based on local properties, selection of local thresholds and dynamic thresholding. Clustering algorithms segment regions by dividing the image into sets or clusters of pixels that are highly similar in element space. The basic operation is to examine each pixel and assign it to a cluster of feature vector values that perfectly represent its feature of interest. Regional growth is another class of region segmentation algorithms that assign pixels or adjacent regions to the identical segment if their image values are close enough via a pre-selected criterion of proximity.

The strategy of edge-based segmentation algorithms is to find the object boundaries and segment regions delineated by these boundaries. These algorithms are generally applicable to board magnitude and/or phase images produced by an on-board operator adapted to the expected image characteristics. For example, most gradient operators such as Prewitt, Kirsch or Roberts are based on the presence of an ideal gradient edge. Other contour-based segmentation techniques are composed of graph searching and contour tracking.

The following section will introduce some classic algorithms by medical imaging.

1.2.1 Thresholding algorithm

Several thresholding techniques have been developed [Davis, 1975] [Fu and Mui, 1981]. They are neither based on the of the image nor local properties, such as the local mean value and standard deviation, or the local gradient. The global thresholding is regarded as the most intuitive approach. When a single threshold is selected for the entire image, according to the image , the thresholding is called global. If the threshold depends on the local properties of certain regions of the image like the local mean grey-level value, the thresholding is called local. If the local thresholds are selected independently for each pixel (or group of pixels), the thresholding is called dynamic or adaptive. Fig.1.1 displays original volume of a 3D aneurysm data-set of CT angiography and a 1D histogram. In order to segment the aneurysm, T is the threshold needed to separate the data-set into two classes.

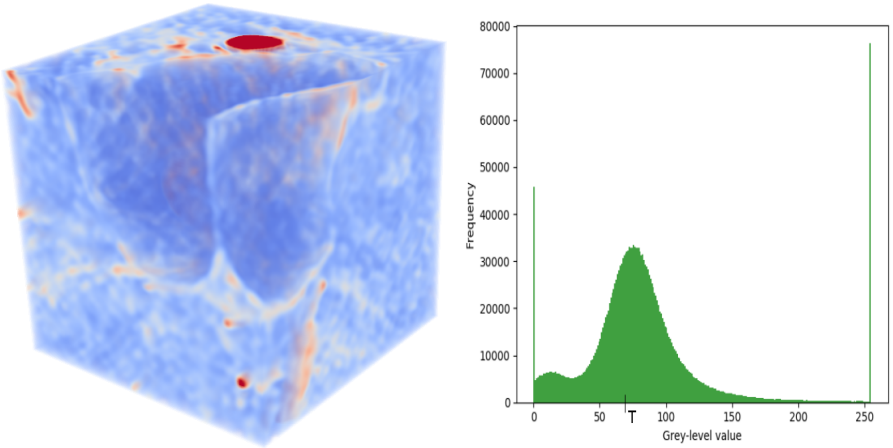

(1) Original CT angiography aneurysm data-set. (2) 1D histogram of the data-set.

Figure 1.1: An example of histogram based thresholding method is used to segment CT angiography data-set.

Typical thresholding method is called Otsu method, which [Sezgin and Sankur, 2004] that an optimum threshold is established by minimizing the weighted sum of within-class variances of the foreground and background pixels, it returns a single intensity threshold that separate pixels into two classes. Recall that minimization of within-class variances is tantamount to the maximization of between-class scatter. This method results in satisfactory results when the numbers of pixels in each class are close to each other, the algorithm is described as follows:

$$g = \frac{\omega_0}{1-\omega_0} \times (u_0 - u)^2 \tag{1.1}$$

where g is inter-class variance, the threshold is computed by maximizing inter-class intensity variance; ω_0 is foreground pixel occupancy ratio; u_0 refers to mean grey-level value of foreground; u represents mean grey-level value of image. However, it is assumed that the image is bimodal (i.e., two classes) and the method breaks down when two classes are extremely unequal (i.e., the classes possess huge different sizes) in this method. Fig.1.2 shows that segmentation of vessel and cranial CT scan, especially on cranial, the segmentation result remains one class.

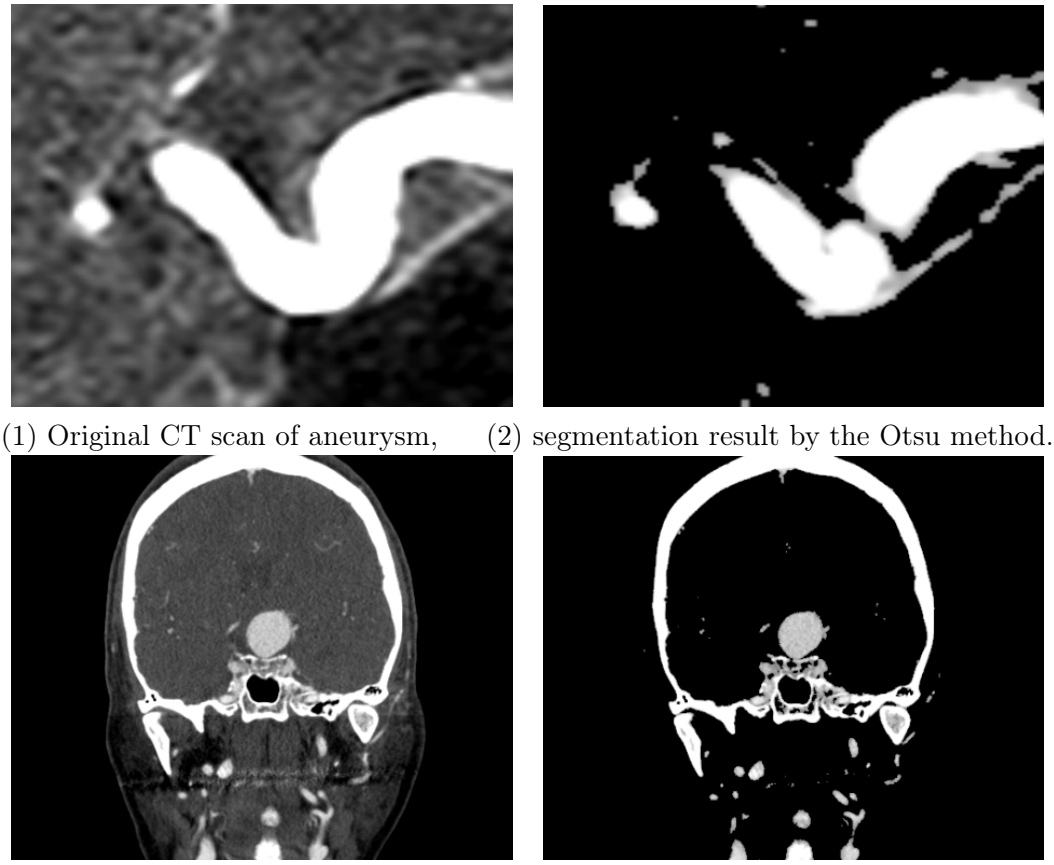

(1) Original CT scan of aneurysm, (2) segmentation result by the Otsu method.

(3) Original CTA of cranial, (4) segmentation result by the Otsu method.

Figure 1.2: An example of segmentation of blood vessel and cranial by the Otsu method, (1) and (3) are the original CT scan images, (2) and (4) are the segmentation results by the Otsu method.

1.2.2 Edge-based algorithm

An edge or boundary on an image can be defined by the local pixel intensity gradient. A gradient is an approximation of the first-order derivative of the image function. For a given image $f(x, y)$ we can calculate the magnitude of the gradient can be calculated as

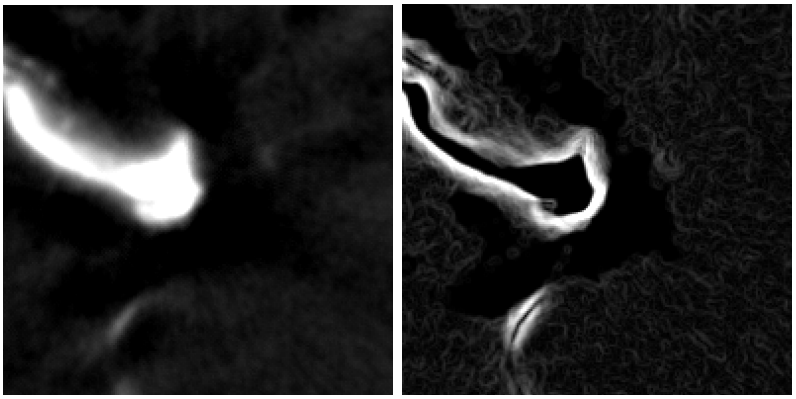

(1) Original CTA of blood vessels, (2) edge magnitude image with Sobel mask.

Figure 1.3: Edge detection by the Sobel operator.

$$|G| = \sqrt{[G_x^2 + G_y^2]} = \sqrt{[(\frac{\partial f}{\partial x})^2 + (\frac{\partial f}{\partial y})^2]}. \tag{1.2}$$

The direction is described as:

$$D = tan^{-1}(\frac{G_y}{G_x}) \tag{1.3}$$

where G_x and G_y stand for gradients in the x and y directions, respectively. Because the discrete nature of the digital image does not allow the direct application of continuous differentiation, the gradient can be calculated by differentiating [Gonzalez and Woods, 2006]. The amplitude and direction of the gradient can be displayed as images. The magnitude image will have a gray-level value that is proportional to the magnitude of the local intensity changes, while the direction image will have a gray-level value that indicates the direction of the maximum local gradient in the original image.

Most gradient operators in digital images involve the calculation of convolutions, such as weighted summaries of pixel intensities in local neighborhoods. The weights could be listed in the form of a digital vector, whose form corresponds to a local nearby area of the image (also known as a mask, window, or kernel). For example, in the case of a Sobel, there are two 363 masks in Eq.1.4:

$$G_x = \begin{bmatrix} -1 & 0 & 1 \\ -2 & 0 & 2 \\ -1 & 0 & 1 \end{bmatrix} G_y = \begin{bmatrix} 1 & 2 & 1 \\ 0 & 0 & 0 \\ -1 & -2 & -1 \end{bmatrix} \tag{1.4}$$

The first mask is used to compute G_x while the second is applied to compute

G_y. The gradient magnitude image is generated by combining G_x and G_y via Eq.3.21. Fig.1.3 shows the edge magnitude image obtained by the sobel operator.

1.2.3 Region-growing algorithm

While thresholding focuses on the difference of the pixel intensity, the regional growth method searches groups of pixels with similar intensities. The growth of a region, also called region fusion, generally begins with a pixel or a group of pixels (called seeds) that belong to the interest structure. The seeds can be selected by an operator or offered by an automatic sowing procedure finishing. In the next step, the neighboring pixels are examined one by one and then added to the growth region, if they are sufficiently similar according to a uniformity test (also called the homogeneity criterion). The procedure continues until no more pixels can be added. Then, the object can be represented by all accepted pixels [Shen et al., 1993] [Torre and Poggio, 1986]. An example of the uniformity test is to compare the difference between the pixel intensity value and average intensity value over a region. If the difference is less than a predefined value, like two standard deviations of intensity in the region, the pixel will be included in the region, while it is considered as an edge pixel. The results of the regional growth depend strongly on the choice of the homogeneity criterion. If it is not correctly chosen, regions spread into or merge with other regions that do not belong to the object of interest. Another issue related to the growth of regions is that distinct starting points may not transform into identical regions. One of advantages of regional cultivation is that It allows the spatially separated regions with the same attributes to be correctly segmented. Another advantage is that it generates connected regions.

1.3 Advanced segmentation method

Variational approaches, such as Mumford Shah model and variational level set approaches (Li et al., 2005; Bara et al., 2011; Zhang et al., 2010), provide relevant results in the medical image segmentation. The idea is to minimize an energy function via a level set evolution process, the variational approaches can evolve the curves stopping at the local or global minima of the energy function.

Some classical Level Set methods, for example the narrow band Level Set method (Lefohn et al., 2004) and Geodesic Active Contour (GAC) model (Caselles et al., 1997; Bresson et al., 2011), can detect the local gradient maximum. How-

Algorithm 1: Region Growing Algorithm.

Input: A level-line field LLA, a seed pixel P, an angle tolerance τ, and a status variable for each pixel.

Output: A set of pixels: region.

```
1  Add P → region
2  θ_region ← cos(θ_region)
3  S_x ← cos(θ_region)
4  S_y ← sin(θ_region)
5  foreach pixel P ∈ region do
6      foreach pixel Q ∈Neighbourhood(P)andStatus(Q)≠ USED do
7          if AngleDiff(θ_region, LLA(Q)) < τ then
8              Add Q → region
9              Status(Q) ← USED
10             S_x ← S_x + cos(LLA(Q))
11             S_y ← S_y + sin(LLA(Q))
12             θ_region ← arctan(S_y/S_x)
13         end
14     end
15 end
16
```

ever, due to their sensitivity to the strong noise in the CTA image and large time–costing in the evolution, the segmentation of medical images resulting from these methods are not acceptable. To overcome this defect, the LBM method is proposed in the framework of Chen's research [Chen, 2009].

1.4 Volume rendering algorithm

The key element of volume rendering [Max, 1995] is utilizing the analysis of image space and data space to assist rendering, which defined different tissues in medical images. Based on the mechanism design, the design of transfer function can be classified into two main areas image-centric and data-centric [Cai et al., 2013]. Data-centric methods are able to extract various features from the volume data and then assign optical properties. Image-centric methods are generally more intuitive. There is no need for users to go through the complex and tedious trial-and-error process of manipulating the transfer function space. Instead, they directly search for the most appealing rendered image in the space of renderings.

1.4.1 Image-centric transfer function

The design of TF needs to manipulate the mapping space, which makes the visualization process not intuitive. In image-centric algorithms, the user interface allows to directly interact with the rendering result to alter the optical properties [Wu and Qu, 2007]. The first image-centred TF design was proposed by [He et al., 1996],where the genetic algorithm was used to produce the desired TFs based on the evaluation of images rendered by users. [Guo et al., 2011] proposed the What You See Is What You Get (WYSIWYG) system that enabled users to directly interact with visualization parameters to find the ROI, as shown in Fig.1.4. For this type of algorithms, users have to manipulate the visual properties to identify the important voxel in volume data-set, which is time-consuming and difficult to fine tune.

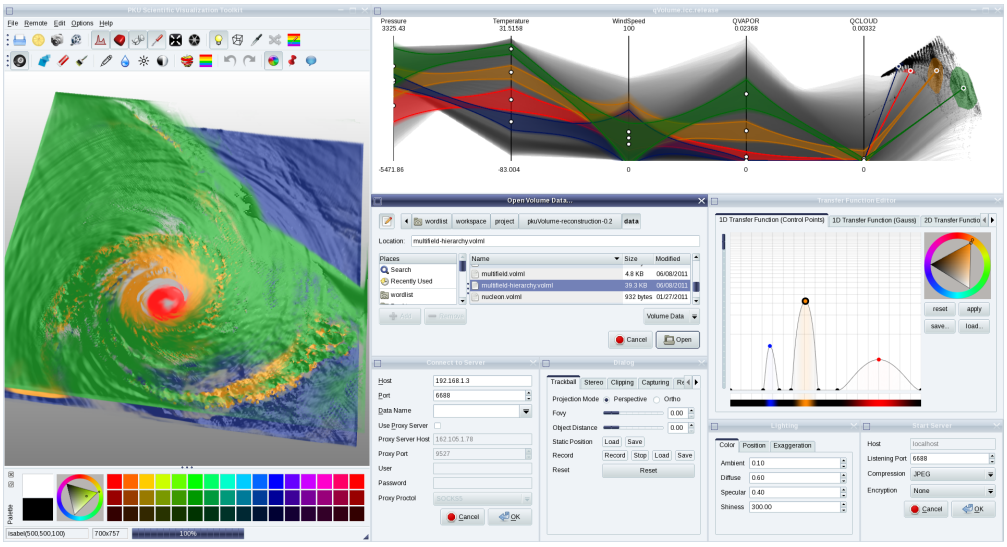

Figure 1.4: WYSIWYG system interface [Guo et al., 2011].

1.4.2 Data-centric transfer function

Data features are introduced to data-centric algorithms. For the first time, [Bajaj et al., 1997] proposed the contour spectrum to assist the user to choose relevant isovalues.This improves the feature-recognition ability of TF by extending or manipulating the feature space [Maciejewski et al., 2009] including visibility [Cai et al., 2013], information divergence [Ruiz et al., 2011], feature clustering [Zhang et al., 2016] and clustering segmentation method [Ulen et al.,] based TF have intrinsic difficulties in visualizing data sets when a data are related to multiple volumetric objects. This limitation can be resolved by extending the scope of the

TF domain to form 2D TFs. The intensity gradient magnitude (IGM) is the most commonly used 2D TF space [Kindlmann and Durkin, 1998]. As shown in Fig.1.5, the gradient magnitude is introduced as a second dimension to ensure a better separation of the object boundaries. More sophisticated features like curvature [Hladuvka et al., 2000], classification certainty [Lundstrom et al., 2006], distance to a reference object [Tappenbeck et al., 2006], entity size [Wesarg and Kirschner, 2009] have been reported as a second dimension for constructing a 2D mapping space with a scalar value. The inclusion of these features provides interesting new separability of volumetric structures.

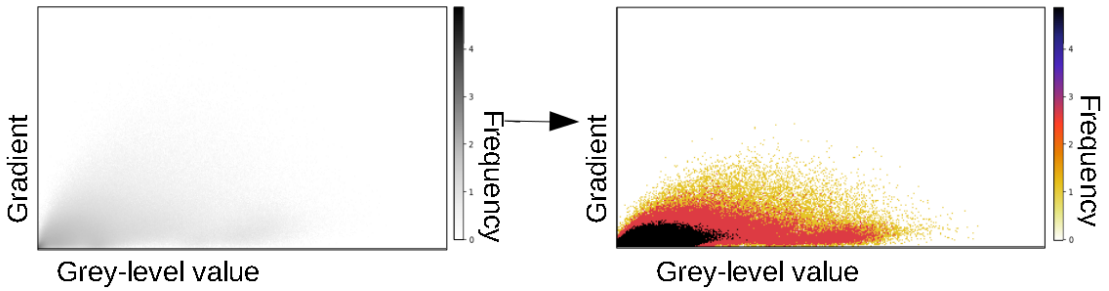

Figure 1.5: Intensity gradient magnitude histogram: original IGM histogram(left), cluster IGM histogram (right).

The discriminatory power of TF can be further greatly enhanced by increasing its dimension beyond two. However, the difficulty of visualizing 3D and larger TF spaces makes it virtually impossible to design an effective user interface. In this regard, the community has made many attempts to develop various methods, including cluster space, machine learning, parallel coordinate plotting (PCP) and dimensional reduction.

The cluster space-based approach has spatially classified large features and transformed the volume data into a representation of the cluster space that can be manipulated by users. Clustering algorithms that have been used to classify high-dimensional volumetric data contain ISODATA (Iterative Self-Organizing Data Analysis Technique) [Tzeng and Ma, 2004]. k-means [Caban and Rheingans, 2008], density estimation [Linsen et al., 2008] and modified dendrogram [Wang et al., 2011].

1.5 Conclusion

However, previous work is either difficult to fine-tune and thus cannot be applied to restricted tasks, or it is difficult to achieve the desired efficiency. As a numerical approach to solve PDE, the LBM is a low-order method with the advantage of parallelization compared with other solution of PDE. The relationship between the segmentation algorithm and hardware is becoming more integrated. Moreover, the implementation of parallel LBM is easy, because simulating the particle propagation performed by LBM only need to compute with the local operation without exchanging data between voxels. And the LBM clearly illustrates this evolution. LBM has the capability to simulate complex fluid flow behaviors [Succi, 2001] and to treat medical images with optimized time of computation [Chen et al., 2008] [Wang et al., 2016] [Ge and Courbebaisse, 2019]. The LBM within a diffusion reaction version of the collision function [He and Luo, 1997] is responsible for image processing. In a recent work [Wang et al., 2016], LBM was used to segment the thrombus part of aneurysm data-sets, and achieve relatively better results, in which it use the Otsu method [Otsu, 1979] to find one threshold as the diffusion penalty value in collision function of LBM. The methods improved the accuracy of aneurysm segmentation. However, it should be noted that the lack of transferability is the main challenge for the LBM segmentation algorithm.

Chapter 2

Lattice Boltzmann method

Abstract

Lattice Boltzmann method (LBM) is developed from lattice gas automata (LGA) which was first proposed in 1973 [Hardy et al., 1973]. In one way, LBM is a model that can describe the fluid flow. Also, LBM could be viewed as the discrete format of the continuous Boltzmann equation. In another way, LBM is a mesoscopic mathematical method that simulate macroscopic phenomenon. In this chapter, the general HPP, FHP and LBM models are presented.

Résumé

La méthode de Boltzmann sur réseau est développée à partir des automates à gaz en réseau (LGA) qui ont été proposés pour la première fois en 1973 [Hardy 1973]. LBM est un modèle qui peut décrire le débit du fluide. En outre, LBM peut être considéré comme le format discret de l'équation de Boltzmann continue. D'une autre manière, la LBM est une méthode mathématique mésoscopique qui simule un phénomène macroscopique. Dans ce chapitre, les modèles généraux HPP, FHP et LBM sont présentés.

2.1 Lattice-gas cellular automata

The lattice-gas cellular automata (LGCA) model is an approach to simulate fluid flow, and firstly proposed in 1973 by Hardy, de Pazzis and pomeau (HPP), which is the original form of lattice LGCA with Boolean pseudo-fluid particles residing on a discrete two-dimensional quadratic grid [Raabe, 2004].

2.1.1 HPP lattice-gas cellular automata

The HPP model is the simplest LGCA, which is a 2-Dimensional cellular LGCA model over a square lattice. At each node there are four cells each associated to a link with the nearest neighbor, each cell may occupied by at most one particle. In order to solve the problems of constructing cellular automate, the update procedure is splitted into 2 parts, collision and propagation (streaming), as shown in Fig.2.1.

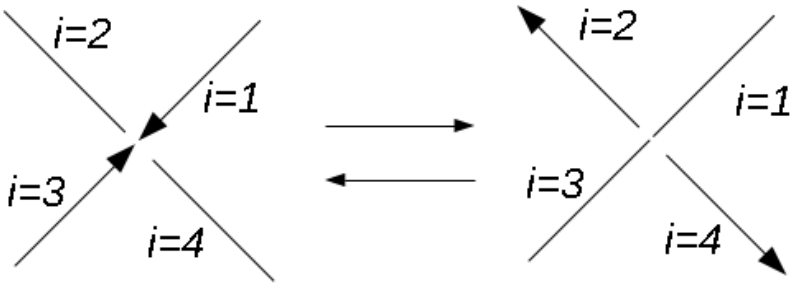

Figure 2.1: HPP Collision configuration and its propagation, after the collision the two cells will occupy the formerly empty cells.

The HPP assume that, in the each node of the lattice there are four cells connecting the nearest neighbors which is lattice vectors or lattice velocities, each cell may be empty or occupied by at most one particle, all particles have the same mass, and after the collision the particles will change their velocity direction. The streaming and collision can be written in Eq.2.1.

$$n_i(\vec{r} + \vec{e}_i, t + \Delta t) = n_i(\vec{r}, t) + \Delta_i \tag{2.1}$$

where $n_i(\vec{r}, t)$ denote the Boolean field at the discrete direction $\vec{r}$ and time t; $\vec{e}_i$ is the unit lattice velocity vectors; Δ_i is collision function which can be given by:

$$\Delta_i = n_{i+1}n_{i+3}(1 - n_i)(1 - n_{i+2}) - n_i n_{i+2}(1 - n_{i+1})(1 - n_{i+3}). \tag{2.2}$$

2.1.2 FHP model

Frish found that it has some deviationwhile solving partical differential equations by HPP model. In 1986 Frisch, Hasslacher and Pomeau (FHP) published a hexagonal grid LGCA model which yield the incompressible Navier-Stokes equation in the macroscope limit [Frisch et al., 1986]. The FHP model has essential properties:

1 At each node the lattice vector has six directions which correspond to six neighbor nodes.

2 All particles have the same mass, and can move along the directions i to neighbor cell.

3 Cell can be empty or occupied by at most one particles.

4 The particle will only locally collide in the each cell.

The collision and steaming of FHP model is shown in Fig.2.2 and its mathematical model is the same with HPP model, but has six directions in Eq.2.3.

$$n_i(\vec{r} + \vec{e}_i, t + \Delta t) = n_i(\vec{r}, t) + \Delta_i \tag{2.3}$$

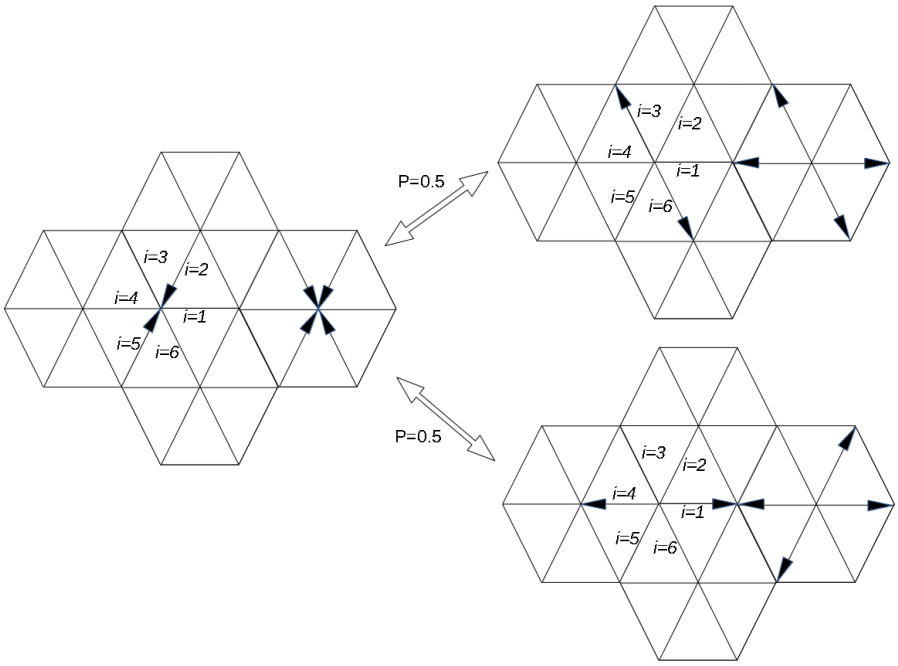

Figure 2.2: FHP model: two possible results of head on particles collision, showing the regular of hexagonal symmetry.

However, HPP model and FHP model has the disadvantages: (1) As the calculation, it produce large amount of numerical noise, for reason that at each node

of grid, each discrete velocity may be taken at most one particle. (2) Higher order correlations between particles are neglected.

2.2 The Boltzmann equation

Recently, LBM has become a common tool for the numerical simulation of fluid flows [Succi, 2001]. LBM is used for the simulation of complex systems and evolves to specific domains such as image processing [Chen et al., 2008]. A key feature is the ability to link the interaction term in the model with a physical model. The numerical LBM scheme is developed by discretizing the continuity Boltzmann equation [Wolf-Gladrow, 2000]. In 1988 McNamara and Zanetti proposed to use mean occupation numbers instead of Boolean fields [McNamara and Zanetti, 1988] so as to reduce the numerical noise. The Boltzmann equation uses the distribution f describe high level system, FHP model by substituting $n_i \to f,\ c_i \to v,\ \Delta \to Q$ gives the Boltzmann equation shown in Eq.2.4:

$$\frac{\partial \rho}{\partial t} + v \bigtriangledown f = Q(f, f). \tag{2.4}$$

$Q(f, f)$ is the collision integral for 2 particles, and this equation considers the following approximations: (1) Only two-particle collisions; (2) The velocities of the two colliding particles are uncorrelated before collision; (3) External forces do not influence the local collision dynamics.

2.3 The Lattice Boltzmann equation

The Boltzmann equation has the the problem of complicated nature of collision integral, therefore Bhatnagar, Goss and Krook (BGK) has proposed an alternative expression in 1954 [Bhatnagar et al., 1954]. It simplified the collision function $Q(f, f)$, and distribution function changes with the collision and steaming. The LBM BGK approximation is shown in Eq.2.5.

$$\frac{\partial f}{\partial t} + v \bigtriangledown f = \omega[f(\vec{r}, t) - f^{eq}(\vec{r}, t)]. \tag{2.5}$$

ω is a relaxation frequency which controls the rate of approaching the equilibrium. The distribution function f depends on space, velocity and time. v is discretized by set of velocities v_i, so the discrete Boltzmann equation is:

$$\frac{\partial f_i}{\partial t} + v_i \bigtriangledown f_i = \omega[f_i(\vec{r},t) - f_i^{eq}(\vec{r},t)] \tag{2.6}$$

where f_i presents the discrete distribution function, and $f_i^{eq}(\vec{r},t)$ is the discrete equilibrium distribution function at node $\vec{r}$ at time t:

$$f_i^{eq} = \omega_i \rho[1 + \frac{\vec{e_i}\vec{u}}{c_s^2} + \frac{(\vec{e_i}\vec{u})^2}{2c_s^4} - \frac{\vec{u}^2}{2c_s^2}] \tag{2.7}$$

where ω_i is constant, ρ is mass density, c_s is constant, $\vec{e_i}$ is lattice velocity, $\vec{u}$ is velocity of fluid. Then keep the parameter length scale reference density, reference speed and time between particle collisions, the non-dimensionalized discrete Boltzmann equation is :

$$\frac{\partial f_i}{\partial t} + c_i \bigtriangledown f_i = \omega[f_i(\vec{r},t) - f_i^{eq}(\vec{r},t)]. \tag{2.8}$$

The discrete form of Eq.2.8 is:

$$\begin{aligned} &\frac{f_i(x,t+\Delta t) - f_i(x,t)}{\Delta t} + c_{ix}\frac{f_i(x+\Delta x, t+\Delta t) - f_i(x,t)}{\Delta x} \\ &+c_{iy}\frac{f_i(x+\Delta y, t+\Delta t) - f_i x,t}{\Delta y} + ... = \omega(f_i - f_i^{eq}) \end{aligned} \tag{2.9}$$

While selecting the lattice spacing as Δx, the lattice velocities at each direction is $c_i = \Delta x/\Delta t$. $\omega = \frac{1}{\tau}$, where τ is a relaxation time. Then the lattice Boltzmann equation is:

$$f_i(x + c_i\Delta t, t + \Delta t) - f_i(r,t) = -\frac{1}{\tau}[f_i - f_i^{eq}]. \tag{2.10}$$

At each simulation step, iteration is mainly separated into two steps: the collision step and the streaming step:

$$f_i(\vec{r}, t + \Delta t) = f_i(x,t) - \frac{1}{\tau}(f_i((\vec{r},t) - f_i^{eq}((\vec{r},t)) \tag{2.11}$$

$$f_i((\vec{r} + e_i\Delta t, t + \Delta t) = f_i((\vec{r},t). \tag{2.12}$$

2.3.1 Lattice Boltzmann Method in 1D

After overcome all of the problems of lattice-gas cellular automata, Qian [Qian et al., 1992] proposed *DdQm* model in 1992 is LBM classic model, the simplest discrete form is in 1-dimensional space, Eq.2.13 is LBM D1Q3 model.

$$\vec{e} = [0, 1, -1], c_s = \frac{c}{\sqrt{3}},$$
$$w_i = \begin{cases} \frac{2}{3}, e_i^2 = 0 \\ \\ \frac{1}{6}, e_i^2 = c^2 \end{cases} \tag{2.13}$$

where w_i and c_s is determined by the geometry of the lattice and isotropy the directions. D1Q3 (one dimension and three directions at each node) geometry model is shown in Fig.2.3. We take D1Q3 as an example, particles can only reside on the nodes and move to their nearest neighbors along links. There are three types of moving particles. Particles of type 1 with lattice velocity $e_i^2 = 0$ stay on the nodes, particles of type 2 move along the axes with lattice velocity $e_i^2 = c$. Here is some models and its parameters.

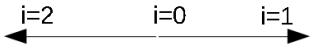

Figure 2.3: LBM D1Q3 lattice.

Eq.2.14 and Fig.2.4 are D1Q5 model.

$$\vec{e} = [0, \pm 1, \pm 2], c_s = c,$$
$$w_i = \begin{cases} \frac{1}{2}, e_i^2 = 0 \\ \\ \frac{1}{6}, e_i^2 = c^2 \\ \\ \frac{1}{12}, e_i^2 = 4c^2 \end{cases} \tag{2.14}$$

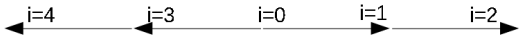

Figure 2.4: LBM D1Q5 lattice.

2.3.2 Lattice Boltzmann Method in 2D

LBM 2D model are introduced in this section. The D2Q7 LBM and model D2Q9 LBM model are shown in Eq.2.15 and Eq.2.16 which mean two dimension with seven directions and nine directions at each node ,as shown in Fig.2.5 and Fig.2.6.

$$\begin{aligned} c_0 &= (0,0) \\ c_{1,3,5,7} &= (cos\theta, sin\theta), \theta = (i-1)\pi/2 \\ c_{2,4,6,8} &= \sqrt{2}(cos\theta, sin\theta), \theta = (i-5)\pi/2 + \pi/4 \end{aligned} \tag{2.15}$$

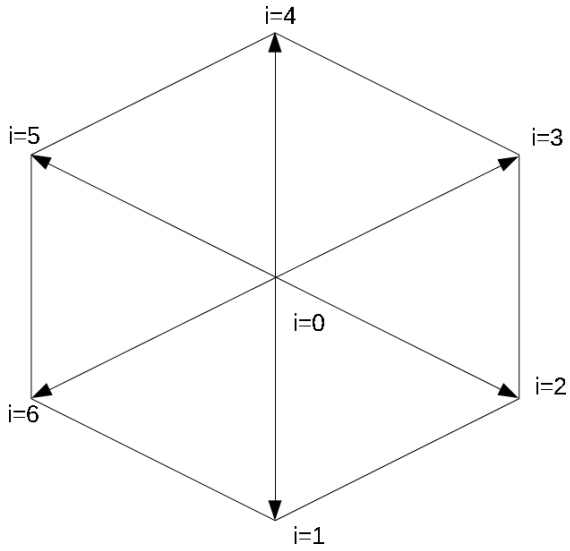

Figure 2.5: LBM D2Q7 lattice.

$$\begin{aligned} c_0 &= (0,0) \\ c_{1,3,5,7} &= (cos\theta, sin\theta), \theta = (i-1)\pi/2 \\ c_{2,4,6,8} &= \sqrt{2}(cos\theta, sin\theta), \theta = (i-5)\pi/2 + \pi/4 \end{aligned} \tag{2.16}$$

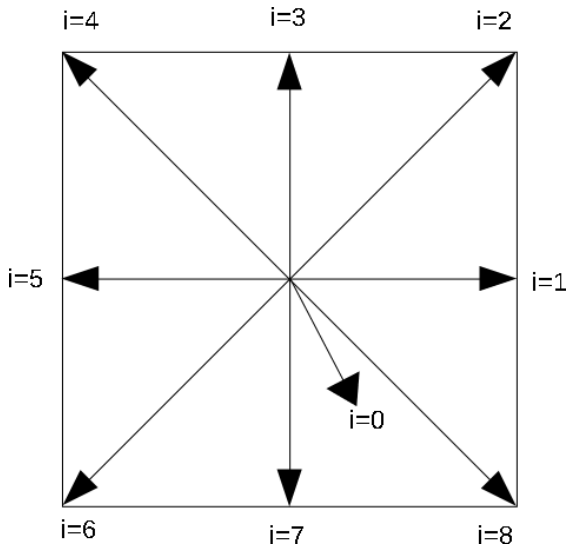

Figure 2.6: LBM D2Q9 lattice.

2.3.3 Lattice Boltzmann Method in 3D

LBM 3D models are introduced in this section. The LBM 3D models are cubic lattice in 3 dimensions in which velocities connecting the nodes. The D3Q9, D3Q15, D3Q19 and D3Q27 model are shown in Eq.2.17, Eq.2.18, Eq.2.19 and Eq.2.20, the lattice structures are shown in Fig.2.7, Fig.2.8, Fig.2.9 and Fig.2.10.

$$\begin{aligned} c_0 = (0,0,0)\ c_1 = (1,1,1)\ c_2 = (1,-1,1) \\ c_3 = (-1,-1,1)\ c_4 = (-1,1,1)\ c_5 = (1,1,-1) \\ c_6 = (1,-1,-1)\ c_7 = (-1,-1,-1)\ c_8 = (-1,1,1) \end{aligned} \tag{2.17}$$

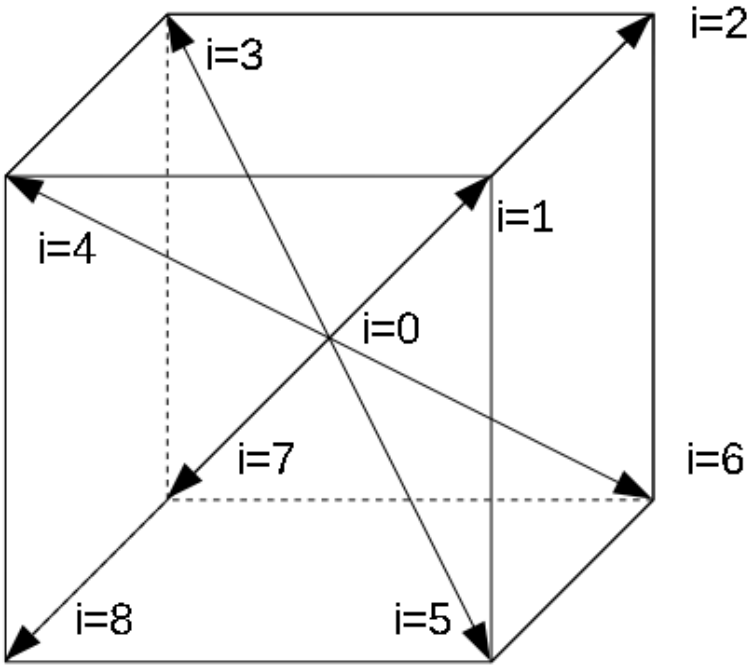

Figure 2.7: LBM D3Q9 lattice.

$$\begin{aligned} c_0 = (0,0) \\ c_{1,2,3,4,5,6} = (\pm 2,0,0),(0,\pm 2,0),(0,0,\pm 2) \\ c_{7,\ldots,14} = (\pm 1,\pm 1,\pm 1) \end{aligned} \tag{2.18}$$

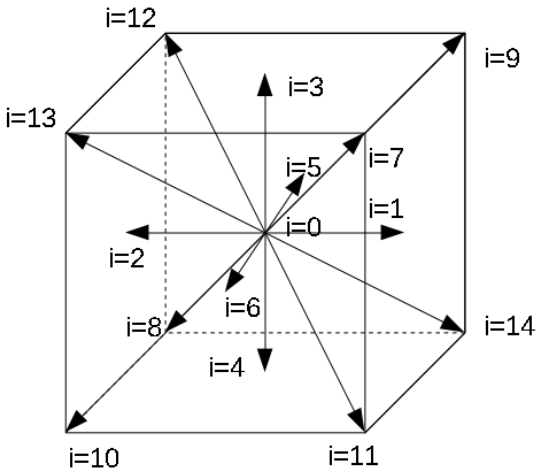

Figure 2.8: LBM D3Q15 lattice.

$$\begin{aligned} c_0 &= (0,0,0) \\ c_{1,2,3,4,5,6} &= (\pm 1,0,0),(0,\pm 1,0),(0,0,\pm 1) \\ c_{7,\ldots,18} &= (\pm 1,\pm 1,0),(\pm 1,0,\pm 1),(0,\pm 1,\pm 1) \end{aligned} \tag{2.19}$$

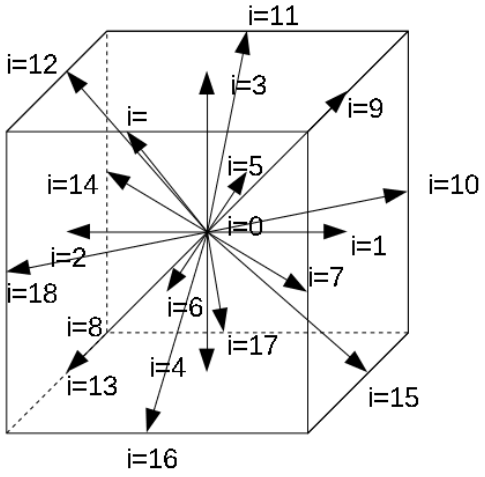

Figure 2.9: LBM D3Q19 lattice.

$$\begin{aligned} c_0 &= (0,0) \\ c_{1,2,3,4,5,6} &= (\pm 1,0,0),(0,\pm 1,0),(0,0,\pm 1) \\ c_{7,\ldots,18} &= (\pm 1,\pm 1,0),(\pm 1,0,\pm 1),(0,\pm 1,\pm 1) \\ c_{19,\ldots,26} &= (\pm 1,\pm 1,\pm 1) \end{aligned} \tag{2.20}$$

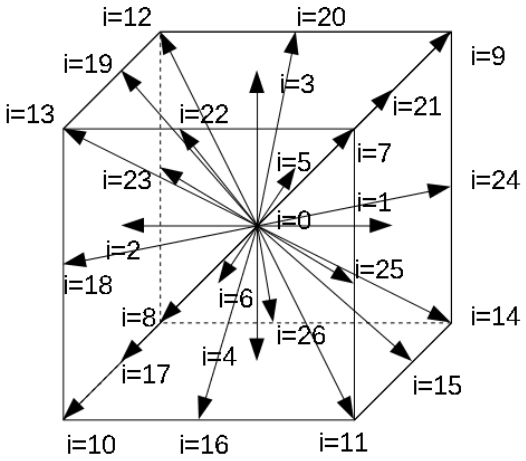

Figure 2.10: LBM D3Q27 lattice.

2.4 Conclusion

Two of the simplest models of lattice gas automata (HPP and FHP) are presented in this chapter. The connection between the lattice automata equation and the lattice Boltzmann equation gives us a general idea of the lattice Boltzmann method. In addition, different discrete speed models dedicated to more complex situations in 2D and 3D are also exhibited in this chapter.

Chapter 3

Lattice Boltzmann method dedicated to image processing

Abstract

The LBM as a numerical tool for solving problems of the partial differential equations (PDE) has been successfully applied to hydrodynamic simulations. It also can facilitate the development of algorithms for image processing like denoising or segmentation. The main problem is the adaptation of the model and its formulation for specific applications. In this chapter, the diffusion equation is firstly introduced, and then LBM is applied for the simulation of the diffusion equation. Thereafter, LBM based smoothing algorithm and LBM anisotropic diffusion function on image segmentation are discussed.

Résumé

Le LBM vu comme un outil numérique pour résoudre les problèmes des équations aux dérivées partielles (EDP) a été appliqué avec succès aux simulations hydrodynamiques. Il peut également faciliter le développement d'algorithmes de traitement d'images tels que le débruitage ou la segmentation. Le problème principal est l'adaptation du modèle et sa formulation pour des applications spécifiques. Dans ce chapitre, l'équation de diffusion est d'abord présentée, puis LBM est appliquée pour la simulation de l'équation de diffusion. Par la suite, l'algorithme de lissage basé sur la LBM et la fonction de diffusion anisotrope de la LBM pour la segmentation d'image sont discutés.

3.1 Diffusion equation on image smoothing

Diffusion equation as a kind of PDE has become an important research topic for image processing. Koenderink [Koenderink, 1984] applied the diffusion function to improve the image in 1984, which is shown in Eq.3.1,

$$\partial\rho = \alpha^2\rho. \tag{3.1}$$

In diffusion function, ρ is the density of the diffusion material. However, Koenderink set K to the 'reference luminance' of the image. The derived image can be obtained by convolution with the Gaussian kernel:

$$\rho(r, r^{'}) = \frac{e^{-(r-r^{'})/4t}}{4\pi t}. \tag{3.2}$$

However, while denoising the boundary edges has become the blurring edges, Perona and Malik [Perona and Malik, 1990] proposed the anisotropic diffusion function (P-M model) in 1990 which is expressed as:

$$\frac{\partial}{\partial t}[c(x, y, t)I_x] = div[c(x, y, t)I_x \bigtriangledown I] \tag{3.3}$$

where c is the diffusion coefficient. the coefficient will descent while the gradient ascents, and vice versa.

3.2 Solving the diffusion equation on image smoothing by LBM

To solve the diffusion equation by LBM, the LBM equation is described as follows:

$$f_i(\vec{r} + \Delta r, t + \Delta t) = f_i(\vec{r}, t) + \frac{1}{\tau}[f_i^{eq}(\vec{r}, t) - f_i(\vec{r}, t)] \tag{3.4}$$

where f_i presents the discrete distribution function, and $f_i^{eq}(\vec{r}, t)$ is the discrete equilibrium distribution function at node $\vec{r}$ at time t. τ is a relaxation time.

To initialize the image, the original image is suitable as the initial value of the proposed method, and the initial values of the particle distribution function $f_i(\vec{r}, 0)$ and equilibrium function $f_i^{eq}(\vec{r}, 0)$ are expressed as follows:

$$f_i(\vec{r},0) = f_i^{eq}(\vec{r},0) = \beta_i \rho(\vec{r},0) \tag{3.5}$$

where β is:

$$\beta_i = \begin{cases} \frac{4}{9}, i = 0 \\ \frac{1}{9}, i = 1,3,5,7,... \\ \frac{1}{36}, i = 2,4,6,8,... \end{cases} \tag{3.6}$$

where $M \in [0,1]$, and ρ is:

$$\rho(\vec{r},t) = \sum_i f_i(\vec{r},t) \tag{3.7}$$

where f_i in Eq.(3.7) gives the density map, which represents the grey value at each lattice node as well as the next iteration. f_i is the density map at each lattice node and at the former iteration. f_i^{eq}represents the local equilibrium distribution which is the volume grey-level value distribution function. β_i and $\vec{e_i}$ are LBM D3Q19 models and represent the direction and lattice velocities are shown in Fig.3.1. They can be expressed as follows :

$$\begin{aligned} \vec{e_0} &= (0,0) \\ \vec{e_{1,2}},\ \vec{e_{3,4}},\ \vec{e_{5,6}} &= (\pm1,0,0),\ (0,\pm1,0),\ (0,0,\pm1) \\ e_{7,\ldots,10},\ e_{11,\ldots,14},\ e_{15,\ldots,18} &= (\pm1,\pm1,0),\ (\pm1,0,\pm1),\ (0,\pm1,\pm1). \end{aligned} \tag{3.8}$$

The evolution function can be written as follows:

$$f_i(\vec{r} + \Delta t\vec{c_i}, t + \Delta t) = f_i(\vec{r},t) + \frac{1}{\tau}[f_i^{eq}(\vec{r},t) - f_i(\vec{r},t)]. \tag{3.9}$$

τ denotes as relaxation time. It shows that the time efficiency of the density distribution tends to be balanced. Moreover, it has been proved that even though the fluid is uniform and τ is larger than 0.5, the LBM still remains steady [Sterling and Chen, 1996]. The distribution function can be expanded by multi-scale technique (Chapman-Enskog expansion) as follows:

$$f_i = f_i^{(0)} + \epsilon f_i^{(1)} + \epsilon^2 f_i^{(2)} + ... \tag{3.10}$$

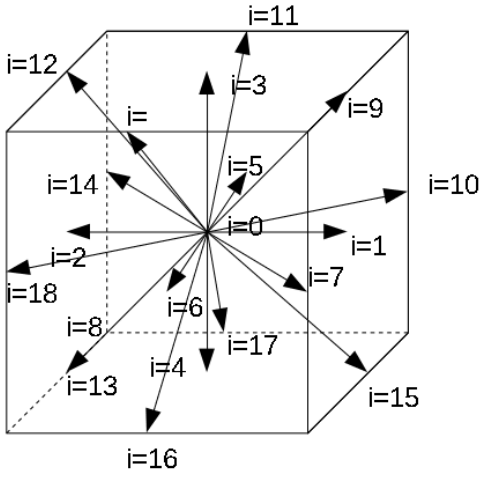

Figure 3.1: Particles directions of D3Q19.

From the Eq.3.9, we calculate an approximation of f_i^{eq} by expanding the left part of Eq.3.9 by Taylor expansion in time and space:

$$f_i(\vec{r},t) + \bigtriangledown \vec{c}_i \Delta t + \frac{\partial}{\partial t}\Delta t = f_i(\vec{r},t) + \frac{1}{\tau}[f_i(\vec{r},t) - f_i^{eq}(\vec{r},t)] + o^2. \tag{3.11}$$

Then based on Eq.3.10 and derivation, we find that the equation is similar to diffusion function as follow:

$$\bigtriangledown \vec{c}_i + \frac{\partial f_i}{\partial t} + \frac{f_i^{(1)}}{\tau \Delta t} = 0 \tag{3.12}$$

then,

$$\epsilon f_i^{(1)} = \tau \Delta t \partial_r f_i + \tau \Delta t \partial_t f_i. \tag{3.13}$$

According to the conservation relation, the formula can be written as :

$$\sum_i [f_i(\vec{r} + \Delta t \vec{c}_i, t + \Delta t) - f_i(\vec{r},t)] = 0. \tag{3.14}$$

The Taylor expansion is then inserted to the left part of Eq.3.14,

$$\sum_i (\partial_r \vec{c}_i f_i + \partial_t f_i + o^2) = 0 \tag{3.15}$$

and therefore,

$$\partial_t \rho = -\sum_i \partial_r \vec{c_i} f_i. \tag{3.16}$$

Next, Chapman-Enskog expansion is inserted to the equation:

$$\partial_t \rho = -\sum_i \partial_{\vec{r}} (\vec{c_i} f_i^{(0)} + \vec{c_i} \epsilon f_i^{(1)}) \tag{3.17}$$

the component velocities $\vec{c_i}$ obey the following equations:

$$\begin{aligned} \sum_i \vec{c_i} &= 0 \\ \sum_i \vec{c_i} f_i^{(0)} &= 0 \end{aligned} \tag{3.18}$$

and therefore,

$$\partial_t \rho = -\sum_i \partial_r \vec{c_i} \epsilon f_i^{(1)} \tag{3.19}$$

based on Eq.3.13, we derive as follow:

$$\begin{aligned} \partial_t \rho &= -\sum_i \partial_r \vec{c_i} (\tau \Delta t \partial_r f_i + \tau \Delta t \partial_t f_i) \\ &= -\tau \Delta t \sum_i \partial_{\vec{r}_\alpha} \partial_{\vec{r}_\beta} \vec{c_{i_\alpha}} \vec{c_{i_\beta}} f_i. \end{aligned} \tag{3.20}$$

In the Eq.3.20, we can see that

$$\sum_i \partial_{\vec{r}_\alpha} \partial_{\vec{r}_\beta} \vec{c_{i_\alpha}} \vec{c_{i_\beta}} f_i \rightarrow \bigtriangledown^2 \rho \tag{3.21}$$

and finally we have

$$\frac{\partial \rho}{\partial t} = -\tau \Delta t \bigtriangledown^2 \rho. \tag{3.22}$$

In LBM-BGK, the diffusion coefficient τ is an adjustable parameter range, which is $\tau > 0.5$. According to Eq.3.11 - 3.22, the LBM method offers a solution for diffusion function, which is the main application of PDE for image segmentation. The key features of LBM are the stability and efficiency to resolve the PDE. While the LBM is difficult on the generalized application mainly due to the implicit parameter. This indicates that it is difficult for the LBM method to find the penalty threshold for volume data-sets. To obtain it, we proposed a novel collision function in the next chapter.

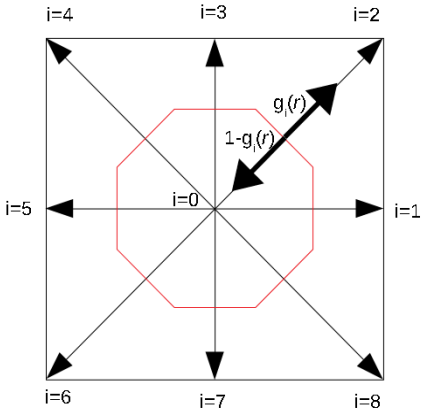

Figure 3.2: LBM D2Q9 lattice.

3.3 LBM on image smoothing

Anisotropic diffusion function has both forward and backward diffusion processes. The backward diffusion process of the P-M model results in a stair-casing effect which demonstrates that the grey-level value rapidly rises at the large grey-level value pixel. In 2008, Yu applied LBM for image smoothing [Chen et al., 2008]]. It revealed that the LBM evolution equation only has a forward diffusion process by Chapman-Enskog expansion, which can effectively overcome the stair-casing effect. The anisotropic diffusion model based on LBM is described in Eq.3.23:

$$\begin{aligned} f_i(\vec{r}+\Delta r, t+\Delta t) &= g_i(\vec{r})\{f_i(\vec{r},t)+\frac{1}{\tau}[f_i^{eq}(\vec{r},t)-f_i(\vec{r},t)]\} \\ &+(1-g_i(\vec{r}))\{f_i(\vec{r}+\Delta r,t)+\frac{1}{\tau}[f_i^{eq}(\vec{r}+\Delta r,t)-f_i(\vec{r}+\Delta r,t)]\} \end{aligned} \tag{3.23}$$

where f_i represents the discrete distribution function and corresponds to a grey-level value at each node linked to image pixel, and $f_i(\vec{r}+\Delta r, t+\Delta t)$ is particle distribution function in each node $\vec{r}+\Delta r$, and at time $t+\Delta t$; Δr and Δt correspond to space and time steps. $f_i^{eq}(\vec{r},t)$ is the discrete equilibrium distribution function at node $\vec{r}$ at time t. τ is the relaxation time.

A semi-permeable membrane g_i acting as a selective filter, is introduced to allow certain molecules to diffuse through the membrane, thereby causing it to diffuse anisotropically. g_i is the possibility of crossing the membrane, and the D2Q9 model is used to show the evolution equation in Fig.3.2.

A CT scan of the aneurysm is used to compare the detail effect between the

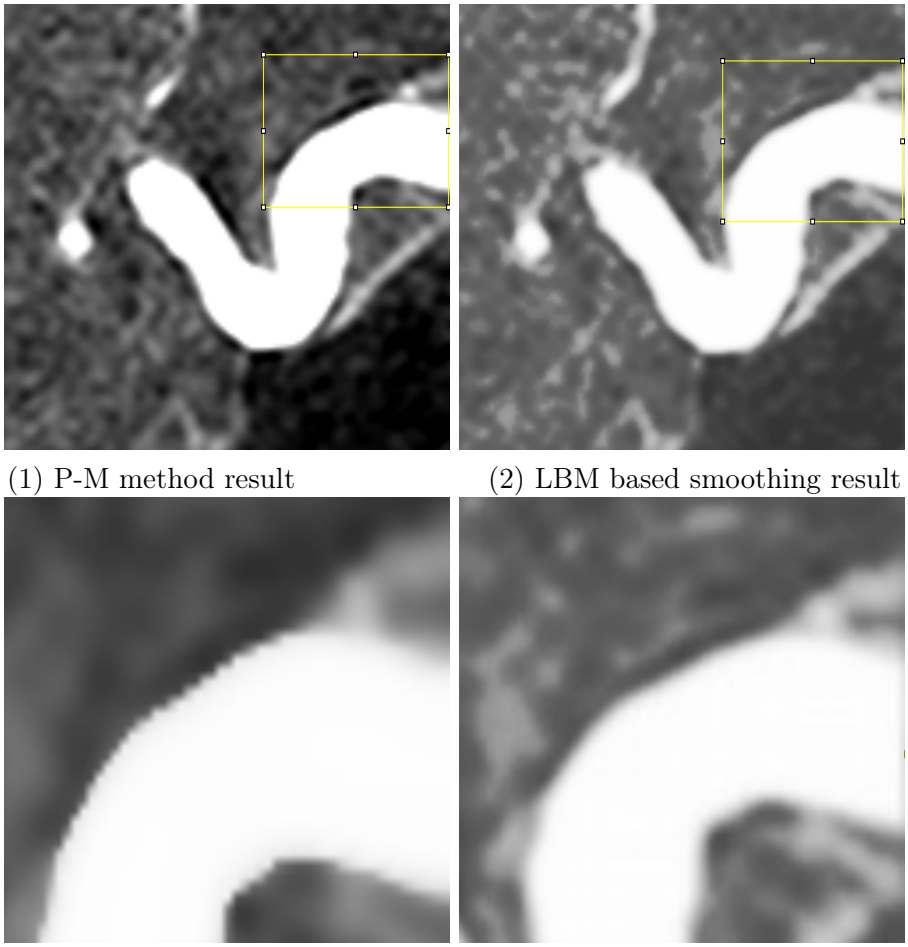

(1) P-M method result (2) LBM based smoothing result

(3) Zoom of the P-M method result (4) Zoom of the proposed method

Figure 3.3: Overcoming the stair-casing effect of classic anisotropic diffusion method in 2D view.

P-M method and LBM method. The result displayed in Fig.3.3 shows that the proposed method can diffuse images while sharpening the boundary information. However, while utilizing the P-M anisotropic diffusion function, the P-M model clearly shows a stair-casing effect compared with the LBM method in Fig.3.3[3][4].

3.4 LBM anisotropic diffusion function on image segmentation

In 2009, Yu [Chen, 2009] proposed image segmentation based on LBM anisotropic diffusion function. As shown in Fig.3.2, he used the same D2Q9 model. In order to enhance the image, a diffusion resource $a\Delta t[T - \rho(\vec{r})]$ was added in the model. The LBM evolution equation is expressed as follows :

$$
\begin{aligned}
f_i(\vec{r}+\Delta r, t+\Delta t) &= g_i(\vec{r})\{f_i(\vec{r},t)+\frac{1}{\tau}[f_i^{eq}(\vec{r},t)-f_i(\vec{r},t)]\} \\
&+(1-g_i(\vec{r}))\{f_i(\vec{r}+\Delta r,t)+\frac{1}{\tau}[f_i^{eq}(\vec{r}+\Delta r,t)-f_i(\vec{r}+\Delta r,t)]\} \\
&+a\Delta t[T-\rho(\vec{r})]
\end{aligned}
\tag{3.24}
$$

where f_i represents the discrete distribution function and corresponds to a grey-level value at each node linked to image pixel, and $f_i(\vec{r}+\Delta r, t+\Delta t)$ is particle distribution function in each node $\vec{r}+\Delta r$, and at time $t+\Delta t$; Δr and Δt correspond to space and time steps. $f_i^{eq}(\vec{r},t)$ is the discrete equilibrium distribution function at node $\vec{r}$ at time t. τ is the relaxation time. Yan [Wang et al., 2016] proposed a segmentation threshold T, calculated by the Otsu method, segmented the lumen portion in Fig.3.4 from the original image. Thereafter, the gray-level values of the lumen region were replaced by the mean value outside it, LBM was applied again on it. Next, level-set was used to optimize the expanding disk in Eq.3.25 in order to define the boundary of thrombus:

$$
s=\frac{disk\cap LBM\ image}{disk} \tag{3.25}
$$

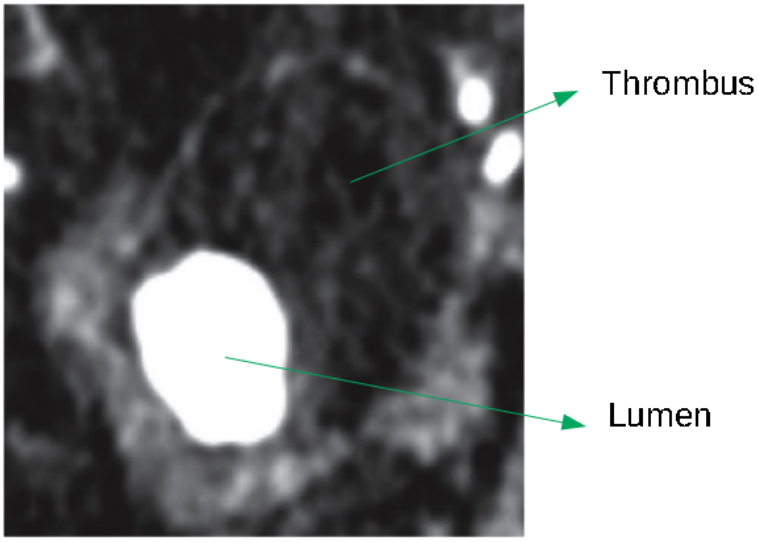

Figure 3.4: The lumen part and thrombus part of cerebral aneurysm.

Then, in 2014, Yu [Chen et al., 2014] presented LBM Geodesic active contour Method (LBGM) to solve the GAC evolution function by LBM. The algorithm includes the following steps:

(1) Initialize the values of the LBM grid as the gray-level value of the image. (2) Particle collision and streaming according. (3) Calculate gradient flow and discrete gradient flow. (4) Update the image according to (3). (5) Proceed to step (1).

The results are acceptable, but the accuracy of this model still needs to be enhanced.

3.5 Conclusion

In this chapter, several LBM-based algorithms for image processing are presented, including image smoothing, image denoising, as well as segmentation. However, it is demonstrated that the advantages of the LBM have not been fully investigated in two aspects. One is flexible control to produce smooth segmentation results, and the other is strong amenability to parallel computing, especially on low-cost, powerful graphics processor units (GPU).

Chapter 4

Segmentation Algorithm coupling LBM and k-means clustering method

Abstract

An original segmentation methodology created by coupling a direct volume rendering technique (2D histogram based clustering method) and a Lattice Boltzmann 3D method is proposed in this chapter. The underlying strategy lies in the opportunity to cluster medical image sequences by considering not only the grey-level value of voxels. Moreover, the gradient magnitude calculated on each voxel could be used as the second property for segmentation. Under this new concept, the purpose of processing a cerebral aneurysm sequence is to segment the aneurysm wall and parent blood vessels.

Résumé

Une méthodologie de segmentation originale créée en couplant une technique de rendu volumique direct (méthode de partitionnement basée sur des histogrammes 2D) et une méthode de Boltzmann sur réseau 3D est proposée dans ce chapitre. La stratégie sous-jacente réside dans la possibilité de partitionner les séquences d'images médicales en tenant compte non seulement de la valeur des niveaux de gris des voxels mais également le gradient de niveau de gris calculé sur chaque voxel utilisé comme deuxième paramètre pour la segmentation. Selon ce nouveau concept, l'objectif du traitement de séquence d'anévrisme cérébral est de segmenter la paroi de l'anévrisme et les vaisseaux sanguins parents.

4.1 Introduction

In this chapter, the most common lattice Boltzmann model is applied. The previous research on LBM dedicated to the image or volume data-set segmentation mainly possess two problems. One problem is the restriction of the Otsu method [Wang et al., 2016] that is to locate the threshold value where the sum of foreground and background spreads reaches its minimum, which is difficult to handle complex data-sets. Another problem is the time efficiency of calculating the large amount of volume data-set. Meanwhile, LBM costs a large amount of memory footprint. Therefore, the threshold calculating from the 2D histogram based k-means clustering method is performed as the key parameter to segment volume data-set to address the first problem.

4.2 LBM methodology and parameter

In this section, the most common lattice Boltzmann model is used. It is based on a linearized BGK collision term, as shown in Eq.4.1 [GE et al., 2017]:

$$f_i(\vec{r}+\Delta r, t+\Delta t) - f_i(\vec{r}, t) = \Omega_i \tag{4.1}$$

and with BGK expression of Ω_i

$$f_i(\vec{r}+\Delta r, t+\Delta t) - f_i(\vec{r}, t) = -\frac{1}{\tau}[f_i(\vec{r}, t) - f_i^{eq}(\vec{r}, t)] \tag{4.2}$$

where f_i represents the discrete distribution function and corresponds to a grey-level value at each node linked to image pixel, and $f_i(\vec{r}+\Delta r, t+\Delta t)$ is particle distribution function in each node $\vec{r}+\Delta r$, and at time $t+\Delta t$; Δr and Δt correspond to space and time steps. $f_i^{eq}(\vec{r}, t)$ is the discrete equilibrium distribution function at node $\vec{r}$ at time t. τ is the relaxation time. LBM is an iterative method performed via successive steps. The first one is the streaming of distribution of particles f_i and the second is the collision phase of f_i at each node of the lattice.

Anisotropic diffusion equation plays an important role in the application of the partial differential equation for image processing. However, there is rare reports about LBM for resolving the anisotropic diffusion equation.The mathematical deduction in chapter 3 shows that the global equation of this model and the diffusion reaction equation are very similar. In this chapter, a lattice Boltzmann anisotropic diffusion model with a specific diffusion resource is proposed. The specific diffusion

resource is shown in Eq.4.3 where the collision function Ω_i is implemented as a reaction-diffusion equation [Chen, 2009]:

$$f_i(\vec{r} + \delta\vec{e_i}\vec{r}, t + \Delta t) = f_i(\vec{e_i}\vec{r}, t) + \frac{1}{\tau}[f_i(\vec{e_i}\vec{r}, t) - f_i^{eq}(\vec{e_i}\vec{r}, t)] + R(T, \rho). \tag{4.3}$$

ρ represents the density of the fluid with $\rho = \sum_i f_i$ on each node. $\vec{e_i}$ is the LBM DdQm model which uses the form of the equilibrium distribution function.There are some differences in the LBM model in 2D as mentioned in section 3 of Chapter 2. T is the threshold. Briefly, the reaction-diffusion LBM solves a reaction-diffusion equation at a microscopic scale. R is diffusion resource in Eq.4.4:

$$R(T, \rho) = a\Delta t[T - \rho(\vec{r})] \tag{4.4}$$

where $R(T, \rho)$ represents the reaction-diffusion resource term(the extra force) in the model [Wang et al., 2016]; T is the threshold calculated from 2D histogram-based k-means clustering method; the algorithm of computing the threshold value T is presented in Section 4.3.

4.3 2D histogram based LBM segmentation method

In the context of TF, the successive iterations of the algorithm lead to finding the appropriate configuration for volume rendering. These one-dimensional TFs solely consider the intensity values of the image, which indicates that all voxels sharing the same intensity values are rendered in the same way. In order to find a way to distinguish those voxels, additional image properties can be taken into account for generating multi-dimensional TFs. One such property is gradient magnitude which can be easily derived from the original image data. How to select voxels with a specific combination of intensity and gradient magnitude values remains challenging. To this end, the 2D Intensity Gradient Magnitude (IGM) histogram [Cai et al., 2013] should reveal several singularities to make it easier to cluster the considered image. Typically, the x-coordinate is intensity; the y axis gradient presents magnitude, and the 2D bin brightness of the 2D histogram is the frequency showing the number of voxels with a specific combination of intensity and gradient size. Fig.4.1 shows two examples of 2D IGM histograms of two aneurysms.

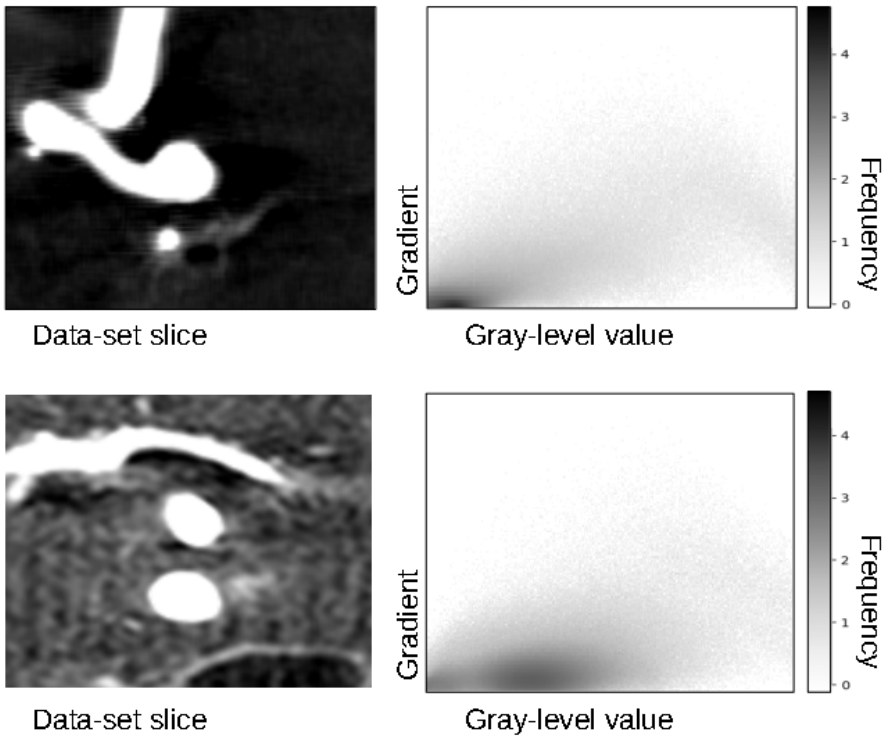

Figure 4.1: Cerebral aneurysm 2D IGM histogram: (1) first aneurysm 2D slice, (2) IGM histogram of the first aneurysm , (3) second aneurysm 2D slice, (4) IGM histogram of the second aneurysm.

For classifying the 2D IGM, the classification method is proposed. Classification methods are mainly considered as three types of approaches that contain supervised, semi-supervised and unsupervised classification. In the first case, classes or labels of certain objects are known in advance to define the training set, and an algorithm is used to obtain the classification criteria. Semi-supervised classification deals with training the algorithm by both labelled and unlabelled data. They are commonly used when manual labelling of a data-set becomes expensive. Finally, unsupervised classification currently called clustering consists of defining classes from the data without knowing the class labels. The objective is to identify classes of objects or clusters, which are more similar to each other than other clusters. Such an approach to data analysis is closely related to the creation of a data model. That is to say, defining a simplified set of attributes can provide an intuitive explanation of the relevant aspects of the data set.. Clustering methods [Guha et al., 2001] are generally more demanding than supervised approaches [Jing et al., 2007] [Camastra and Verri, 2005], but they provide more information on complex data. Current work generally focuses on the clustering method [Lloyd, 2006].

4.3.1 k-means clustering

The K-means clustering is a hard-clustering unsupervised algorithm [MacQueen, 1967], which represents a typical strategy of the prototype-based objective function clustering methods. K-means clustering is utilized for importance curves clustering [Wang et al., 2008]. In our algorithm, the K-means clustering method is used to compute the threshold for clustering tissues in volume data-set. The basic k-means clustering pipeline is shown in Fig.4.2. Eq.4.5 is the k-means formula of minimizing within-cluster distance.

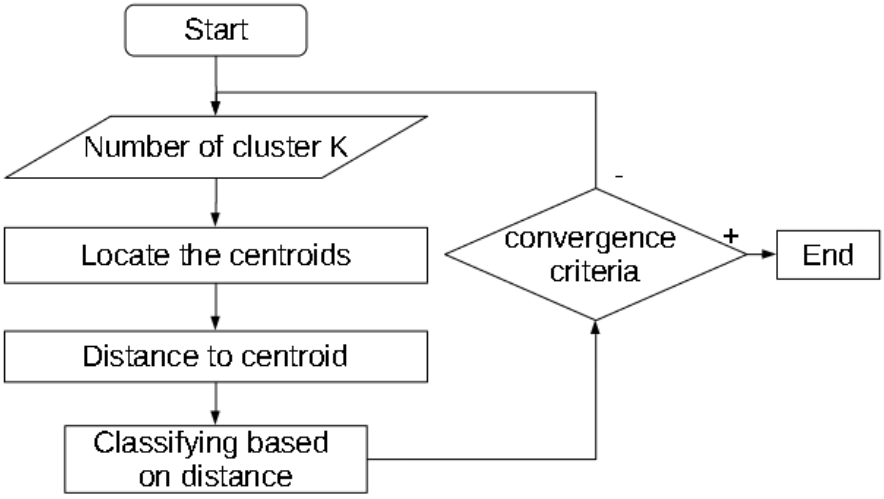

Figure 4.2: K-means algorithm pipeline.

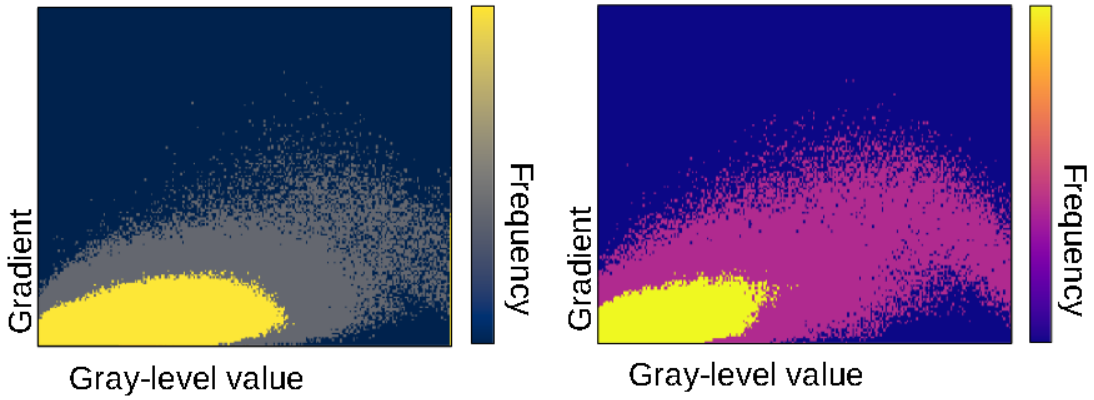

Figure 4.3: Two cerebral aneurysm data-set clustered 2D IGM histogram example.

$$\arg\min_{C} \sum_{j=1}^{k} \sum_{\rho \in C_j} |\rho - m_j|^2 , T_j = m_j \tag{4.5}$$

where ρ is the grey-level value of volume data-set; m_j is the average value of the class C_j. T is the threshold which is the parameter of LBM reaction diffusion equation in Eq.4.4. Fig.4.3 shows two aneurysm cases computing the threshold using the 2D histogram based k-means clustering method.

4.3.2 Segmentation algorithm methodology

Medical imaging makes great contributions to the detection and analysis of brain aneurysm of patients. In light of this, computed tomography angiography (CTA) can provide a diagnosis for the care and follow-up of patients with brain aneurysms. In this chapter, the studied aneurysm is recorded on 464 slices with a 3D CTA scan (Fig.4.4) and issued from the data base of the Thrombus project (FP7-269966). A brain aneurysm is a vascular disorder as a small hernia due to weakened blood vessel walls, which occur mainly at the bifurcation of blood vessels. An aneurysm may rupture and thus lead to a subarachnoid hemorrhage with the consequence of high mortality rates sometimes. Many projects work on the analysis and treatment of brain aneurysms, and specific needs are required to estimate the evolving of an aneurysm after endovascular treatment. In this framework, image processing techniques such as volume rendering bring essential means of patient follow-up.

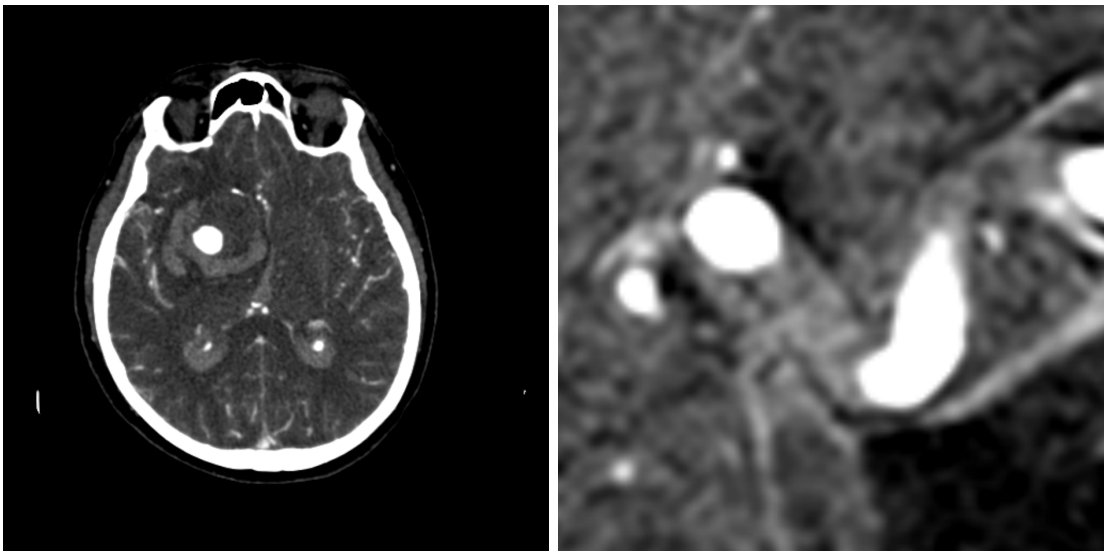

Figure 4.4: CT scan of cranial (left) and cerebral aneurysm (right).

Fig.4.5 exhibits a synoptic of our LBM-based k-means clustering algorithm design method for medical image segmentation. Two major algorithms in our segmentation algorithm are LBM and K-means clustering methods.

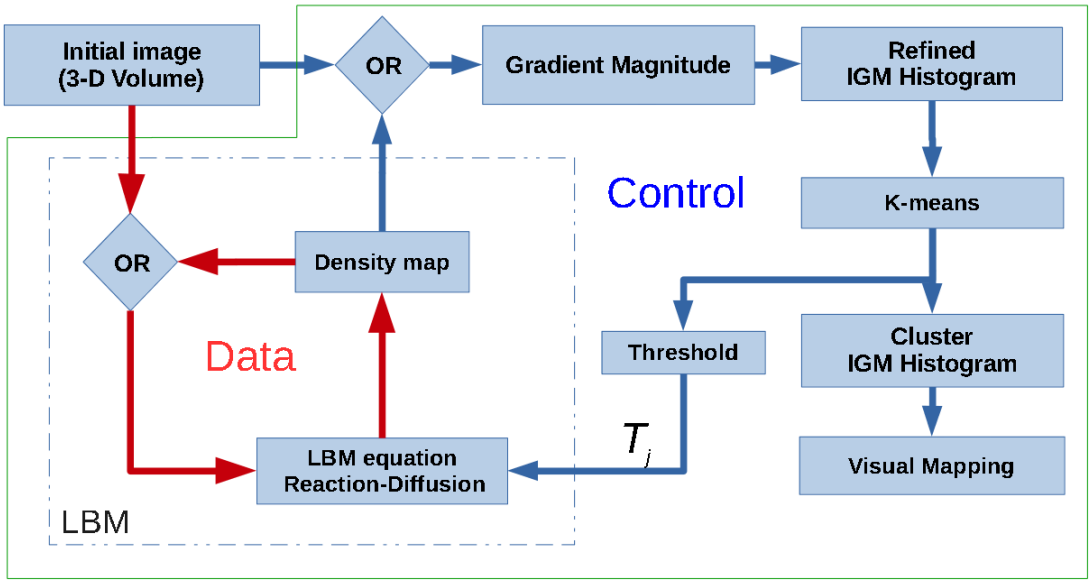

Figure 4.5: Matching LBM and k-means clustering method.

Using the gray value of each pixel in the image or volume data set, the gradient of each pixel or voxel can be calculated using the gradient function in Eq.4.6 :

$$\bigtriangledown f(x_0, x_1, ..., x_n) = (\frac{\partial f}{\partial x_0}, ..., \frac{\partial f}{\partial x_j}, ..., \frac{\partial f}{\partial x_n}). \tag{4.6}$$

In the proposed algorithm, the norm of the gradient vector at each voxel is computed by Eq.4.7:

$$|\bigtriangledown f| = \sqrt{(\frac{\partial f}{\partial x_0})^2 + ... + (\frac{\partial f}{\partial x_j})^2 + (\frac{\partial f}{\partial x_n})^2}. \tag{4.7}$$

The 2D IGM histogram is constructed with two synthetic data-sets, which are gradient and grey-level values. Then, using the density map generated in each LBM iteration, the K-means clustering algorithm clusters the classes in the volume and then calculates the optimal threshold to distinguish the living tissues. These thresholds are addressed to the LBM block in Fig.4.5 for solving a reaction-diffusion equation at a microscopic scale. This innovative segmentation scheme continuously iterates and modifies the data-set. With the refined data-set, the 2D IGM histogram is computed at each iteration until meeting the iteration convergence. Next, the IGM is clustered into several regions, and each region corresponds to a specific tissue by K-means the algorithm. Subsequently, the refined IGM and volumetric data-set are applied to render the volume and generate the segmentation result.

4.4 Aneurysm segmentation result

The 2D CTA segmentation result is shown in Fig.4.6 and Fig.4.7. The red contours are superimposed on the original image, which is the boundary of the vessel. The proposed algorithm in this section is used to segment the two patient CTA with 131 slices and 128 slices, respectively, and the results contain ROI.

The proposed algorithm and k-means clustering method is applied to segment 3D cerebral aneurysm sequence in Fig.4.8 and Fig.4.9. Fig.4.8 (top) displays the IGM histogram calculation results of the K-means clustering algorithm (without LBM). It can be seen that the K-means algorithm clusters IGM into two parts, in which the red part is the vessel boundary and the yellow part is the blood within intra-cranial aneurysms and parent blood vessel.

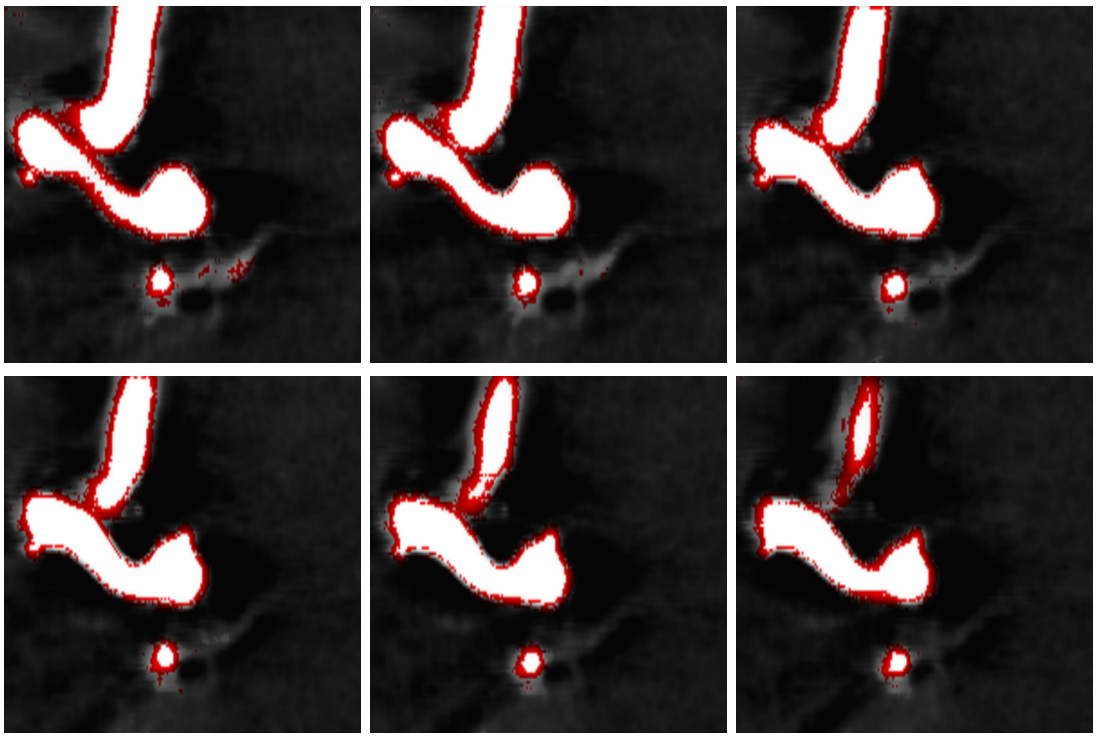

Figure 4.6: The cerebral aneurysm CTA segmentation result of the first patient, which takes six slices of cerebral aneurysm as examples of 2D segmentation. The red part is the vascular borders, the white part refers to the interior of the vessel. The black and gray parts correspond the other tissues.

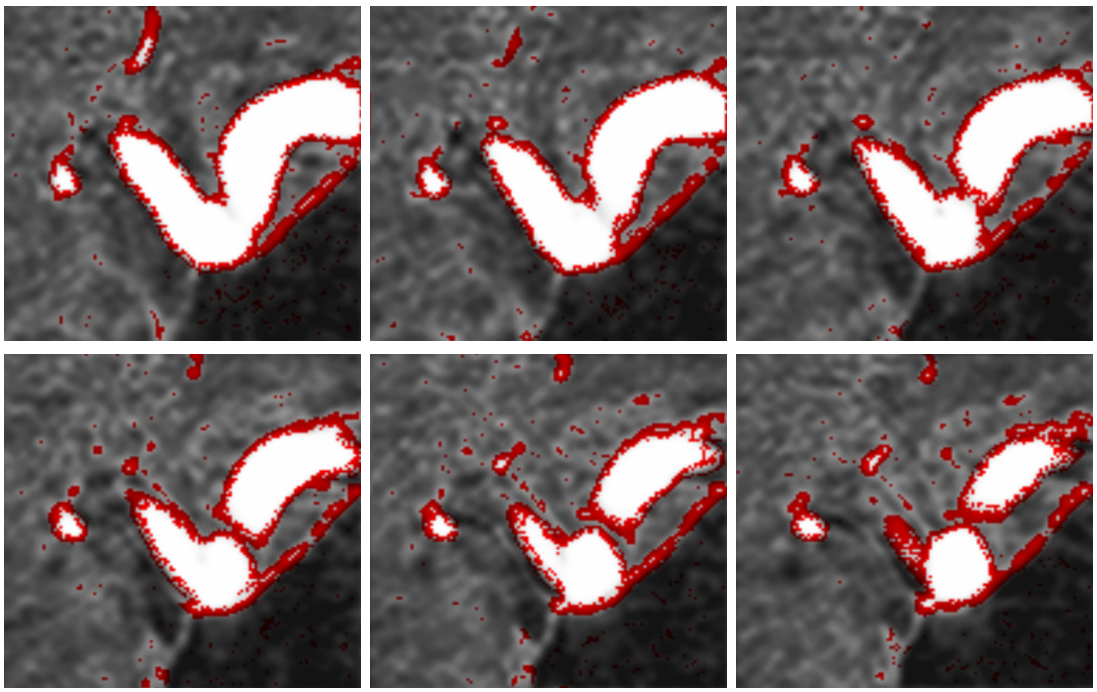

Figure 4.7: The cerebral aneurysm CTA segmentation result of the second patient, which takes six slices of cerebral aneurysm as examples of 2D segmentation. The red part is the vascular borders, the white part refers to the interior of the vessel. The black and gray parts correspond the other tissues.

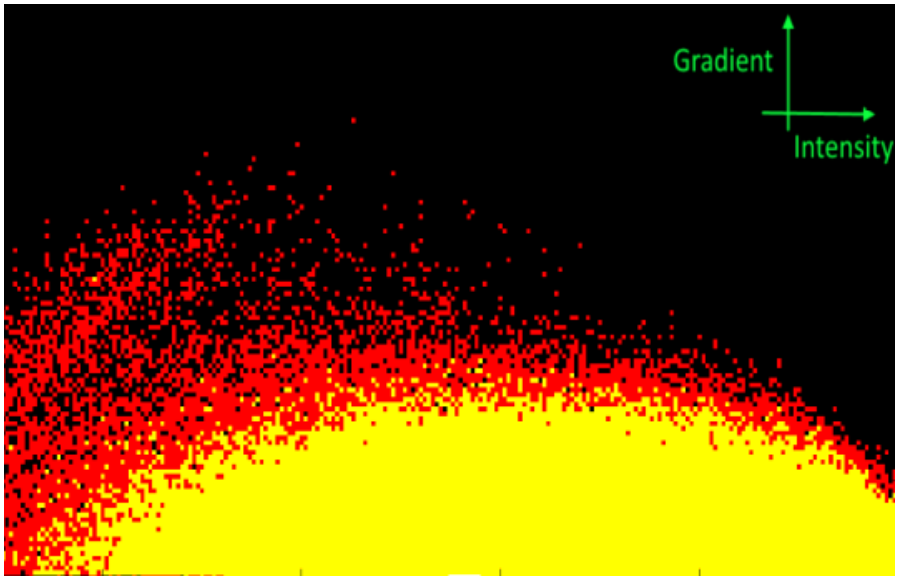

Figure 4.8: IGM histogram clustering result without LBM, which is classified to 2 cluster (red part and yellow part).

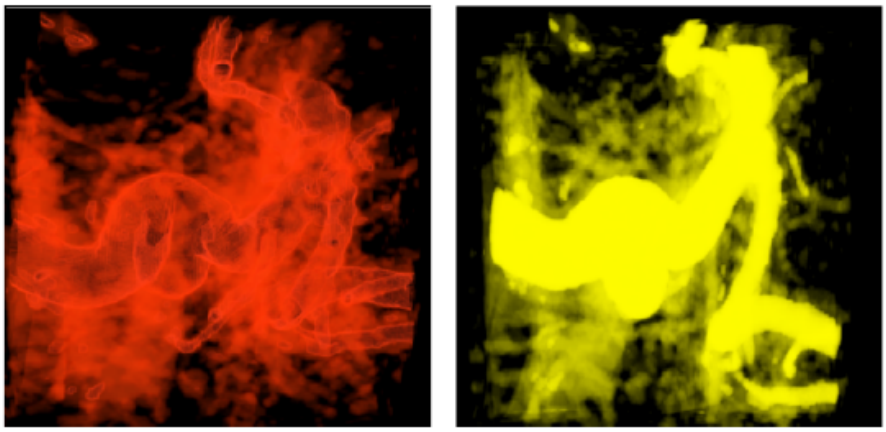

Figure 4.9: Clustering result without LBM, the parent vessel (red) and lumen part of a blood vessel (yellow).

Fig.4.10 displays the IGM histogram of the proposed method with LBM. It can be seen that the data-set is less sensitive to noise than without LBM compared to the results in Fig.4.11. The volume rendering results are more distinctive and clearer than Fig.4.9. The underlying objective is to reveal arches within 2D IGM histogram in order to detect different living tissues in medical images via LBM [Wu and Qu, 2007]. Based on one threshold T issued from K-means, the solving of the reaction-diffusion equation via LBM can reveal several arches. In this example, the yellow arches correspond to the blood, and the red arches represent the parent vessel.

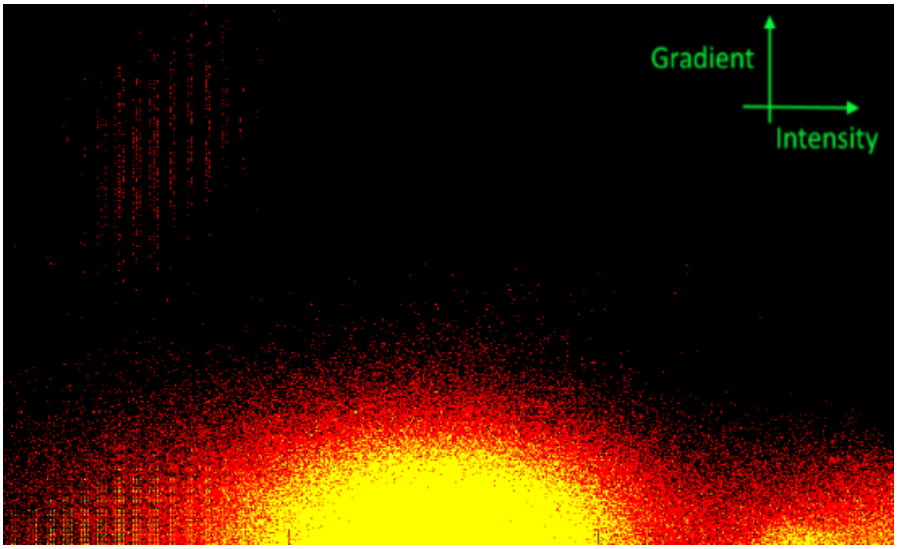

Figure 4.10: IGM histogram clustering result with LBM, which is classified to 2 cluster (red part and yellow part).

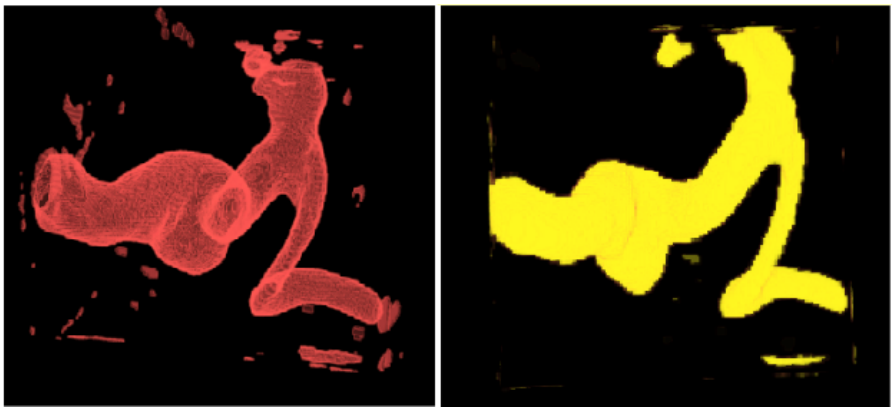

Figure 4.11: Clustering result with LBM, the parent vessel (red) and lumen part of a blood vessel (yellow).

4.5 Conclusion

This chapter presents a new segmentation algorithm in which reconstruct the reaction diffusion equation at a mesoscopic scale via the LBM method leads to the optimization of a consistent volume rendering method in regard to the complexity of the cranial medical images with cerebral aneurysms. The promising potential of the proposed method lies in the using of several thresholds, updated along with the successive iterations of the LBM code, which leading to the concept of dynamic clustering of medical images sequences and improving the calculation efficiency.

Chapter 5

Lattice Boltzmann multi-thresholds method design

Abstract

In the image processing domain, the Lattice Boltzmann method is basically implemented for segmentation by solving a reaction-diffusion equation which only considers one threshold. In this chapter, an innovative multi-thresholds collision function is elaborated, a new formulation of the lattice Boltzmann method for 2D image and 3D volume data-set clustering is proposed, where the threshold is fixed by the clustering method. In order to test its effectiveness, 2D natural images and 3D medical volume data-sets are segmented and the performances are validated by the Dice similarity coefficient, Relative volume difference and Hausdorff distance. Compared to the 3D visual perception and quantitatively, the results of the proposed method are superior to those of the existing methods for dealing with the stent-assisted intra-cranial aneurysm. As an alternative, a LBM-based segmentation method is constructed through an innovative multivariate collision function for clustering 3D volume data-sets. The centroids of the collision function are still determined by 2D histogram-based k-means clustering algorithm. According to this new concept, the cranial volume data-set and brain aneurysm sequence are segmented to evaluate the performances. The experimental validation of this concept is performed by the Dice similarity coefficient and Hausdorff distance.

Résumé

Dans le domaine du traitement d'images, la méthode de Boltzmann sur réseau est essentiellement mise en œuvre pour l'opération de segmentation en résolvant une équation de réaction-diffusion prenant en compte un seuil couramment calculé via la méthode d'Otsu. Dans cette thèse, une fonction innovante de collision multi-seuils est élaborée, qui aboutit à une nouvelle formulation de la méthode de Boltzmann sur réseau pour le partitionnement d'images 3D, les seuils étant fixés par la méthode de partitionnement. Les performances sont validées en segmentant des images angiographiques par tomographie tridimensionnelle (3D), et sont évaluées par calcul du coefficient de similarité de Dice, la différence de volume relatif et la distance de Hausdorff. En comparant à partir de la perception visuelle 3D et quantitativement, les résultats de la méthode proposée sont supérieurs aux méthodes existantes pour traiter les anévrismes intracrâniens traités par stent. Comme alternative, une fonction de collision multivariée innovante est développée, contribuant à une nouvelle formulation de la LBM pour partitionner des données volumiques 3D. Les centres de gravité de la fonction de collision sont déterminés par l'algorithme de partitionnement par k-moyennes via un histogramme 2D. Selon ce nouveau concept, l'ensemble des données sur le volume du crâne et la séquence de l'anévrisme cérébral sont segmentés pour évaluer la performance. La validation expérimentale de ce nouveau concept est effectuée en calculant le coefficient de similarité de Dice et la distance de Hausdorff.

5.1 Introduction

In this chapter, a LBM-based segmentation algorithm is proposed using multiple thresholds calculated by the K-means clustering method. Firstly, the methodology pipeline of Lattice Boltzmann multi-thresholds method algorithm (LBMTM) is presented in Section 5.2.1. Secondly, the design of the multi-thresholds clustering collision function is given in Section 5.2.2. Thirdly, data sources consist of 2D images data-set and 3D volume data-sets segmentation experiments, and the results are presented in Section 5.3.1. Thereafter, evaluation methods are introduced to validate the segmentation results by the proposed algorithm, which are used to calculate the differences between the segmentation result and reference. To test the accuracy of the new approach, three types of evaluation function, including Dice similarity coefficient (DSC), Relative volume difference (RVD) and Hausdorff distance, are discussed in Section 5.3.2. Afterwards, the LBMTM is applied to segment data source including 2D images and 3D volume data-set, and the segmentation result is presented in Section 5.3.3. In addition, the proposed method is compared with the Chan-Vese algorithm and K-means clustering methods in Section 5.3.2 by the segmentation result of 3D volume data-set, respectively. This contains cranial, cerebral aneurysm and stent-assisted aneurysm, and is presented at the end of Section 5.3.3.

5.2 Segmentation framework design

While applying the proposed method in Chapter 4 to segment a more complex volumetric data-set, it is found that the method in the last chapter does not show ideal accuracy and computational performance. There are two mainly purposes of our method:

- The definition of nearby diffuse objects (lumen, stent, boundary and the whole aneurysm).
- The segmentation result should have high contrast in the whole volume.

5.2.1 Segmentation methodology pipeline

However, the two purposes conflict with each other when dealing with diffuse objects. After applying LBM segmentation on the whole volume, it is impossible

to segment the diffuse objects especially after the placement of the stent. Herein, a Lattice Boltzmann multi-threshold method is introduced to increase the contrast among the diffuse objects and segment the different tissues from volume data-set. Fig.5.1 exhibits the proposed method pipeline for image segmentation.

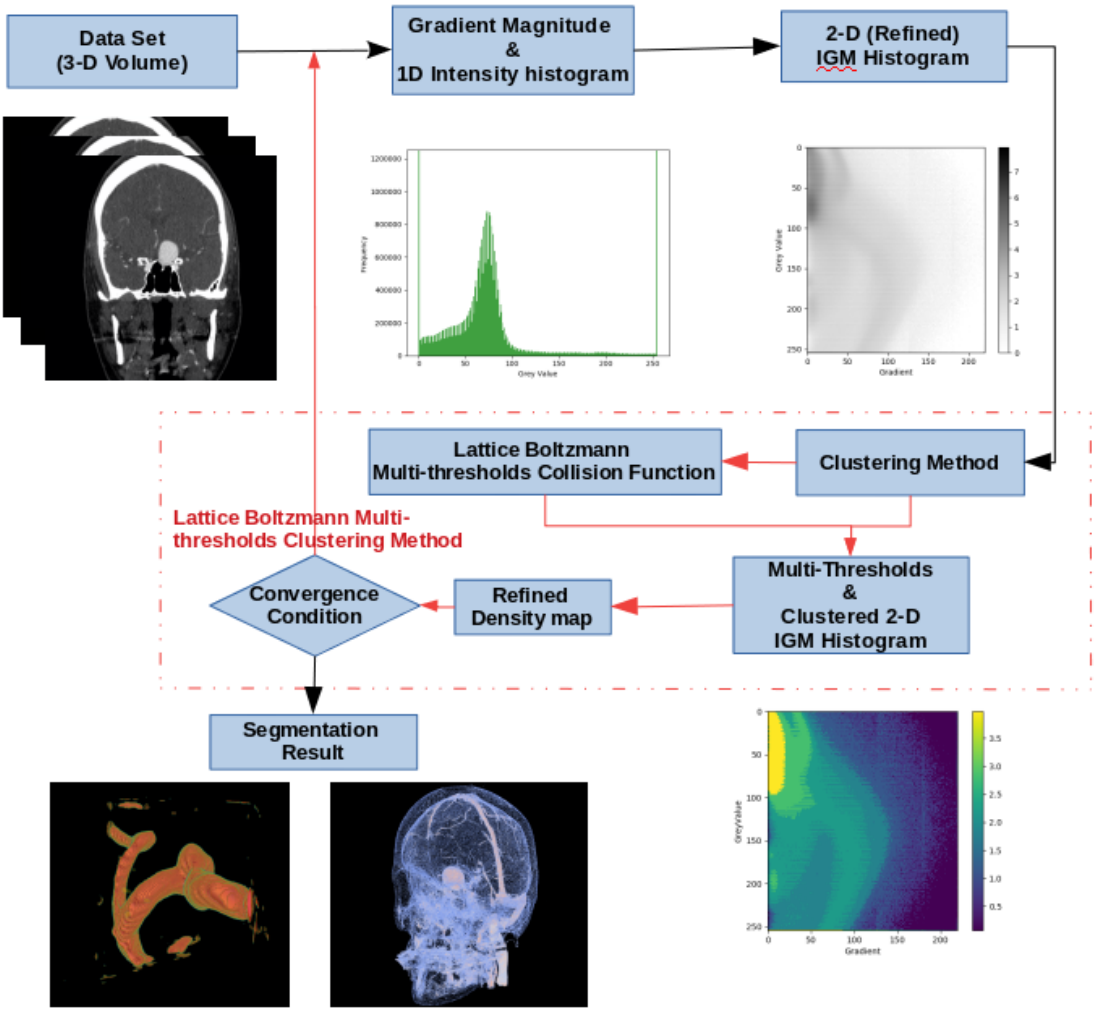

Figure 5.1: Main pipeline of the proposed algorithm.

In the proposed method, the grey-level value from the whole volume data-set of CT scan is firstly conduced to get the density map and gradient magnitude on each voxel; Thereafter, a 2D intensity-gradient magnitude histogram (IGM histogram) with the density map and gradient magnitude is produced. By applying the IGM histogram as the input of the clustering algorithm, the clustered IGM histogram and the threshold of different clusters can be obtained. The application of thresholds contributes to the LBM reaction-diffusion function, and the optimized density map is obtained for the data visualization or as the input volume of the

next iteration.

By introducing the clustering algorithm, thresholds are continually optimized to differentiate living tissues. These thresholds are addressed to the LBM block (Fig.5.1) which is implemented for dealing with a reaction-diffusion equation at a microscopic scale for the purpose of image processing. This innovative method continuously iterates and modifies the data-set. With the refined data-set, the IGM is clustered into several regions, and each region corresponds to a specific tissue. Subsequently, the refined IGM and volumetric data-set are applied to render the volume and generate the segmentation result.

5.2.2 Multi-thresholds clustering collision function design

To remove the staggered invariants in LBM models, Qian [Qian, 1997] proposed to use *fractional propagation* as an effective strategy for suppressing undesired invariants. During the propagation step, the updating procedure is described as follows:

$$f_i(\vec{r}+\Delta r, t+\Delta t) = (1-g_i(\vec{r}))f_i(\vec{r}+\Delta r, t) + g_i(\vec{r})f_i(\vec{r}, t) \tag{5.1}$$

where g_i ,the possibility of one voxel to go through the encountered medium, describes the *fractional propagation*, which is based on encountered medium values from 0 to 1. In this algorithm, $g_i = 1$. [Chen, 2009] suggested a diffusion resource based on Eq.5.1, and the LBM evolution equation is expressed as Eq.5.2,

$$\begin{aligned} f_i(\vec{r}+\Delta r, t+\Delta t) &= f_i(\vec{r}, t) + \frac{1}{\tau}[f_i^{eq}(\vec{r}, t) - f_i(\vec{r}, t)] \\ &+ R(\rho, T) \end{aligned} \tag{5.2}$$

where ρ represents the grey-value on each node. In chapter 5, only one threshold [Wang et al., 2016] calculated and fit into the LBM-based segmentation framework. Especially when segmenting the complex data-set (data-sets with multiple tissues), the result is not ideal. Herein, the collision function of LBM proposed in a specific version, $R(\rho, T)$ represents the new collision term (the extra force) in the LBM model [Wang et al., 2016]. In the novel algorithm, multiple threshold value T_j is replaced the original T , as shown in Eq.5.2.

$$f_i(\vec{r}+\Delta r, t+\Delta t) = f_i(\vec{r}+\Delta r, t) + \frac{1}{\tau}[f_i^{eq}(\vec{r}+\Delta r, t) - f_i(\vec{r}+\Delta r, t)] + R(\rho, T_j) \tag{5.3}$$

where $f_i(\vec{r}+\Delta\vec{r}, t+\Delta t)$ corresponds to the grey value distribution function at $\vec{r}+\Delta\vec{t}$ at time $t+\Delta t$. $\Delta\vec{r}$ and Δt are sampling interval and time step, respectively. τ is relaxation time ($1/\tau$ is collision frequency). f_i^{eq} is local equilibrium distribution which represents the volume grey-level value distribution function. In this novel algorithm, according to Eq.5.3, a new multi-thresholds collision term is proposed, as shown in Eq.5.4. In terms of reaction function in Eq.5.3, T_j is used as multi-thresholds as the main condition criterion to regulate ρ. However, multiple thresholds T_j are introduced into the algorithm. A new scheme which finds the nearest threshold value is designed in Eq.5.4.

$$R(\rho, T_j) = \alpha(T_m - \rho), \exists m : |T_m - \rho| = min|T_j - \rho| \tag{5.4}$$

where T_m is nearest grey-level value threshold for each pixel. To achieve automatically segmentation at different forms, T_j by histogram-based K-means hard-clustering algorithm is obtained, which is a representative of the prototype-based objective function clustering methods. And $\alpha = \frac{2}{1+\frac{1}{1+\nabla\rho}}$ is a non decreasing function to ensure the propagation procedure enhance the contrast at boundary as shown in Fig.5.2. 2D histogram-based K-means clustering is utilized for the importance curve clustering [Wang et al., 2008]. In the proposed method, the clustering method aims to compute the thresholds for clustering tissues in volume data-set. The clustering algorithm is described as follows,

$$\arg\min_{T} \sum_{j=1}^{k} \sum_{\rho \in T_j} |\rho - m_j|^2, T_j = m_j \tag{5.5}$$

where ρ is one voxel of volume data-set; m_j is the center value of class T_j. (ρ and m_j are both multidimensional variables). T_j is the thresholds that are used as parameters of LBM segmentation.

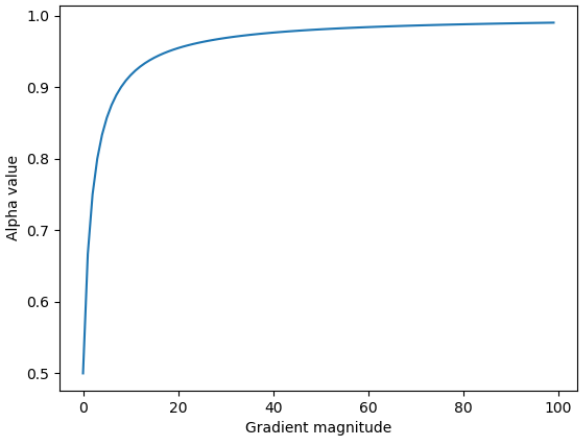

Figure 5.2: The α non-decreasing function.

5.3 Experiments and results

5.3.1 Application data

The proposed segmentation method was performed on 2D images and 3D volume data-sets, the description are as follows, and the 2D images and slices of 3D volume are shown in Fig.5.3 and Fig.5.4:

2D images: The 2D images we use for validating our proposed segmentation algorithm are derived from the Berkeley segmentation data-set [Martin et al., 2001] that is an open source data-set with hand-labeled segmentation.

Data_ 1: The whole cardiac volume data-set aims to validate the proposed method on different types of medical images. In this chapter, the studied cardiac data-set has been recorded on 320 slices with a 3D CTA scan.

Data_ 2: The whole CT brain volume aims to test our method on the segmentation of the entire brain. In the light of this, computed tomography angiography (CTA) plays a crucial role in providing diagnosis for the care and follow-up of patients with cerebral aneurysms. In this chapter, the studied aneurysm has been recorded on 464 slices with a 3D CTA scan, and it is issued from the data base of the Thrombus project (FP7-269966).

Data_ 3: A brain aneurysm is a vascular disorder as a small hernia due to weakened blood vessel walls, which occur mainly at the bifurcation of blood vessels. An aneurysm may rupture and thus lead to a subarachnoid hemorrhage with the consequence of high mortality rates sometimes. The aneurysm has been recorded on 131 slices with a 3D CTA scan.

Data_ 4: One of the intra-cranial aneurysm treatment methods is to use tubular support(stent) placed temporarily inside a blood vessel, or canal, which can facilitate to aid healing or relieve an obstruction. In this chapter, for precisely locating the vascular stent of the stent-assisted intra-cranial aneurysm, we use patient data which is recorded on 512 slices of 3D CTA scan.

Figure 5.3: The 2D images data-set.

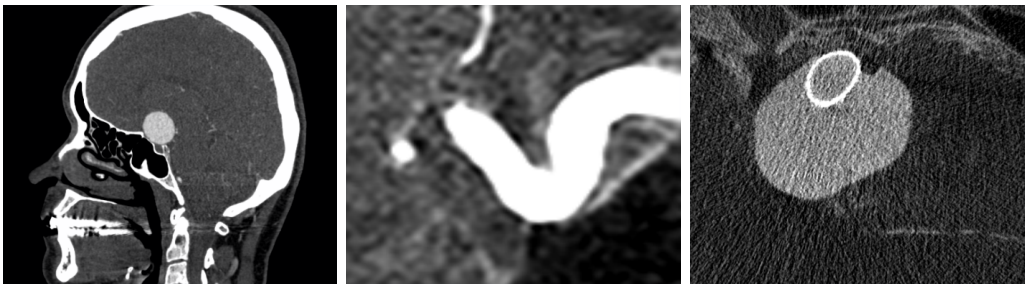

Figure 5.4: Three phases of the treatment of an aneurysm. Left: the CT scan of the head; Middle: locate the position of an aneurysm; Right: stent-assisted aneurysm.

5.3.2 Evaluation Function

In this chapter, Dice similarity coefficient (DSC) [Sørensen, 1948], Relative volume difference (RVD) [Altman and Bland, 1983] and Hausdorff distance [Rockafellar and Wets, 2009] are applied to assess the accuracy of our method [Bernard et al., 2018]. For data set segmentation results V_{sr} and references V_{ref}, the DSC and RVD are defined as:

$$DSC = \frac{2(|V_{sr} \cap V_{ref}|)}{(|V_{ref},| + |V_{ref}|)} \tag{5.6}$$

$$RVD = \frac{V_{sr} - V_{ref}}{V_{ref}} \tag{5.7}$$

where V_{sr} represents the volume of segmentation results, and V_{ref} denotes the volume of references which are manually segmented by clinical doctors. DSC is a magnitude value from 0 to 1 (no match to complete match), and smaller RVD indicates high accuracy. Meanwhile, Hausdorff distance d_H is also calculated to measure the distance between two subsets. The equation for Hausdorff distance is defined as:

$$\begin{aligned} d_H(V_{sr}, V_{ref}) = max\{ & \sup_{V_{sr} \in V} \inf_{V_{ref} \in V} d(V_{sr}, V_{ref}), \\ & \sup_{V_{ref} \in V} \inf_{V_{sr} \in V} d(V_{sr}, V_{ref})\} \end{aligned} \tag{5.8}$$

where sup represents the upper bound(supremum) and inf represents the lower bound (infimum). In this paper we use 3D d_H for evaluate the segmentation result in order to avoid management of missing segmentation problem on end slices.

5.3.3 Segmentation Result

2D images

In this section, the proposed method is compared with the Chan-Vese [Chen et al., 2014] segmentation method from Fig.5.5 to Fig.5.10. The first images are the original one; the second images are segmentation results of the Chan-Vese segmentation method; the third images are the results of the proposed method. The last images are hand-labeled segmentation.

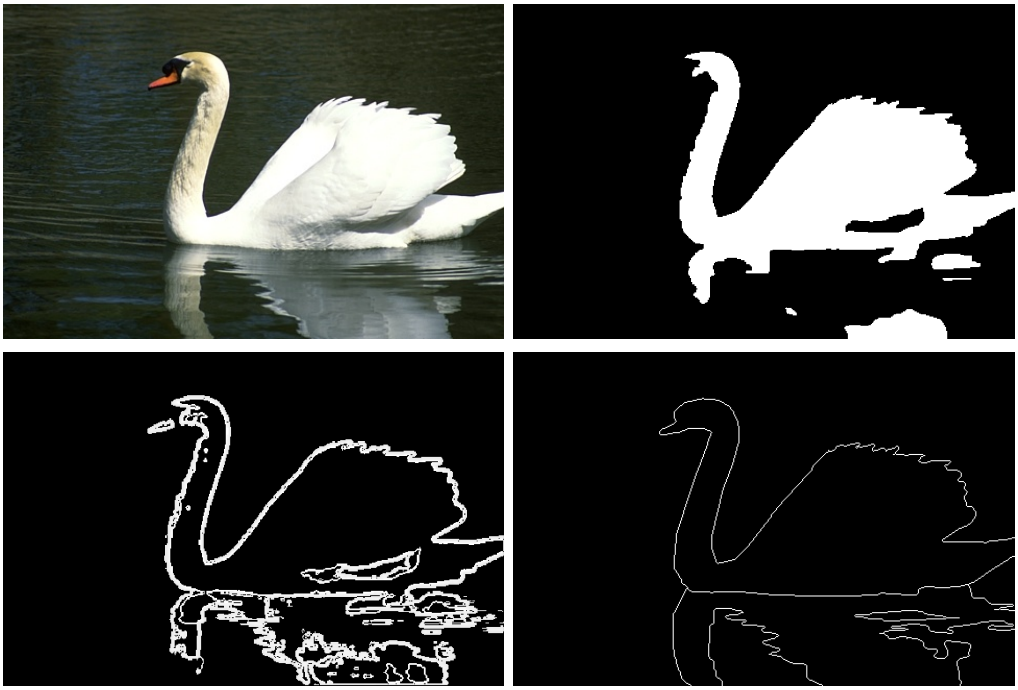

Figure 5.5: 2D image segmentation results: (1) 2D origin image (2) the Chan-Vese method (3) the proposed method (4) reference.

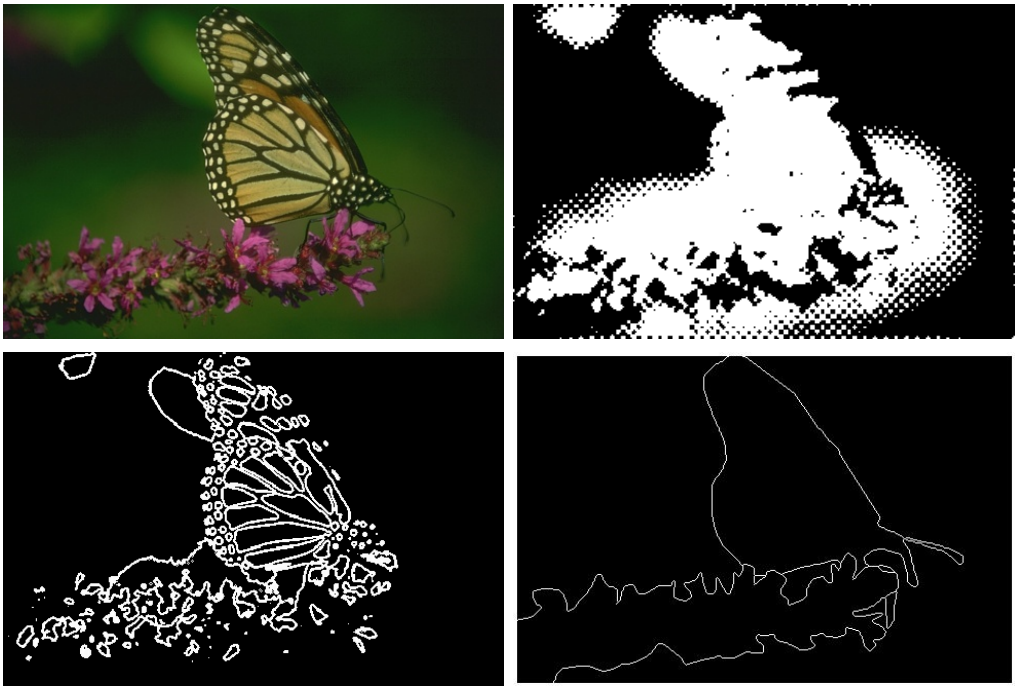

Figure 5.6: 2D image segmentation results: (1) 2D origin image (2) the Chan-Vese method (3) the proposed method (4) reference.

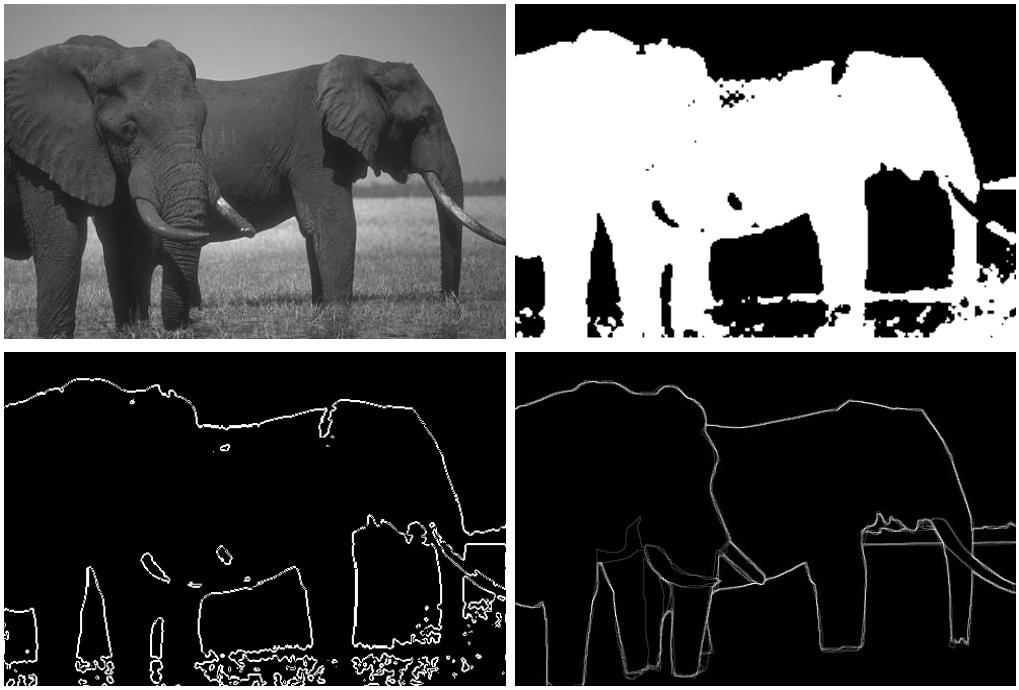

Figure 5.7: 2D image segmentation results: (1) 2D origin image (2) the Chan-Vese method (3) the proposed method (4) reference.

Figure 5.8: 2D image segmentation results: (1) 2D origin image (2) the Chan-Vese method (3) the proposed Method (4) reference.

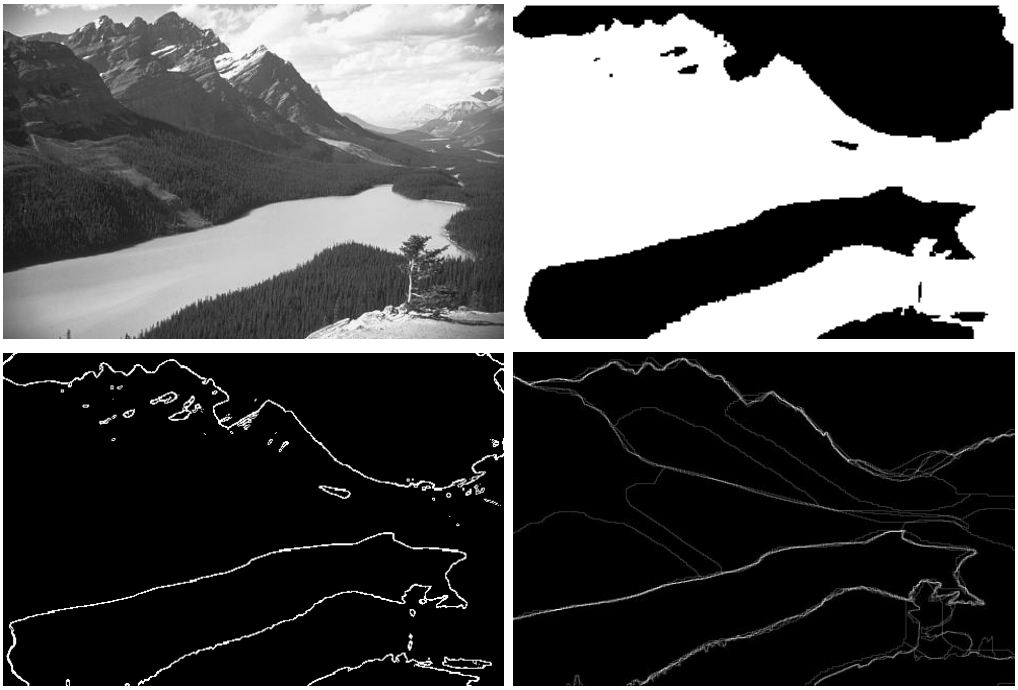

Figure 5.9: 2D image segmentation results: (1) 2D origin image (2) the Chan-Vese method (3) the proposed method (4) reference.

Figure 5.10: 2D image segmentation results: (1) 2D origin image (2) the Chan-Vese method (3) the proposed method (4) reference.

3D volume data-sets

Then, the proposed method on 3D cardiac volume data-set is applied. The implemented parameters of reaction-diffusion function $R(T_j, \rho)$ are thresholds T_j calculated from the 2D histogram with the clustering algorithm in Eq.5.5. Based on all accomplished parameters, the histogram is computed for assessing the amount of the data. Then, for counting the intensity of the data-set, bins of the 2D histogram is computed by the grey-level value and the gradient magnitude calculated on each voxel. X-coordinate is gradient magnitude value, and Y-coordinate is grey-level value in Fig.5.11(1). Then, using the 2D histogram as the input of the the proposed method, the 2D histogram is clustered into *ths* classes by clustering method in Eq.5.5, as showed in Fig.5.11(2). Next, thresholds are used as the key parameters of the multi-thresholds collision function Eq.5.2 and Eq.5.4. Based on *iter* iterations, it can be clearly found that the whole volume is clustered into *ths* clusters. And compared with other parts, the outline of the aneurysm has a high contrast, and it is not difficult to identify nearby diffuse objects.

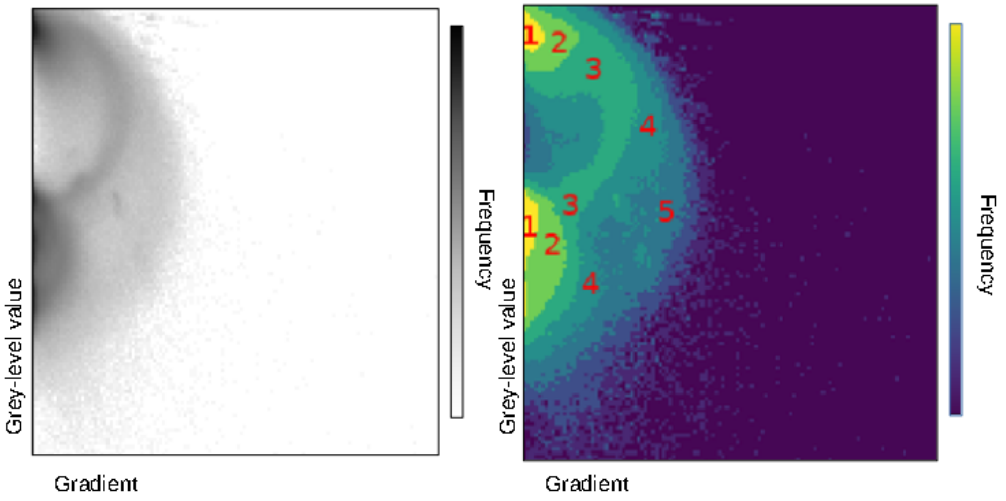

(1) IGM histogram (2) Clustered IGM histogram

Figure 5.11: Cardiac IGM histogram (left) and clustered IGM histogram of cardiac volume data-set (right), each color corresponds to a cluster.

Here, a short implementation of each step on pipeline is constructed to show how we manipulate 2D histogram and apply it for segment 3D cardiac image. The 5 clusters are shown in Fig.5.12(1)-(5), and the corresponding 4 grey-level value thresholds of volume data are 1.3, 5.7, 28.7 and 125.0, respectively.

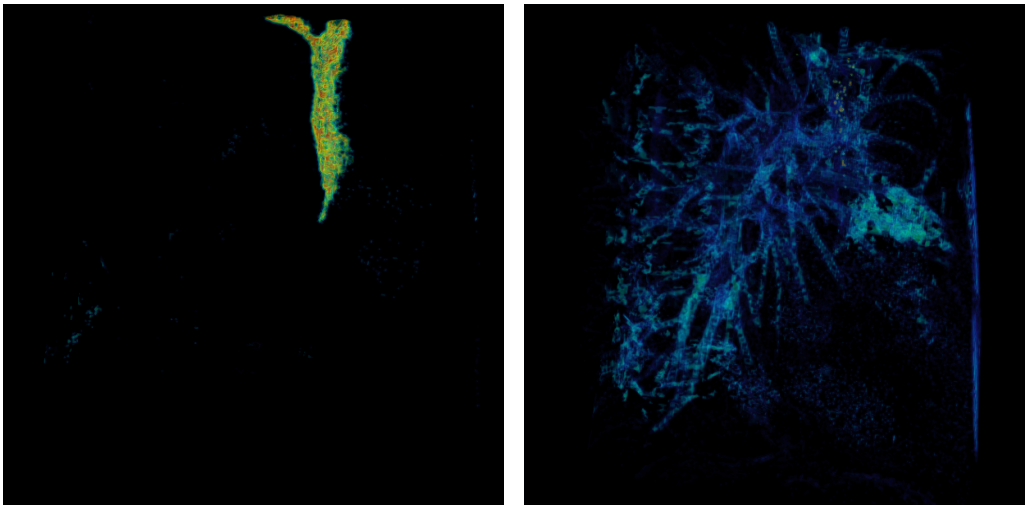

(1) Cluster_1 (2) Cluster_2

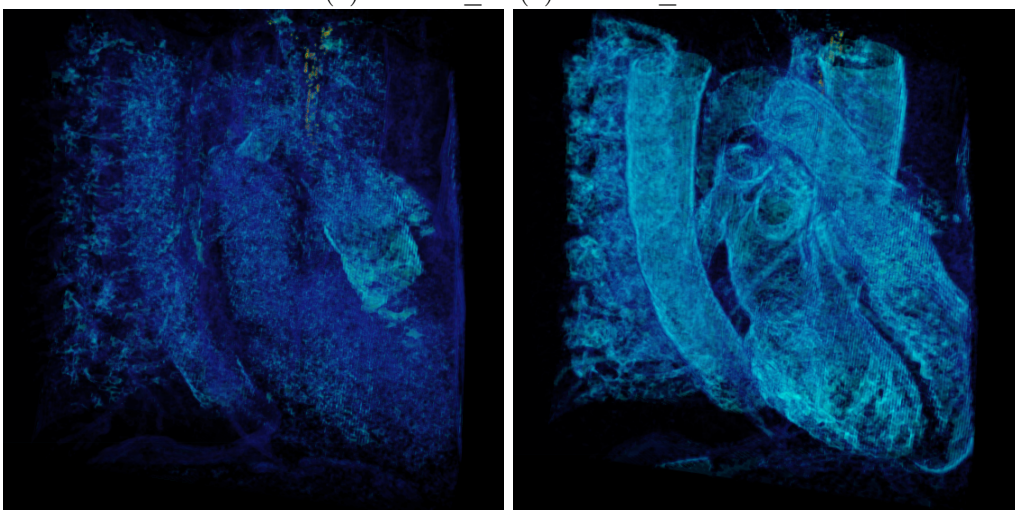

(3) Cluster_3 (4) Cluster_4

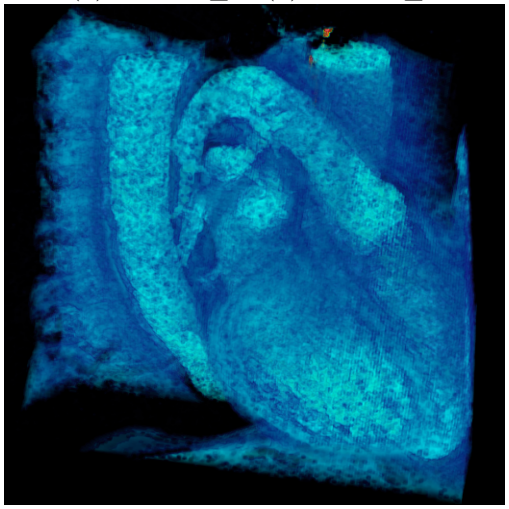

(5) Cluster_5

Figure 5.12: Cardiac volume data-sets segment to five clusters, which correspond to the clusters in Fig.5.11.

Then, we use the proposed method on the 3D volume dataset from dataset-2 to dataset-4, which shows all data in the form of 1D histogram, 2D histogram, and 2D cluster histogram. The histograms in Fig.5.13, Fig.5.15 and Fig.5.17 firstly illustrate the frequency of each grey value (from 0-255). There are two types of the 2D histogram. The first one shows the gradients calculated on each voxel. Based on the grey-level value and histogram, the 2D histogram is generated. The third figure in Fig.5.13, Fig.5.15 and Fig.5.17 are the second type of 2D histogram, calculated by clustering method in which the thresholds are applied as the input parameter of the LBM collision function. Meanwhile, each color corresponds one cluster of the whole volume.

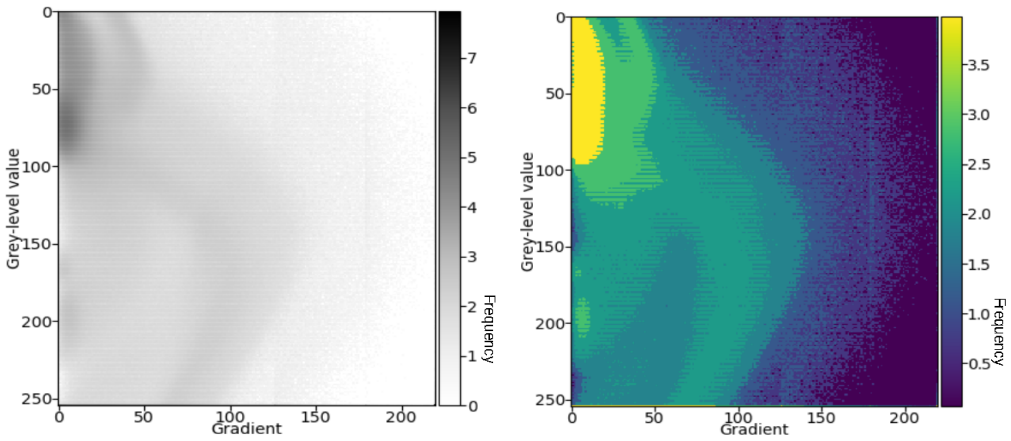

Figure 5.13: Cerebral data-set presented in the IGM Histogram (left) and 2D multi-threshold clustered histogram (right).

The parameters that depend on the histogram and histogram are used as inputs for a multi-threshold LBM. At each iteration of our method, we continuously optimize the grey value of each voxel through multi-thresholds collision function in Eq.(5.4). Hence we can obtain the region of interest(ROI). Fig.5.16, Fig.5.14 and Fig.5.18 correspond to three patient data, respectively. The first images are the origin 3D volumes data-set rendering by hundreds of CT scans slices. The second images are the half-result volumes data-set to make the position comparison with original volume. The third images are the 3D segmentation results, and the fourth images are the slices from 3D segmentation results.

In Fig.5.14, it can be seen that the aneurysm frame is segmented from the CT scan of cranial. After segmenting the aneurysm contour based on the method in the cranial part, we focus our work on the aneurysm local part. In Fig.5.16, we applied our method on the aneurysm part. At the end of the algorithm, we obtain

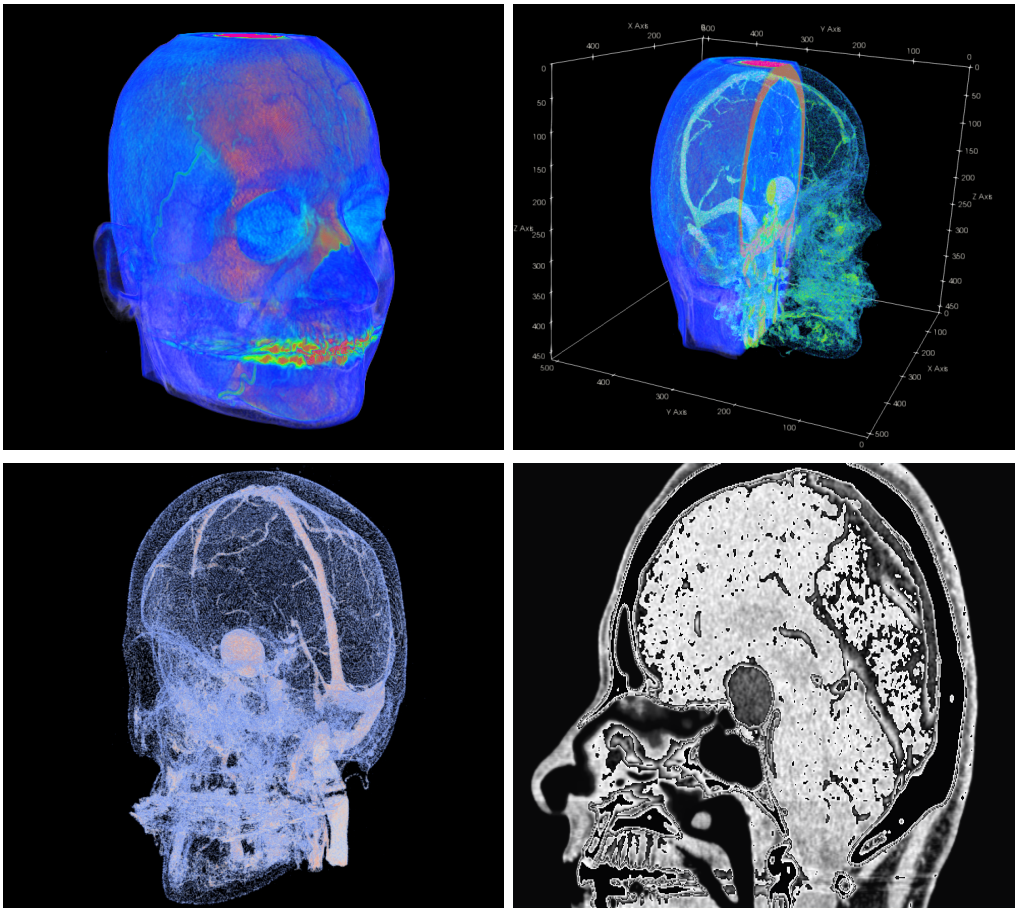

Figure 5.14: Cranial segmentation results: CTA of segmented cranial by using $iter = 2, ths = 7$. (1) Original volume data-set, (2) half-volume data-set in 3D, (3) segmentation result in 3D, (4) segmentation result in 2D.

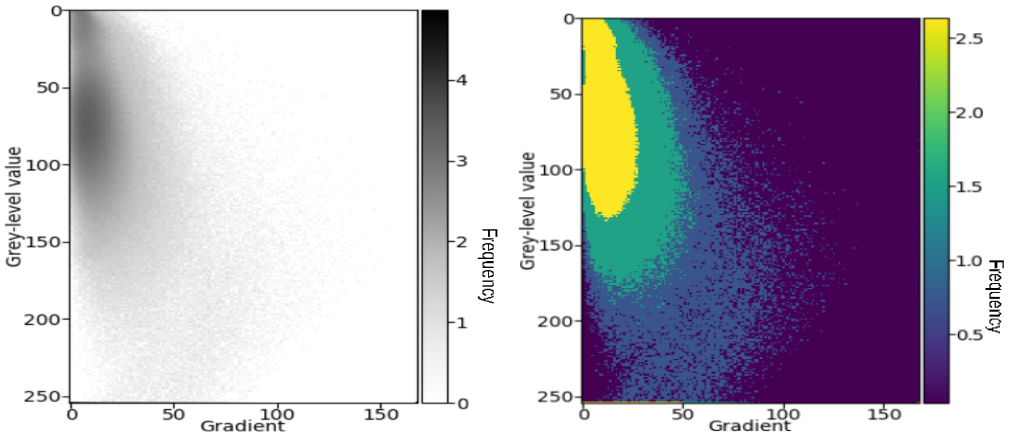

Figure 5.15: Aneurysm presented in the IGM histogram (left) and 2D multi-threshold histogram (right).

the contour by using a non-incremental convex hull algorithm. Then, we applied

the above method to a stent-assisted aneurysm in Fig.5.18. It is noticed that parts of the stent are not that clear especially for the aneurysm part, because the stent and vascular are close to the neighbor tissues in this region.

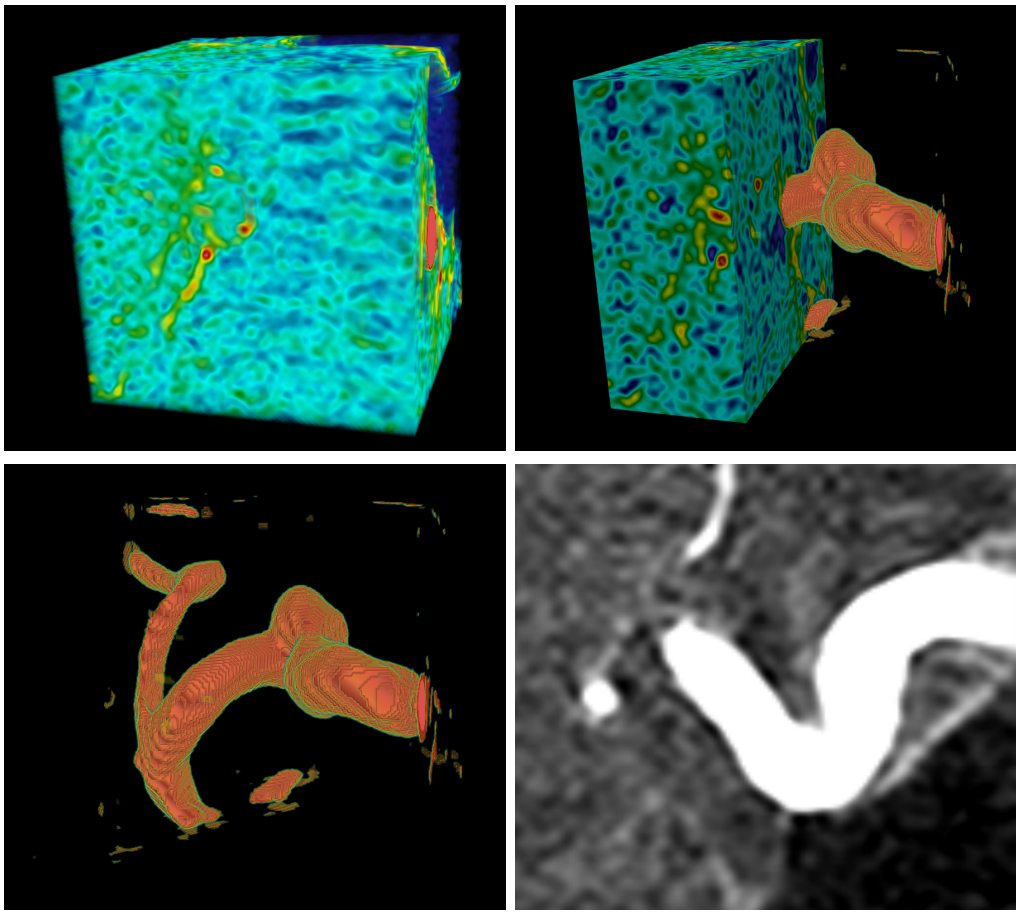

Figure 5.16: Aneurysm segmentation results: segmented aneurysm by using $iter = 3, ths = 4$. (1) Original volume data-set, (2) half-volume data-set in 3D, (3) segmentation result in 3D, (4) segmentation result in 2D.

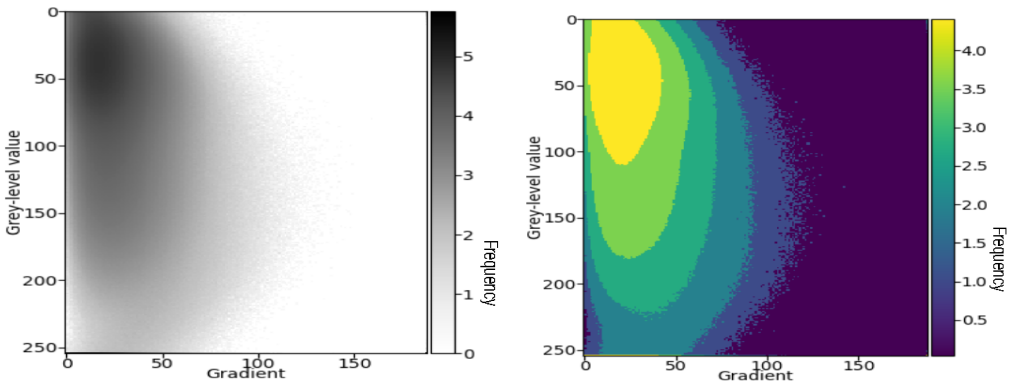

Figure 5.17: Stent-assisted aneurysm presented in the IGM histogram (left) and 2D multi-threshold histogram (right).

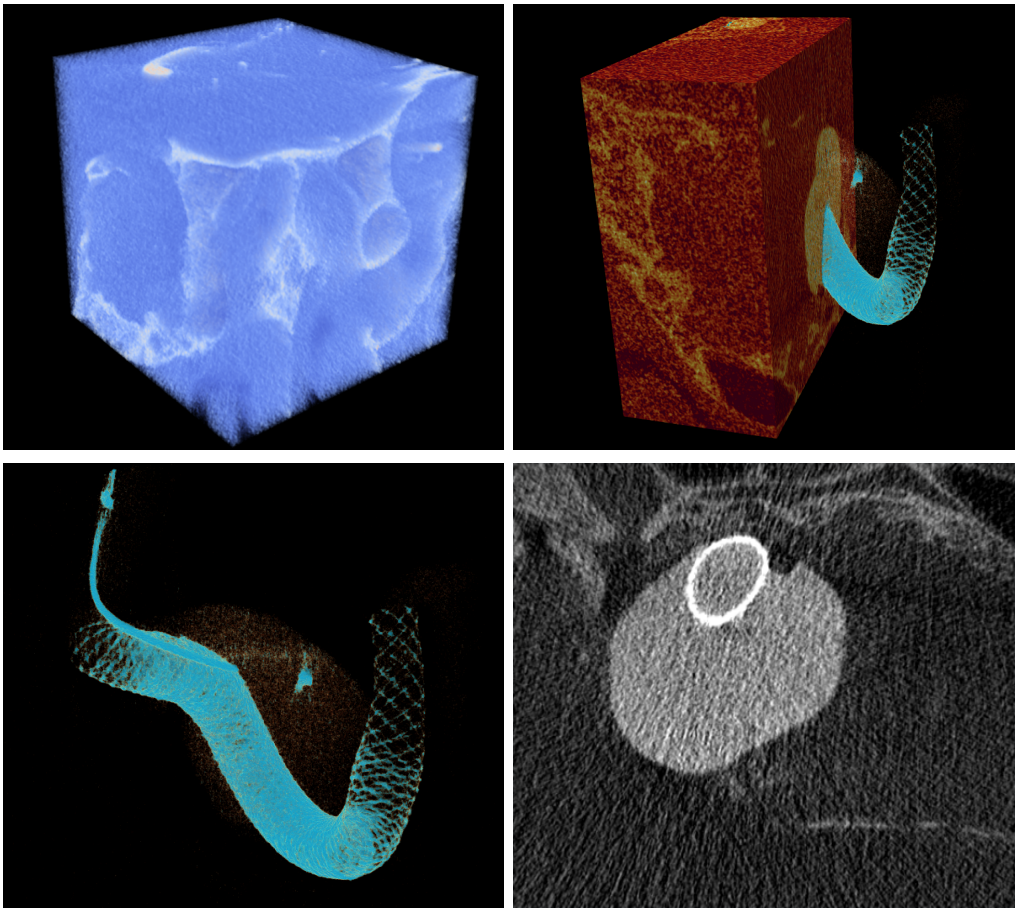

Figure 5.18: Stent-assisted aneurysm segmentation results: the segmented stent-assisted aneurysm by using $iter = 3, ths = 5$. (1) Original volume data-set, (2) half-volume data-set in 3D, (3) segmentation result in 3D, (4) segmentation result in 2D.

To evaluate the multi-thresholds collision function segmentation method, the compared references are the manual segmentation by clinical doctors. Based on these references, the Relative Volume Difference, Dice Similarity Coefficient and Hausdorff Distance can be calculated, and results are displayed in Tab5.1. The segmentation results of stent-assisted aneurysm 512 slices are validated by the Hausdorff distance, it shows in Fig.5.20. It should be noted that all these three evaluation methods are based on the 3D scale,and the mistake errors are magnified when comparing with 2D slices errors. The DSC values, which are greater than 60%, are quite acceptable in the 3D scale. Furthermore, the data sets are used to compare with the Chan-Vese's model [Chan et al.,], 2D histogram clustering method and the proposed model. Tab.5.1 summarized detail information of each model; Fig.5.16, Fig.5.14 and Fig.5.18 show cases. The different segmentation method results of intra-cranial aneurysm are 0.89, and 0.6732 in terms of the Dice similarity coefficients, 0.0010, and 0.0183 in terms of the Relative volume differ-

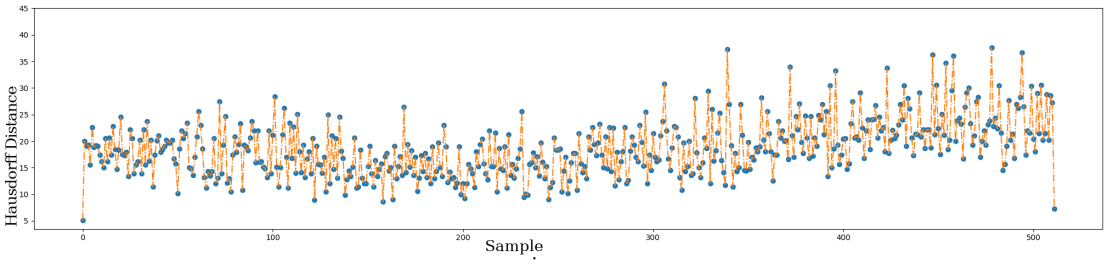

Figure 5.20: Hausdorff distance values of 512 stent-assisted aneurysm slices.

ence, 32.2491, and 64.5058 in terms of the Hausdorff Distance. The segmentation results of stent-assisted intra-cranial aneurysm are 0.0551, and 0.8245 in terms of the Dice similarity coefficients, and 0.0684 in terms of the Relative volume difference, and 12.0830 in terms of the Hausdorff Distance. The results reflect that the proposed method shows better accuracy when dealing with a stent-assisted intra-cranial aneurysm in terms of Dice similarity coefficients, Relative volume difference and Hausdorff Distance, respectively. In addition, the 2D histogram clustering algorithm and Chan-Vese's model have better accuracy when segmenting the intra-cranial aneurysm. Fig.5.19 presents the proposed method converges with the iteration. Nevertheless, the proposed multi-threshold collision function framework can split stent-assisted aneurysm by quantifying the multidimensional information.

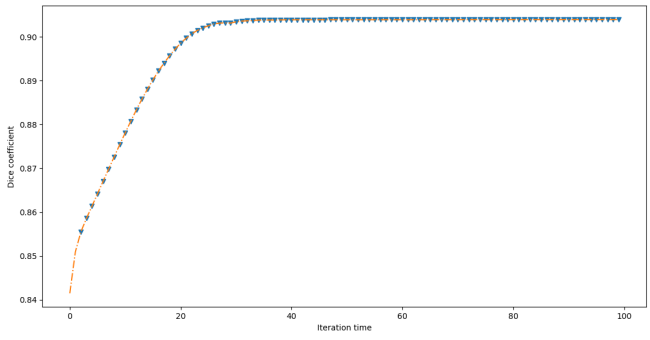

Figure 5.19: Dice similarity coefficient by choosing the different iterations.

Table 5.1: Values of RVD, DSC and d_H from the Chan-Vese method, K-means clustering method and the proposed method.

Data-sets	Evaluation Values	Chan-Vese	K-means	Proposed method
Data_1	DSC	0.8905	0.9479	0.6732
	RVD	0.0010	0.0221	0.0183
	d_h	32.2491	61.0164	64.5058
Data_2	DSC	0.0551	0.7922	0.8254
	RVD	0.0583	0.0933	0.0684
	d_h	34.2491	46.4004	12.0830

5.4 Clustering with curvature information

5.4.1 Objective

The other main problem of image segmentation is difficult because different regions have distinct feature patterns. Features like color, texture, intensity and edge are some widely used in image segmentation. A variety of methods have been proposed for image segmentation [Li and Tian, 2007] [Zhang and Wu, 2009]. Given that, it also should consider to integrate the advantages of two or more feature spaces [Liu et al., 2015]. But how to combine different features for image segmentation is still a challenging issue.

Two feature spaces are integrated into the LBMTM algorithm and propose a multivariate collision function in the LBM framework. The gradient and curvature of the volume data-set are considered to help the algorithm segment image, which aims to elaborate a universal image segmentation approach.

The subject of this section is to further introduce the new approach LBMTM and apply it to the volumes with more complex compositions. In the LBMTM algorithm, the gradient value calculated in 2D histogram effectively improved the segmentation result. Therefore, other potential properties are introduced to the algorithm. For testing the performance of the LB multi-variable segmentation algorithm, two volume data-sets are segmented. The results demonstrate that the multivariate clustering-based collision function of the LBM can greatly improve the segmentation result.

5.4.2 LBM multivariate clustering-based collision function

A new method for image segmentation is proposed in this section by fitting a multivariate feature space and a clustering method integrated with LBM. Fig.5.21

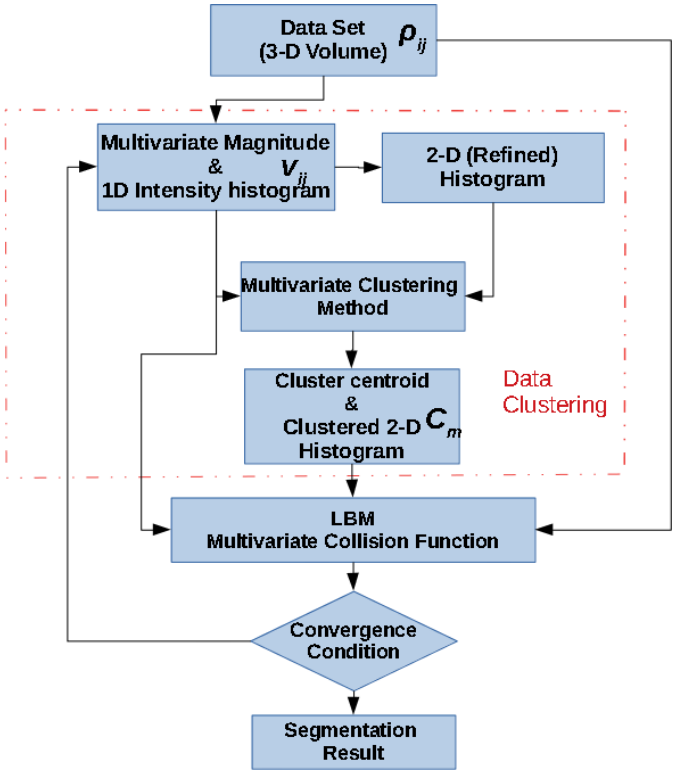

Figure 5.21: Main pipeline of the LBM multivariate method.

exhibits the pipeline of the proposed method, which includes five steps as follows:

Step.1 Based on the volume data-set, we can calculate the corresponding multiple variables at each voxel.

Step.2 Construct 2D histogram with the corresponding variable magnitude.

Step.3 The K-means clustering method is used to classify the 2D histogram and compute the optimal centroids.

Step.4 Then, the thresholds are addressed to the LBM block for anisotropic diffusion.

Step.5 Back to Step.1 until the segmentation results meet the convergence condition.

The proposed method continuously iterates and refines the data-set. Meanwhile, the 2D density histogram is also computed at each iteration and clustered into regions, and each region corresponds to a kind of tissue by K-means algorithm. Subsequently, the refined 2D density histogram and volumetric data-set are applied to render the volume and locate the clusters in image or volume data-set.

The grey-level value and gradient value are collected to construct a 2D histogram. Moreover, the IGM histogram is segmented into several regions, and each

approximates a spatially connected structure by the k-means clustering algorithm. This clustered IGM histogram is applied as a "reference page" to calculate the corresponding thresholds of the LBMTM algorithm. Nevertheless, the gradient also restricts the transferability of the proposed algorithm. It is found that other geometry or statistic properties of the volume data-set can be served as features of the k-means clustering method to increase segmentation accuracy. Therefore, the collision function in LBMTM is reconstructed which is the multivariate clustering-based collision function. In this section, the curvature is selected as an attempt in this direction. After the computation of the gradient and curvature, the proposed method is recursively applied onto the 2D histogram, and a different color is assigned to different features in the 2D histogram. Segmentation can be performed on the 3D volume to the exact different regions of the volume data-set. Herein, the LBM is used in a specific version where the collision function Ω_i is implemented as a reaction-diffusion equation [Qian et al., 1992]:

$$f_i(\vec{r}+\Delta\vec{r},t+\Delta t) = f_i(\vec{r},t) + \frac{1}{\tau}[f_i^{eq}(\vec{r},t) - f_i(\vec{r},t)] + R(C_j,\rho) \tag{5.9}$$

where $R(C_j,\rho)$ is a diffusion term. ρ represents the grey-value on each node.

Herein, a new multivariate clustering-based collision function is proposed, as shown in Eq.5.10, in which C_j is performed as the geometric information and statistics criterion to regulate ρ. Currently, the gradient, curvature [Koenderink and van Doorn, 1992] and the frequencies of them in terms of the multiple threshold values are considered in Chapter 5.

$$R(C_j,\rho) = \alpha(C_m-\rho), \exists m : |C_m-\rho| = min|C_j-\rho| \tag{5.10}$$

where $\alpha = \frac{2}{1+\frac{1}{1+\nabla\rho}}$ is a non decreasing function to ensure the propagation procedure enhance the contrast at boundary. When handling volume data-set with multiple compositions, we still utilize the k-means clustering algorithm to obtain the C_j by segmenting the images shown in Eq.5.11:

$$\arg\min_{C} \sum_{l}\sum_{m} \sqrt{w_1(v_{1,1}-c_1)^2 + ... + w_k(v_{l,m}-c_j)^2} \tag{5.11}$$

where v is the multivariate derived from the voxels of volume data-set; w refers to the weight coefficient of each variate; c_j represents the average value of class C (cluster center). The C_j denotes as the centroids that are used as the main parameter in the proposed collision function.

5.4.3 Experimental result

Segmentation result

In this section the Data_1 and Data_2 are segmented to perform the proposed method. Firstly, the proposed method calculates the magnitude of the considered variable and constructs the 2D histogram in Fig.5.22. Then, based on the 2D histogram from the k-means clustering method, the centroids of all variables are obtained. Because of the limitation of the 2D histogram, only two features can be considered. Next, based on the clustered 2D histogram and centroids from the previous step, the corresponding grey-level value can be derived.

Finally, with the gray value as the main criterion, the gray value in the LBM method is adjusted until the convergence condition is satisfied, which includes the tolerance and max iteration time. We applied the proposed method on the whole cranial volume data-set, and the clustered 2D histograms are displayed in Fig.5.23.The whole cranial is segmented into four parts, and each color on the 2D histogram reflects a cluster. Fig.5.24 reveals all of the corresponding clusters .

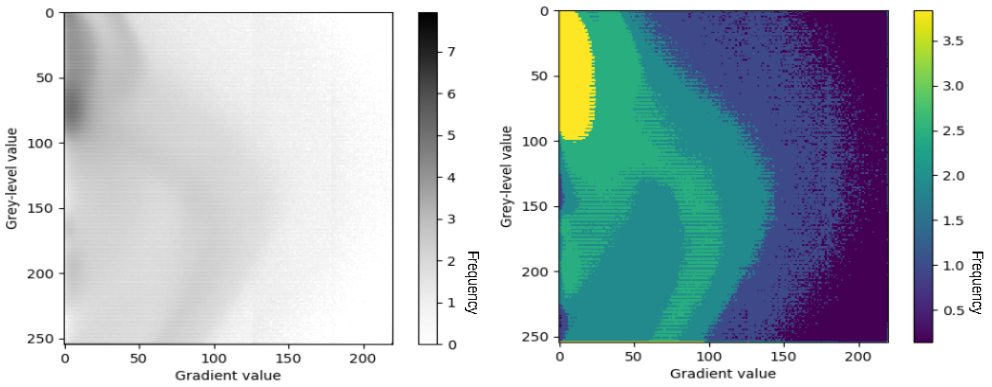

(1) 2D IGM histogram (2) Clustered IGM 2D histogram

Figure 5.22: Multivariate 2D histogram of cranial; Left: Grey-level Value with gradient magnitude. Right: Clustered Gradient-Grey-level 2D histogram.

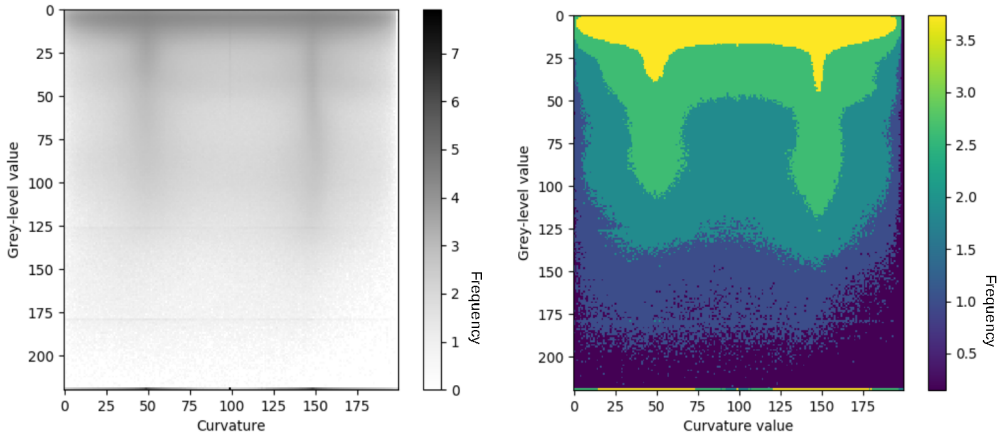

(1) Curvature-grey-level histogram (2) Clustered curvature-Grey histogram

Figure 5.23: Multivariate 2D histogram of cranial; Left: curvature-grey-level histogram. Right: clustered curvature-grey-level histogram.

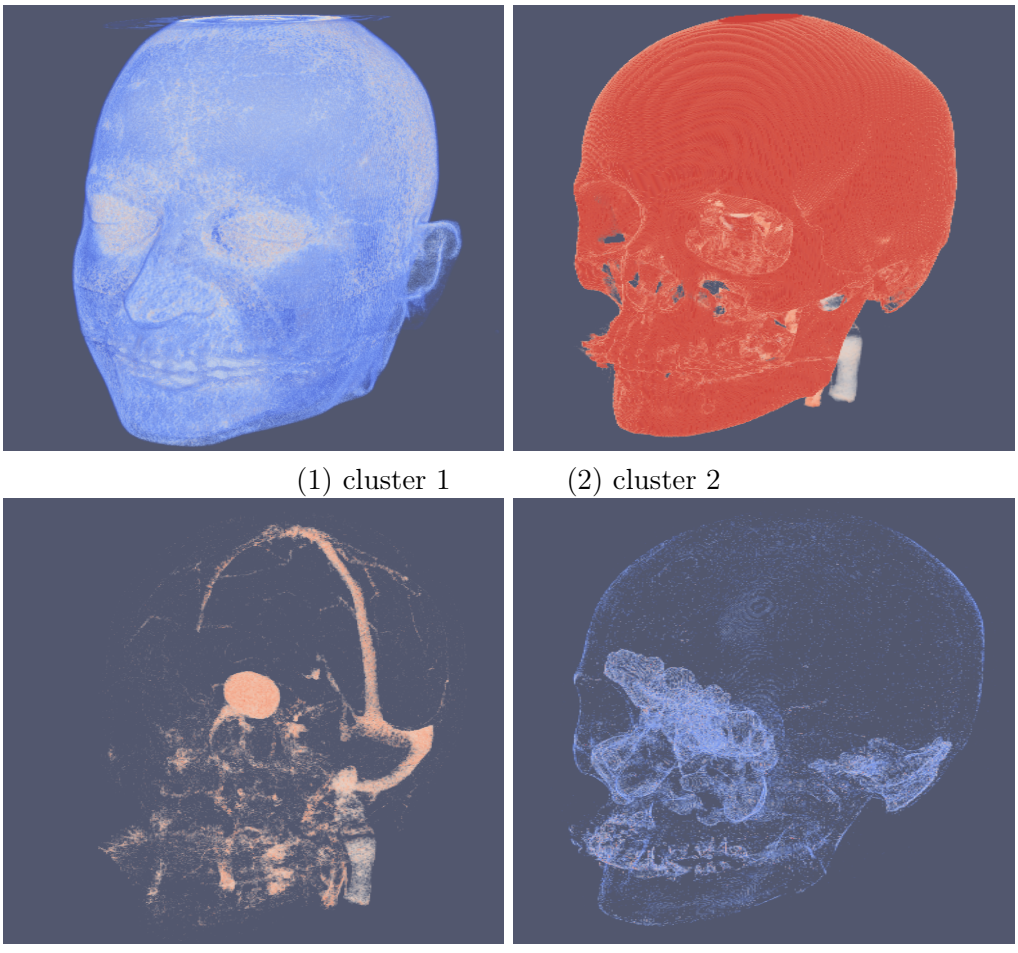

(1) cluster 1 (2) cluster 2

(3) cluster 3 (4) cluster 4

Figure 5.24: The cranial segmentation result of each cluster in the 3D view.

Table 5.2: The Dice similarity coefficient and Hausdorff Distance in different segmentation methods.

	Validation method	**Cerebral Aneurysm**
Chan-Vese	DSC	0.8905
	d_H	32.2491
K-means	DSC	0.9479
	d_H	61.0164
Proposed method	DSC	0.9557
	d_H	56.5509

Validation

For this purpose, we use Dice similarity coefficient (DSC) and Hausdorff distance are conducted to assess the accuracy of our method [Bernard et al., 2018].With respect to data-set segmentation results of V_{sr} and references of V_{ref}, the DSC is defined as:

$$DSC = \frac{2(|V_{sr} \cap V_{ref}|)}{(|V_{ref},| + |V_{ref}|)} \tag{5.12}$$

where V_{sr} represents the volume data-set of segmentation results, and V_{ref} is the volume data-set of references which are the volumes manually segmented by clinical doctors. The DSC is a magnitude value from 0 to 1 (no match to complete match). Meanwhile, Hausdorff distance d_H is also calculated to measure the distance between two subsets, and it is defined as follows:

$$d_H(V_{sr}, V_{ref}) = max\{\sup_{V_{sr}\in V}\inf_{V_{ref}\in V} d(V_{sr}, V_{ref}), \sup_{V_{ref}\in V}\inf_{V_{sr}\in V} d(V_{sr}, V_{ref}) \tag{5.13}$$

where sup represents the upper bound (supremum), and inf represents the lower bound (infimum). In this section, 3D d_H is used to evaluate the segmentation result in order to avoid the management of missing segmentation problems on the end slices. While dealing with volume data-set (whole cranial) with several compositions, the result in Tab.5.2 show that the proposed method is more accurate than that of the k-means and Chan-Vese method in DSC.

5.5 Conclusion

This chapter proposed a novel multi-threshold LBM framework to solve a reaction-diffusion equation at a macroscopic scale via the multi-thresholds collision function. This framework can effectively optimize a consistent segmentation method in regard to the complexity of the cerebral medical images with cranial, cerebral aneurysms and stent-assisted intra-cranial aneurysm. By introducing the clustering algorithm and 2D IGM histogram, the potential of the proposed framework depends on updating with several thresholds and successive iterations of the LBM code, leading to the concept of dynamic clustering of medical image sequences. Then in order to demonstrate the potential possibility of the LBM based segmentation frame work, the lattice Boltzmann multi-variate segmentation algorithm is proposed, in which a reaction-diffusion equation at a macroscopic scale is solved via the clustering-based multi-variate collision function. The promising potential of the proposed method lies in the fitting of derived geometric properties and statistic information of optimized images along with the successive iterations of the LBM framework, which results in the concept of dynamic clustering of medical images sequences. Two data-sets are utilized in experiments to verify the validity and applicability of the proposed method. The segmentation result is compared with the Chan-Vese algorithm as well as k-means clustering method.

Chapter 6

Parallel LBM-based algorithm design

Abstract

In this chapter, a parallel scheme for large scale volume data-set segmentation is proposed. This scheme originates from the LBM-based framework in chapter 5, which takes advantage of local propagation of LBM. The method is implemented on graphics processing unit (GPU) architectures. We operated four volume data-set on our GPU cluster 'Saki', where the computation was completely GPU-based (data write and read once). The results show that the parallel computational scheme is suitable for GPU computing, which can greatly improve the method efficiency. This scheme is also applicable for the large data-set segmentation. The method of parallel segmentation has been executed on the NVIDIA graphic card, and demonstrates that the proposed method can obtain the acceleration at least 131 times under the same precision.

Résumé

Nous proposons un concept de segmentation parallèle basé sur le LBM pour une image médicale à grande échelle. Cette approche reconstruit la fonction de collision de la méthode de Lattice Boltzmann (LBM) par une méthode de classification basée sur un histogramme 2D. Dans ce chapitre, nous élaborons une nouvelle formulation de LBM pour le traitement de volume 3D. Pour traiter les images à grande échelle, nous tirons parti du LBM parallèle en utilisant des architectures d'unités de processeur graphique (GPU) afin d'améliorer les performances du LBM. Nous avons prouvé son efficacité en segmentant la paroi d'un anévrisme traité par stent et des vaisseaux sanguins parents. La méthode de segmentation parallèle a été exécutée sur la carte graphique NVIDIA et démontre que la méthode proposée peut obtenir une reduction du temps de calcul d'un facteur 100 et ceci avec la même précision.

6.1 Introduction

The relationship between the segmentation algorithm and hardware is becoming much more integrated. The LBM has the capability to simulate the fluid flow behavior [Wolf-Gladrow, 2000] and can be used for image processing recently [Wang et al., 2016]. It is easy to implement the parallel computation because of the local operation of LBM that uses the gray-level value on each node of the volume lattice for propagation without data transmission. Therefore, it is feasible to map and calculate the lattices on the thread of GPU. For solving the Computational Fluid Dynamics (CFD) field [Zhao, 2007] and image processing field [Hagan and Zhao, 2009], its parallel computing ability on GPU has been proved. However, because of the complexity of the medical image, the high-performance medical image segmentation still is a challenge. While dealing with large scale volumetric data-set, it has been revealed that the proposed method is not ideal for computational performance. LBM as a numerical approximation method exhibit the following advantages:

- Easy to implement with the core program only with a few lines of code;
- Implicit computation of curvatures;
- Flexible control of generating smooth segmentation results;
- Strong amenability to parallel computing, especially on low-cost, powerful graphics hardware (GPU)

there are already some LBM implementations of CFD on GPUs, but the implementation of LBM on image segmentation is still difficult. In 2009, Aaron used LBM to solve the level-set method [Hagan and Zhao, 2009], in which the proposed scheme was not ideal for complex data-set. Hence, in this section, the proposed LBMTM is implemented on the GPU cluster by CUDA-10.0 in order to accelerate its computation efficiency.

6.2 Differences between CPUs and GPUs

The design of GPU and CPU is different. The reason behind the discrepancy in floating-point capability between the CPU and GPU is that GPU is dedicated to

highly parallel computing and accurately achieves the purpose of graphics rendering. Therefore, it is designed so that more transistors are dedicated to data processing than data caching and flow control [NVIDIA, 2019]. Thus, the complexity is greatly reduced. For example, the GPU does not have CPU intelligence, no prefetching, no branch prediction, etc. The GPU dedicates most of its transistors to the processing in Fig.6.1. This makes GPUs ideal for compute-intensive, highly parallel computation. More specifically, GPUs excel at data-parallel computations. Just like the AVX (SIMD) units in CPUs. GPUs have a reasonable amount of High Bandwidth Memory (HBM) onboard. This memory has greater bandwidth than server RAM, while the drawback is less of it. GPUs attach to a server via the PCIe bus except for NVLink power systems, which ultimately limits communication speed between a CPU and GPU.

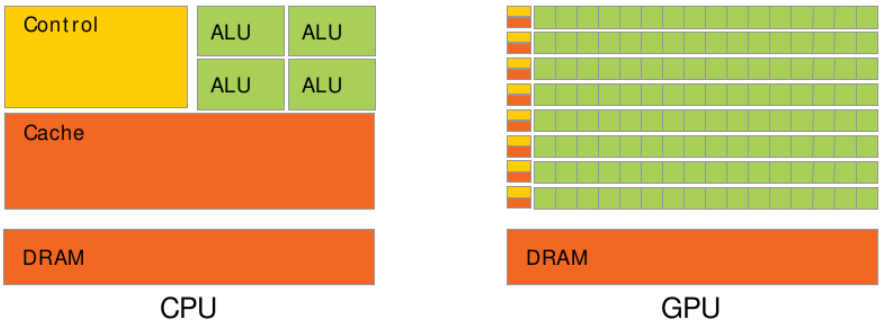

Figure 6.1: GPU devotes more transistors to Data processing[NVIDIA, 2019].

6.3 GPU memory architecture

The LBMTM algorithm is mainly implemented on NVIDIA GPU Tesla P100, and the memory architecture is shown in Fig.6.2.GPU is a hardware device that contains multiple small hardware units called Streaming Multiprocessors (SM). Each SM can execute many threads concurrently. Each one of these SM exists a cache called L1 that is much smaller than that on CPU, but the bandwidth is much larger. As seen in Fig.6.2, all GPUs have a cache called L2 cache, and its on GPU is much smaller than the size of L2 or L3 cache on CPU. But again, the bandwidth of L2 cache in GPU is much larger than that of L2 cache on CPU. On Tesla P100, this GPU Memory has 16 gigabytes memory, which is used to store the volume data-set and particle distribution and equilibrium distribution.

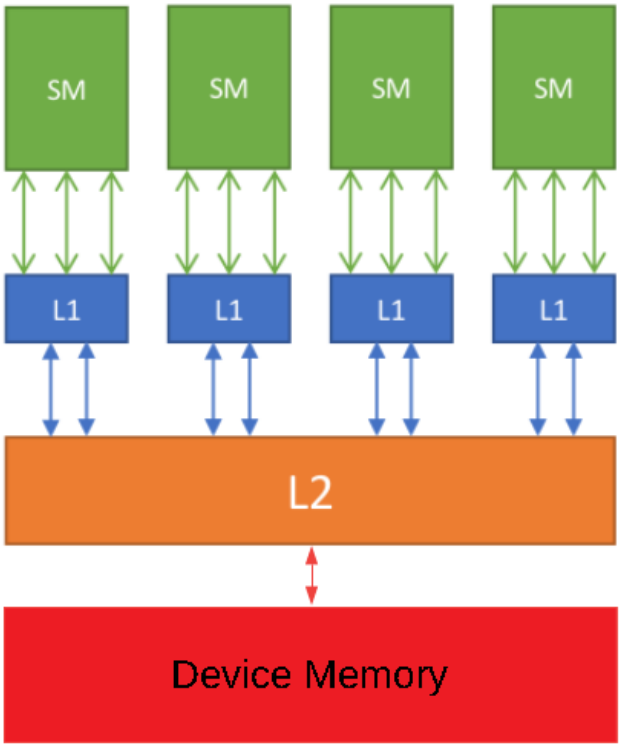

Figure 6.2: GPU memory architecture.

6.4 LBM-based segmentation algorithm

LBM is derived from the cellular automaton scheme, which models particles on a discrete grid. Each point of the grid contains a specific network structure and is linked to its neighbors. Lattice structures we proposed in this section are defined by D3Q7 and D3Q19 which refers to the dimensions and number of connected links between the lattice and its neighbors. Fictitious particles moving along the links and their averaging behaviors are firstly used to simulate traditional fluid dynamics. Based on the numerical computation process derived from microscopic statistical physics, it recovers the Naiver-Stokes equations that govern flow behavior. The independent variables of the LBM equation are particle distribution functions of each link from a grid point to one of its neighbors. Particle distribution functions model the probability that a particle packet will flow through a lattice link to its corresponding neighbor. Between two consecutive steps of the continuous calculation, the function is modified by performing a local relaxation that models inter-particle collisions. This section will introduce a complete physical description and its application in visual simulations.

The first step of the algorithm is to initialize the model which discretes the

simulation space to a grid, and each node of the grid generates a lattice structure. Each node of the grid is regarded as a voxel of the volume data-set. The particle distribution function and equilibrium function are show in Eq.6.1 and Eq.6.2.

$$f_i(\vec{r},0) = f_i^0(\vec{r},0) = \beta_i \rho(\vec{r},0) \tag{6.1}$$

where ρ is the volume data-sets and β_i is given by:

$$\beta_i = \begin{cases} \frac{4}{9}, i = 0 \\ \frac{1}{9}, i = 1,3,5,7,... \\ \frac{1}{36}, i = 2,4,6,8,... \end{cases} \tag{6.2}$$

with ρ and β_i the initial values of the particle distribution and equilibrium function can be calculated.

Then, at each simulation step, iteration is mainly separated into two phases that are the steaming phase in Eq.6.3 and collision phase in Eq.6.4.

$$f_i((\vec{r} + e_i \Delta t, t + \Delta t) = f_i((\vec{r},t) \tag{6.3}$$

$$f_i(\vec{r}, t + \Delta t) = f_i(x,t) - \frac{1}{\tau}(f_i((\vec{r},t) - f_i^{eq}((\vec{r},t)) + R(\rho, T_j) \tag{6.4}$$

where $R(\rho, T_j)$ represents the collision term(the extra force) in the LBM model [Wang et al., 2016]:

$$R(\rho, T_j) = \alpha(T_m - \rho), \exists m : |T_m - \rho| = min|T_j - \rho|. \tag{6.5}$$

At a given time step t, each particle distribution function f_i , along one link vector e_i at a lattice point. $\vec{r}$ is updated by a relaxation process with respect to f_i^{eq} . The collision process is controlled by a relaxation parameter τ. τ controls the rate at which the equation approaches an equilibrium state. $\alpha \Delta t(T_m - \rho)$ is an additional external force, in which T_m is the nearest threshold from the k-means clustering method. The particle distribution function f_i is updated according to Eq.6.4. Then, ρ and equilibrium function f_i^{eq} will be updated in Eq.6.6 and Eq.6.7.

$$\rho(\vec{r},t) = \sum_{i}^{19} f_i(\vec{r},t) \tag{6.6}$$

$$f_i^{eq}(\vec{r}, t + \Delta t) = \beta_i \rho(\vec{r}, t + \Delta t) \tag{6.7}$$

where β_i is the same formula in Eq.6.2. With the updated ρ, T_j is re-calculate by the 2D histogram based k-means clustering algorithm in section 4.3.1.

The segmentation algorithm from Eq.6.1 to Eq.6.7, it reveals that if we have enough memory to store the distribution data-set, the calculation at each node of the grid and at each iteration is independent. This makes the LBM-base segmentation algorithm suitable for carrying into GPUs.

6.5 Parallel LBMTM algorithm

6.5.1 Overview of implementation

The main implementation procedure of parallel computing is to design the kernel function of GPU. The kernel function of LBM is the concrete implementation of the parallel computing, which assigns LBM cell (voxels of volume data) on each thread of GPU, as shown in Fig.6.3. In this method, because the LBM D3Q19 model is utilized, a 4-D matrix is applied on GPU to store the LBM Data in the kernel, including 3-D volumetric data and its corresponding 19 velocities data.

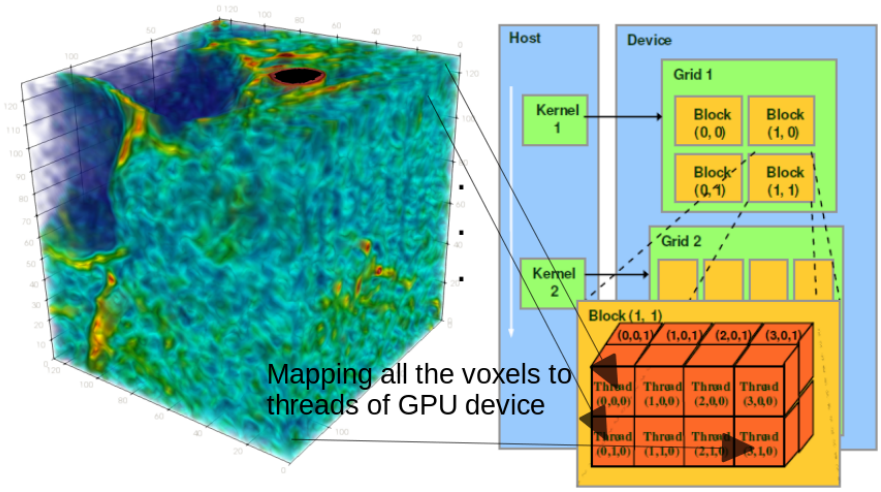

Figure 6.3: Assignment of volume data on GPU.

6.5.2 Computational procedure

The LBMTM image segmentation algorithm is implemented in the following steps:

Algorithm 2: Parallel LBMTM algorithm part 1.

Input: The volume data-set ρ , LBM model D2Q9 or D3Q19, relaxation time τ, maximum iteration time N, center number m,

Output: Volume data-set

1 Initialize the $\bigtriangledown f_i(\vec{r}, t)$ on each node of the grid from the grey-level value;

2 Initialize the value of the $\rho(\vec{r}, 0)$;

3 Initialize the f_i^{eq} according to the two functions as follows:

$$f_i(\vec{r}, 0) = f_i^{eq}(\vec{r}, 0) = \beta_i \rho(\vec{r}, 0) \tag{6.8}$$

$$\beta_i = \begin{cases} \frac{4}{9}, i = 0 \\ \frac{1}{9}, i = 1, 3, 5, 7, ... \\ \frac{1}{36}, i = 2, 4, 6, 8, ... \end{cases} \tag{6.9}$$

4 Initialize the $f_i(\vec{r}, t)$ with function:

5

$$f_i(\vec{r}, 0) = f_i^{eq}(\vec{r}, 0) \tag{6.10}$$

6 Set the maximum iteration time N;

7 **while** *iteration* $<N$ **do**

8 Calculate T_j with function

$$\arg\min_{C} \sum_{j=1}^{k} \sum_{\rho \in C_j} |\rho - m_j|^2 , T_j = m_j \tag{6.11}$$

9 Steaming with function:

$$f_i((\vec{r} + e_i \Delta t, t + \Delta t) = f_i((\vec{r}, t) \tag{6.12}$$

Algorithm 3: Parallel LBMTM algorithm part 2.

1 Collision with function

2

$$f_i(\vec{r}, t+\delta t) = f_i(x,t) - \frac{1}{\tau}(f_i((\vec{r},t) - f_i^{eq}((\vec{r},t)) + \alpha\Delta t(T_m - \rho) \tag{6.13}$$

3 Update the voxel with:

4

$$\rho(\vec{r}, t+\Delta t) = \sum_{i}^{19} f_i(\vec{r}, t+\Delta t) \tag{6.14}$$

5 Calculate $\bigtriangledown f_i(\vec{r}, t)$ and construct 2D histogram and equilibrium function with:

6

$$f_i(\vec{r}, 0) = f_i^{eq}(\vec{r}, 0) = \beta_i \rho(\vec{r}, 0) \tag{6.15}$$

7

$$\beta_i = \begin{cases} \frac{4}{9}, i = 0 \\ \frac{1}{9}, i = 1, 3, 5, 7, ... \\ \frac{1}{36}, i = 2, 4, 6, 8, ... \end{cases} \tag{6.16}$$

8 **End**

9 Output the segmentation result

The main task running on GPU here is to compute the evolution of the density map f_i. The evolution is initialized by the equilibrium distribution function, gradient, thresholds T_j and the distance from clustering thresholds T_j. Next, the collision process is computed. Each voxel of the volume (lattice node) is mapped to a thread of GPU, and the equilibrium distribution for the 3D lattice with 19 velocities is calculated. The total number of voxel times 19 is the number of threads. The $f_i(\vec{r}+\Delta, t+\Delta t)$ is computed on each thread. Next, all 19 velocities are added together to update the density map of the current iteration. The computation will be terminated by the convergence criteria or max iteration time. The pseudo kernel code is displayed in Fig.6.4.

```
__global__ void Kernel_3DLBMD3Q19(float *result, float *fin, float *feq)
{
  Obtain the 19 LBM velocities by *fin

  Parameter initialization

  for iterations{

          for 19 velocities{

           Compute the equilibrium distribution function to *feq

           Compute the centroids of gradient *d

           Calculate the distrubution(density map) of next time step
           by proposed collision function(*fin and *feq)

           Add all 19 velocities together to current *result

          if(meet the convergence condition)
          break;
         }
 }
}
```

Figure 6.4: Pseudo kernel code on GPU.

6.6 Performance result

Parallel computing can be regarded as one of the main advantages of LBM. At first, the proposed method is implemented on a NVIDIA graphic card of the laptop, the Quadro M1000M with 4 gigabytes of GPU memory and programming by python and CUDA-10.0. However, it is found that when the large scale data-set is segmented by LBMTM, the memory of GPU is not enough. Hence, the LBM method is then implemented on NVIDIA graphic card Tesla-P100 with 16GB memory in the cluster "saki" of CREATIS. The results show that when the aneurysm of $128 \times 128 \times 128$ is segmented by proposed method under 15 iterations, it costs 0.24 s on GPU in terms of 31.50 s running on CPU. In order to assess the performance of the proposed method, a comparison is made by running the proposed code on one thread of CPU i7- 6820HQ CPU at 2.70GHz. Tab.6.1 compares the performance between CPU and GPU. The result shows that the proposed method on GPU exhibits efficiency (at least 131 times) and accuracy (Tab.5.1).

Table 6.1: Performance comparison between GPU and CPU.

3D Volume	Volume size	Calculation time on CPU	Calculation time on GPU	time per iteration on GPU	time per slice on GPU	Speed-up-ratio
Aneurysm_1	128*128*128	31498 ms	240 ms	16.0 ms	0.13 ms	131.24
Aneurysm_2	201*201*131	75157 ms	310 ms	20.1 ms	0.10 ms	240.44
Brain/head	512*512*464	2270650 ms	3690 ms	246.0 ms	0.48 ms	615.35
Stent-assisted aneurysm	512*512*512	3571335 ms	5329 ms	349 ms	0.68 ms	670.17

Chapter 7

Conclusion and perspective

7.1 Conclusion

The central theme of this thesis is the LBM for image segmentation. The LBM operates at a mesoscopic scale dealing with distributions of particles in order to simulate macroscopic phenomenon, it is also a numerical tool for solving partial differential equation. The challenge of this thesis is the transformation and adaptation of the LBM to image processing treatment such as image segmentation operation. The main contributions of this thesis are synthesized as follow.

First an original segmentation methodology created by coupling a 2D histogram based clustering method and 3D LBM is constructed, the strategy lies in the opportunity to cluster medical images sequences by taking into consideration not only the grey-level value of voxels but also some geometric characteristics such as curvature index. Under this new concept, a cerebral aneurysm sequence has been processed with the objective of segmenting the wall of a patient specific aneurysm and the associated parent blood vessels.

Then this thesis follows for overcoming the disadvantage of large volume data-set containing multiple components, the lattice Boltzmann multi-thresholds segmentation algorithm is proposed. A novel multi-thresholds collision function (LBM-TM) is elaborated leading to a new formulation of the LBM for the clustering of 3D images, the thresholds being fixed by a 2D histogram-based clustering method. In order to test the performance, 2D images from Berkeley segmentation open source database and volume data-set including a cerebral aneurysm medical imaging sequence, and more challenging a deployed stent in the parent vessels of the cerebral aneurysm are segmented and compared. The results are quantified in term of Dice similarity coefficient, Relative volume difference and Hausdorff distance.

Thirdly based on the segmentation framework, the 2D histogram based clustering method opens the opportunity to integrate other geometric or statistic properties into the method. The first results obtained with this concept are very fruitful and open new perspectives of research in the domain.

Then we found that while segmenting large scale volume data-set, the performances of the proposed method were not ideal, so we propose and implement a parallel LBM based segmentation algorithm implemented on GPU. Concretely the parallel segmentation method has been run on nVIDIA graphic card Tesla P100, the experiment demonstrate that the proposed method accelerates the calculation on GPU by at least a factor of 131 speedup with the same precision reached with CPU, and also accompanied by the characteristic which is the larger the volume data-set, the greater the relative computational efficiency.

7.2 Perspective

Scientific researches based on the LBM contributing to enlarge the landscape of image processing are very rare to find; In this context, this thesis proposes an framework that combines the LBM and clustering method. The results demonstrate its great adaptability to the segmentation of both 2D images and 3D volume data-sets. In future works, the LBM-based segmentation algorithm could be universally used in the image processing field as a specific way to characterize properties of image. And it may also contribute to provide learning matrix or dictionaries of machine learning system. And the other advantage of the proposed framework is its intrinsic adaptability to parallel computation, the LBM-based framework also has the superiority to segment or process 4D volumes of data-set or 3D real-time segmentation [Wang et al., 2016].

7.3 Author's publications

F. Ge, R. Noël, L. Navarro, and G. Courbebaisse, Volume Rendering and Lattice-Boltzmann Method, GRETSI 2017, ID168, Juan Les Pins (France), September 2017.

R. Noël, F. Ge, Y. Zhang, L. Navarro, and G. Courbebaisse, Lattice Boltzmann method for modelling of biological phenomena, the 25th European Signal Processing Conference EUSIPCO, Greek island of Kos, pp. 2654–2658, 2017.

F. Ge, and G. Courbebaisse. A novel parallel lattice Boltzmann method on large scale medical image segmentation. International Conference on Biomedical & Health Informatics, IEEE EMBS BHI 2019, USA, Chicago, May 2019.
F. GE, and G. Courbebaisse. Multi-Thresholds Image Segmentation coupling Lattice Boltzmann Method and clustering Method, J. of Computer Physics Communication, Elsevier Ed., Submitted in December 2019.

Bibliography

[Altman and Bland, 1983] Altman, D. G. and Bland, J. M. (1983). Measurement in medicine: the analysis of method comparison studies. *Journal of the Royal Statistical Society: Series D (The Statistician)*, 32(3):307–317.

[Bajaj et al., 1997] Bajaj, C. L., Pascucci, V., and Schikore, D. R. (1997). The contour spectrum. In *Proceedings of the 8th Conference on Visualization '97*, VIS '97, pages 167–ff., Los Alamitos, CA, USA. IEEE Computer Society Press.

[Bernard et al., 2018] Bernard, O., Lalande, A., and Zotti, C. (2018). Deep Learning Techniques for Automatic MRI Cardiac Multi-structures Segmentation and Diagnosis: Is the Problem Solved? *IEEE Transactions on Medical Imaging*, pages 1 – 1.

[Bhatnagar et al., 1954] Bhatnagar, P. L., Gross, E. P., and Krook, M. (1954). A Model for Collision Processes in Gases. I. Small Amplitude Processes in Charged and Neutral One-Component Systems. *Physical Review*, 94(3):511–525.

[Caban and Rheingans, 2008] Caban, J. J. and Rheingans, P. (2008). Texture-based transfer functions for direct volume rendering. *IEEE Transactions on Visualization and Computer Graphics*, 14(6):1364–1371.

[Cai et al., 2013] Cai, L. et al. (2013). Automatic transfer function design for medical visualization using visibility distributions and projective color mapping. *Computerized Medical Imaging and Graphics*, 37(78):450 – 458.

[Camastra and Verri, 2005] Camastra, F. and Verri, A. (2005). A novel kernel method for clustering. *IEEE Transactions on Pattern Analysis and Machine Intelligence*, 27(5):801–805.

[Chan et al.,] Chan, T. F., Sandberg, B., and Vese, L. A. Active contours without edges for vector-valued images. 11(2):130–141.

[Chen, 2009] Chen, Y. (2009). Lattice boltzmann method based medical image segmentation. In *Image and Signal Processing, 2009. CISP'09. 2nd International Congress on*, pages 1–5. IEEE.

[Chen et al., 2014] Chen, Y., Navarro, L., Wang, Y., and Courbebaisse, G. (2014). Segmentation of the thrombus of giant intracranial aneurysms from CT angiography scans with lattice Boltzmann method. *Medical Image Analysis*, 18(1):1–8.

[Chen et al., 2008] Chen, Y., Yan, Z., and Qian, Y. (2008). An anisotropic diffusion model for medical image smoothing by using the Lattice Boltzmann method. In *7th Asian-Pacific conference on medical and biological engineering*, pages 255–259. Springer.

[Davis, 1975] Davis, L. S. (1975). A survey of edge detection techniques. *Computer Graphics and Image Processing*, 4(3):248 – 270.

[Drebin et al., 1988] Drebin, R. A., Carpenter, L., and Hanrahan, P. (1988). Volume rendering. In *ACM Siggraph Computer Graphics*, volume 22, pages 65–74. ACM.

[Frisch et al., 1986] Frisch, U., Hasslacher, B., and Pomeau, Y. (1986). Lattice-Gas Automata for the Navier-Stokes Equation. *Physical Review Letters*, 56(14):1505–1508.

[Fu and Mui, 1981] Fu, K. and Mui, J. (1981). A survey on image segmentation. *Pattern Recognition*, 13(1):3 – 16.

[Ge and Courbebaisse, 2019] Ge, F. and Courbebaisse, G. (2019). A novel parallel lattice boltzmann method on large scale medical image segmentation. In *2019 IEEE EMBS International Conference on Biomedical & Health Informatics (BHI) (IEEE BHI 2019)*, Chicago, USA.

[GE et al., 2017] GE, F., NOËL, R., NAVARRO, L., and COURBEBAISSE, G. (2017). Volume rendering and lattice-boltzmann method. In *GRETSI 2017*.

[Gonzalez and Woods, 2006] Gonzalez, R. C. and Woods, R. E. (2006). *Digital Image Processing (3rd Edition)*. Prentice-Hall, Inc., Upper Saddle River, NJ, USA.

[Guha et al., 2001] Guha, S., Rastogi, R., and Shim, K. (2001). Cure: an efficient clustering algorithm for large databases. *Information systems*, 26(1):35–58.

[Guo et al., 2011] Guo, H., Mao, N., and Yuan, X. (2011). Wysiwyg (what you see is what you get) volume visualization. *IEEE Transactions on Visualization and Computer Graphics*, 17(12):2106–2114.

[Hagan and Zhao, 2009] Hagan, A. and Zhao, Y. (2009). Parallel 3d image segmentation of large data sets on a gpu cluster. In *Advances in Visual Computing*, pages 960–969, Berlin, Heidelberg. Springer Berlin Heidelberg.

[Hardy et al., 1973] Hardy, J., Pomeau, Y., and de Pazzis, O. (1973). Time evolution of a two-dimensional model system. I. Invariant states and time correlation functions. *Journal of Mathematical Physics*, 14(12):1746–1759.

[He et al., 1996] He, T., Hong, L., Kaufman, A., and Pfister, H. (1996). Generation of transfer functions with stochastic search techniques. In *Proceedings of Seventh Annual IEEE Visualization'96*, pages 227–234. IEEE.

[He and Luo, 1997] He, X. and Luo, L.-S. (1997). Theory of the lattice boltzmann method: From the boltzmann equation to the lattice boltzmann equation. *Phys. Rev. E*, 56:6811–6817.

[Hladuvka et al., 2000] Hladuvka, J., König, A., and Gröller, E. (2000). Curvature-based transfer functions for direct volume rendering. In *Spring Conference on Computer Graphics*, volume 16, pages 58–65. Citeseer.

[Jing et al., 2007] Jing, L., Ng, M. K., and Huang, J. Z. (2007). An entropy weighting k-means algorithm for subspace clustering of high-dimensional sparse data. *IEEE Transactions on Knowledge and Data Engineering*, 19(8):1026–1041.

[Kindlmann and Durkin, 1998] Kindlmann, G. and Durkin, J. W. (1998). Semi-automatic generation of transfer functions for direct volume rendering. In *IEEE Symposium on Volume Visualization (Cat. No. 989EX300)*, pages 79–86. IEEE.

[Koenderink, 1984] Koenderink, J. J. (1984). The structure of images. *Biological Cybernetics*, 50:363–370.

[Koenderink and van Doorn, 1992] Koenderink, J. J. and van Doorn, A. J. (1992). Surface shape and curvature scales. *Image and Vision Computing*, 10(8):557 – 564.

[Li and Tian, 2007] Li, X. and Tian, Z. (2007). Multiscale stochastic hierarchical image segmentation by spectral clustering. *Science in China Series F: Information Sciences*, 50(2):198–211.

[Linsen et al., 2008] Linsen, L., Van Long, T., Rosenthal, P., and Rosswog, S. (2008). Surface extraction from multi-field particle volume data using multi-dimensional cluster visualization. *IEEE Transactions on Visualization and Computer Graphics*, 14(6):1483–1490.

[Liu et al., 2015] Liu, C., Zhou, A., Wu, C., and Zhang, G. (2015). Image segmentation framework based on multiple feature spaces. *IET Image Processing*, 9(4):271–279.

[Lloyd, 2006] Lloyd, S. (2006). Least squares quantization in pcm. *IEEE Trans. Inf. Theor.*, 28(2):129–137.

[Lundstrom et al., 2006] Lundstrom, C., Ljung, P., and Ynnerman, A. (2006). Local histograms for design of transfer functions in direct volume rendering. *IEEE Transactions on visualization and computer graphics*, 12(6):1570–1579.

[Maciejewski et al., 2013] Maciejewski, R. et al. (2013). Abstracting attribute space for transfer function exploration and design. *IEEE Transactions on visualization and Computer Graphics*, 19(1):94–107.

[Maciejewski et al., 2009] Maciejewski, R., Woo, I., Chen, W., and Ebert, D. (2009). Structuring feature space: A non-parametric method for volumetric transfer function generation. *IEEE Transactions on Visualization and Computer Graphics*, 15(6):1473–1480.

[MacQueen, 1967] MacQueen, J. (1967). Some methods for classification and analysis of multivariate observations. In *Proceedings of the Fifth Berkeley Symposium on Mathematical Statistics and Probability, Volume 1: Statistics*, pages 281–297, Berkeley, Calif. University of California Press.

[Martin et al., 2001] Martin, D., Fowlkes, C., Tal, D., and Malik, J. (2001). A database of human segmented natural images and its application to evaluating segmentation algorithms and measuring ecological statistics. In *Proc. 8th Int'l Conf. Computer Vision*, volume 2, pages 416–423.

[Max, 1995] Max, N. (1995). Optical models for direct volume rendering. *IEEE Transactions on Visualization and Computer Graphics*, 1(2):99–108.

[McNamara and Zanetti, 1988] McNamara, G. R. and Zanetti, G. (1988). Use of the boltzmann equation to simulate lattice-gas automata. *Phys. Rev. Lett.*, 61:2332–2335.

[Mitiche and Aggarwal, 1985] Mitiche, A. and Aggarwal, J. (1985). Image segmentation by conventional and information-integrating techniques: a synopsis. *Image and Vision Computing*, 3(2):50 – 62.

[NVIDIA, 2019] NVIDIA (2019). Cuda c++ programming guide v.10.2.89.

[Otsu, 1979] Otsu, N. (1979). A Threshold Selection Method from Gray-level Histograms. *IEEE Transactions on Systems, Man and Cybernetics*, 9(1):62–66.

[Perona and Malik, 1990] Perona, P. and Malik, J. (1990). Scale-space and edge detection using anisotropic diffusion. *IEEE Transactions on Pattern Analysis and Machine Intelligence*, 12(7):629–639.

[Qian et al., 1992] Qian, Y., d'Humières, D., and Lallemand, P. (1992). Lattice bgk models for navier-stokes equation. *EPL (Europhysics Letters)*, 17(6):479.

[Qian, 1997] Qian, Y.-H. (1997). Fractional propagation and the elimination of staggered invariants in lattice-bgk models. 8:753–761.

[Raabe, 2004] Raabe, D. (2004). Overview of the lattice boltzmann method for nano- and microscale fluid dynamics in materials science and engineering.

[Rockafellar and Wets, 2009] Rockafellar, R. T. and Wets, R. J.-B. (2009). *Variational analysis*, volume 317. Springer Science & Business Media.

[Ruiz et al., 2011] Ruiz, M. et al. (2011). Automatic transfer functions based on informational divergence. *IEEE Transactions on Visualization and Computer Graphics*, 17(12):1932–1941.

[Sezgin and Sankur, 2004] Sezgin, M. and Sankur, B. (2004). Survey over image thresholding techniques and quantitative performance evaluation. *Journal of Electronic imaging*, 13(1):146–166.

[Shen et al., 1993] Shen, L., Rangayyan, R. M., and Desautels, J. L. (1993). Detection and classification of mammographic calcifications. *International Journal of Pattern Recognition and Artificial Intelligence*, 7(06):1403–1416.

[Sonka et al., 2007] Sonka, M., Hlavac, V., and Boyle, R. (2007). *Image Processing, Analysis, and Machine Vision*. Thomson-Engineering.

[Sørensen, 1948] Sørensen, T. J. (1948). *A method of establishing groups of equal amplitude in plant sociology based on similarity of species content and its application to analyses of the vegetation on Danish commons*. I kommission hos E. Munksgaard.

[Sterling and Chen, 1996] Sterling, J. D. and Chen, S. (1996). Stability analysis of lattice boltzmann methods. *Journal of Computational Physics*, 123(1):196 – 206.

[Succi, 2001] Succi, S. (2001). *The lattice Boltzmann equation for fluid dynamics and beyond*. Numerical mathematics and scientific computation. Clarendon Press ; Oxford University Press, Oxford : New York.

[Tappenbeck et al., 2006] Tappenbeck, A., Preim, B., and Dicken, V. (2006). Distance-based transfer function design: Specification methods and applications. In *SimVis*, pages 259–274.

[Torre and Poggio, 1986] Torre, V. and Poggio, T. A. (1986). On edge detection. *IEEE Transactions on Pattern Analysis and Machine Intelligence*, PAMI-8(2):147–163.

[Tzeng and Ma, 2004] Tzeng, F.-Y. and Ma, K.-L. (2004). A cluster-space visual interface for arbitrary dimensional classification of volume data. In *Proceedings of the Sixth Joint Eurographics-IEEE TCVG conference on Visualization*, pages 17–24. Eurographics Association.

[Ulen et al.,] Ulen, J., Strandmark, P., and Kahl, F. An efficient optimization framework for multi-region segmentation based on lagrangian duality. 32(2):178–188.

[Wang et al., 2008] Wang, C., Yu, H., and Ma, K.-L. (2008). Importance-driven time-varying data visualization. *IEEE Transactions on Visualization and Computer Graphics*, 14(6):1547–1554.

[Wang et al., 2011] Wang, L., Zhao, X., and Kaufman, A. E. (2011). Modified dendrogram of attribute space for multidimensional transfer function design. *IEEE transactions on visualization and computer graphics*, 18(1):121–131.

[Wang et al., 2016] Wang, Y., Zhang, Y., Navarro, L., Eker, O. F., Corredor Jerez, R. A., Chen, Y., Zhu, Y., and Courbebaisse, G. (2016). Multilevel segmentation of intracranial aneurysms in ct angiography images. *Medical physics*, 43(4):1777–1786.

[Wesarg and Kirschner, 2009] Wesarg, S. and Kirschner, M. (2009). 3d visualization of medical image data employing 2d histograms. In *2009 Second International Conference in Visualisation*, pages 153–158. IEEE.

[Wolf-Gladrow, 2000] Wolf-Gladrow, D. A. (2000). *Lattice-gas cellular automata and lattice Boltzmann models: An Introduction*. Number 1725. Springer Science & Business Media.

[Wu and Qu, 2007] Wu, Y. and Qu, H. (2007). Interactive transfer function design based on editing direct volume rendered images. *IEEE Transactions on Visualization and Computer Graphics*, 13(5).

[Zhang et al., 2016] Zhang, T. et al. (2016). A clustering-based automatic transfer function design for volume visualization. *Mathematical Problems in Engineering*, 2016.

[Zhang and Wu, 2009] Zhang, Y. and Wu, L. (2009). Segment-based coding of color images. *Science in China Series F: Information Sciences*, 52(6):914–925.

[Zhao, 2007] Zhao, Y. (2007). Lattice boltzmann based pde solver on the gpu. *The Visual Computer*, 24:323–333.

Appendix A

Software development

A software has been developed develop under the framework of the lattice Boltzmann method based image segmentation method, programmed with Python and the interface is constructed by utilizing Qt libraries. The software mainly consists of three parts, 3D volume data-set view, 2D slice view and parameter control panel. The algorithms to be implemented in this software are the lattice Boltzmann Multi-threshold method (LBMTM) and lattice Boltzmann multi-variates method (LBMVM-curvature) , the software also integrates several classic segmentation algorithms including: diffusion method, k-means clustering method, 2D histogram-based clustering method, Otsu method, level-set method, Chan-Vese method. then for comparison, the evaluation method also integrated including Dice similarity coefficient, relative volume difference and Hausdorff distance. The basic functions of 3D visualization software are also developed, for example: load 2D image (*.jpg, *.png file) or volume data-sets (*.mhd and *.raw file), save segmentation result to a specific file name and visualize the 2D/3D segmentation result to 2D/3D view. The Graphic user interface is shown in Fig.A.1 and Fig.A.2.

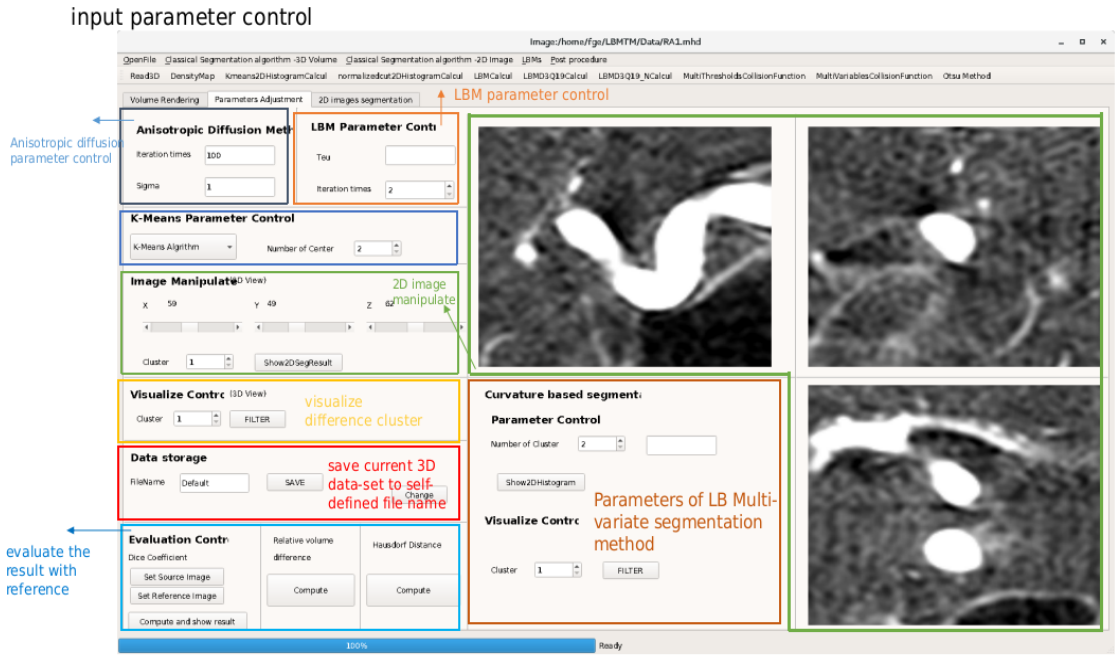

Figure A.1: 2D view and parameter input widget of the software.

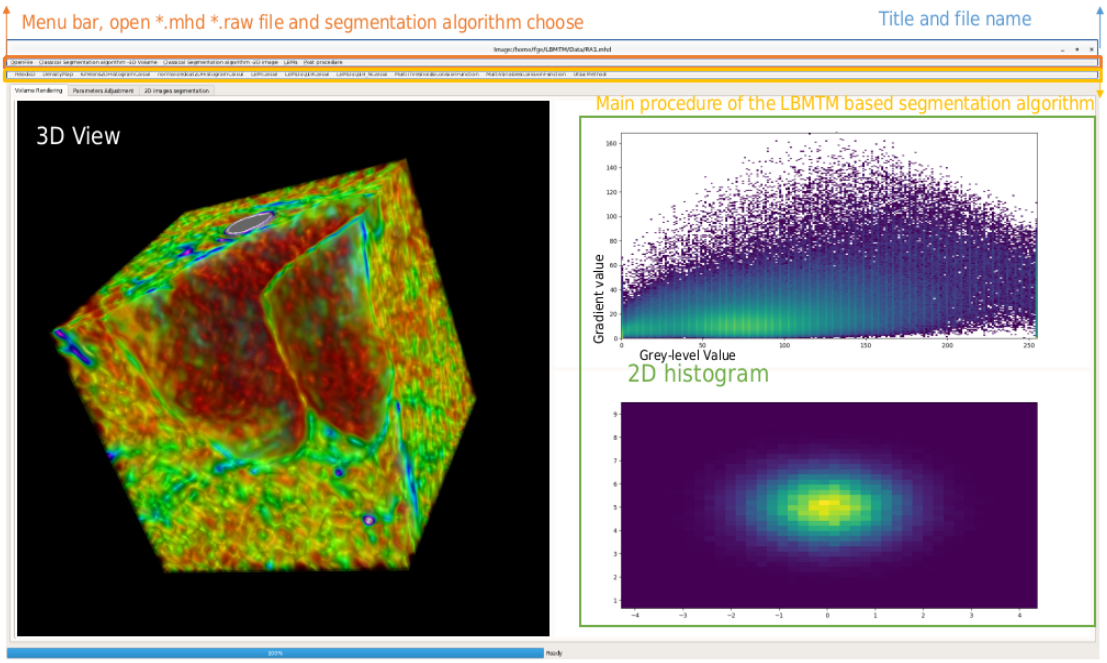

Figure A.2: 3D view of the software.

FOLIO ADMINISTRATIF

THESE DE L'UNIVERSITE DE LYON OPEREE AU SEIN DE L'INSA LYON

NOM : GE
(avec précision du nom de jeune fille, le cas échéant)

DATE de SOUTENANCE : 14/02/2020

Prénoms : Fei

TITRE : La méthode de Boltzmann sur réseau dédiée au traitement d'image
The lattice Boltzmann method dedicated to image processing

NATURE : Doctorat

Numéro d'ordre : 2020LYSEI012

Ecole doctorale : EEA

Spécialité : Traitement du Signal et de l'Image

RESUME :
La méthode de Boltzmann sur réseau est un outil de simulation numérique dont la formulation à l'échelle mésoscopique permet d'éviter la résolution d'une équation différentielle, et repose sur des mécanismes de propagation et de collision au cours du temps, de distributions de particules se propageant sur un réseau régulier. Si les lois de conservation sont imposées en chaque nœud du réseau, alors la solution générée correspondra à la modélisation de phénomènes physiques à l'échelle macroscopique. Dans ce contexte la méthode de Boltzmann est tout à fait adaptée pour résoudre un problème de mécanique des fluides qui équivaut à résoudre indirectement l'équation de Navier-Stokes. Récemment des travaux en traitement d'images ont été réalisés en adaptant la méthode de Boltzmann sur réseau à des opérations de segmentation, de dé bruitage, etc. Par ailleurs la méthode Boltzmann est intrinsèquement adaptée au calcul parallèle sur cartes graphiques permettant ainsi d'optimiser les temps de calculs. Dans ce cadre, l'objectif de cette thèse est de développer une stratégie générale de segmentation multi-seuils appliquée à des données 3D. L'élaboration d'une fonction de collision originale couplée à un algorithme des k-moyennes réalisant une division en "K" partitions ("clusters") des niveaux de gris de l'image considérée, permet une segmentation efficace à seuils multiples. La précision et l'efficacité de la solution proposée ont été validées sur des images de références et sur des séquences d'imagerie médicale traitant d'anévrismes cérébraux.
Egalement la méthode proposée couplant la méthode de Boltzmann et la méthode des k-moyennes, a été testée sur cartes graphiques n'VIDIA attestant que la méthode proposée permet une accélération des calculs d'un facteur au moins supérieur à cent et avec une précision identique relevée notamment lors de la segmentation de la paroi d'anévrismes intracrâniens.

MOTS-CLÉS :algorithme de segmentation, segmentation de l'anévrisme cérébral, méthode de Boltzmann sur réseau, algorithme de clustering, anévrisme traité par stent, histogramme 2D, accélération GPU.

Laboratoire (s) de recherche :CREATIS

Directeur de thèse: Guy COURBEBAISSE

Président de jury :Thierry FOURNEL

Composition du jury :

RUAN Su, Professeure des Universités, Université de Rouen	Rapporteuse
THIRAN Jean-Philippe, Professeur ordinaire , EPFL	Rapporteur
NAVARRO Laurent, Chargé de Recherche - HDR,ENSMSE	Examinateur
CHEN Yu, Professeur associé, YanchengTeachers University	Examinateur
FOURNEL Thierry, Professeur des Universités, Université Jean Monnet	Examinateur
COURBEBAISSE Guy, IR HC - HDR, INSA Lyon	Directeur de thèse